A Numerical Study and Tracer Evaluation of Transport and Diffusion in the Lake Breeze

by
Joseph L. Eastman

Department of Atmospheric Science
Colorado State University
Fort Collins, Colorado

EPA Grant #R-816486-01-0
University of Alabama Grant #UCAR S9148
Roger A. Pielke, P.I.

Colorado State University

Department of Atmospheric Science

Paper No. 531

A NUMERICAL STUDY AND TRACER EVALUATION OF TRANSPORT AND DIFFUSION IN A LAKE BREEZE

Joseph L. Eastman

Department of Atmospheric Science
Colorado State University
Fort Collins, Colorado
Summer 1993

Atmospheric Science Paper No. 531

ABSTRACT

A NUMERICAL STUDY AND TRACER EVALUATION OF TRANSPORT AND DIFFUSION IN A LAKE BREEZE

This study focuses on modeling transport and diffusion in a lake breeze using two different dispersion models. First, a case day was modeled using the CSU-RAMS atmospheric model. A variety of grid spacings in a 2D mode were used, which in turn helped evaluate the grid spacing used to run 3D versions of the model. In addition, a run was conducted in 3D in which all water was removed from the data used to integrate the model. Next the meteorology produced by RAMS was used to drive a Lagrangian Particle Dispersion Model (LPDM), and provide input to a Gaussian plume model called the Industrial Source Complex Short Term (ISCST) model. Both dispersion models were then run to compare with a tracer release conducted on the day modeled. The results were then compared to the concentration fields measured during aircraft flights conducted during, and after, the tracer release. Comparison procedures were used. In their brief comparison the solutions found by the LPDM and the ISCST differed greatly, with the LPDM representing the observed concentration fields remarkably well, provided that RAMS input used a Δx of 4km or less. The 3D simulations produced the highest correlations, followed by 2D simulations in order of increasing grid spacing; next was the no lake simulation, and finally, the ISCST model. ISCST is used by the Environmental Protection Agency to evaluate the potential impact of an industrial source on a given region. It has been applied to areas with complex terrain, such as Rocky Flats in Colorado. After reviewing the results of this study, it is apparent that this is not a correct approach when mesoscale motions are dominant in the vicinity of an industrial complex.

Joseph L. Eastman
Department of Atmospheric Science
Colorado State University
Fort Collins, Colorado 80523
Summer 1993

ACKNOWLEDGEMENTS

I would first like to thank my adviser, Dr. Roger A. Pielke. Together with Dr. Walter A. Lyons, these two men provided support and guidance that made this study proceed coherently. I have known these gentlemen for several years and believe that without their expertise the coherent structure of this study would have never been realized. In addition, my committee members, Drs. Robert N. Meroney and Thomas H. Vonder Haar, need to be accredited with helping me produce a polished finished product. Finally, technical support on using the RAMS and LPDM models was graciously provided by Drs. Craig Tremback and Bob Walko.

There are several others with non-academic backgrounds that need mention. Firstly, my wife, Sara, whom I owe some of my deepest gratitude. She maintained an encouraging attitude throughout the entire process, and provided impetus when results were not turning out as expected. The entire secretarial staff of Dr. Pielke's, Dallas McDonald, Tony Smith, and Bryan Critchfield spent numerous hours preparing the final thesis.

Finally, this study was supported by EPA Grant #R-816486-01-0 and computational support was provided by a grant from the EPA to the University of Alabama through Grant #UCAR S9148.

TABLE OF CONTENTS

LIST OF FIGURES

LIST OF TABLES

Chapter 1

INTRODUCTION

Air quality in the Lake Michigan area has been the subject of numerous studies (Lyons, 1970, 1975; Lyons and Olsson, 1973, Lyons and Pease, 1973; Lyons and Cole, 1974; Haney et al., 1989). The summertime conditions in the region lends itself to numerous episodes of high ozone levels. In addition, the lake-water itself is generally colder than the overlying air mass often resulting in the formation of an intense conduction inversion in the lowest 300 meters. This has an impact on the photochemistry of the region (Lyons and Cole, 1976). During the 1980's there were over 200 days where ozone levels exceeded the federal one-hour ozone standard in this region (Haney et al., 1989). These episodes generally coincide with stagnant, summertime high pressure systems in the area. Under these conditions lake breeze circulations develop and it has been theorized that ozone, and its chemical precursors are trapped in some way and recirculated within the lake breeze circulation. Subsequently, the chemicals can spiral up the coast, or be injected into the return flow aloft.

During the summer of 1991 an extensive set of data was taken in conjunction with the Lake Michigan Ozone Study (LMOS). Two days were the object of intensive measurement programs, June 26 and July 16 of 1991. The 1991 field program included special soundings, ship data, and profiler data at a variety of locations. Shown in Figure 1.1 are the locations of the special sounding sites as well profiler sites. On both of these days sulfur hexafluoride (SF6) was released. SF6 levels were then measured by aircraft and a mobile van. The flight and van paths are shown in Figure 1.2. On both of these days a lake breeze developed, providing an excellent chance to verify theorized helical transport (Lyons and Cole, 1976).

July 16, 1991 was chosen for meteorological and dispersion modeling. This day exhibited features common to development of a lake breeze. Shown in Figure 1.3 is a surface

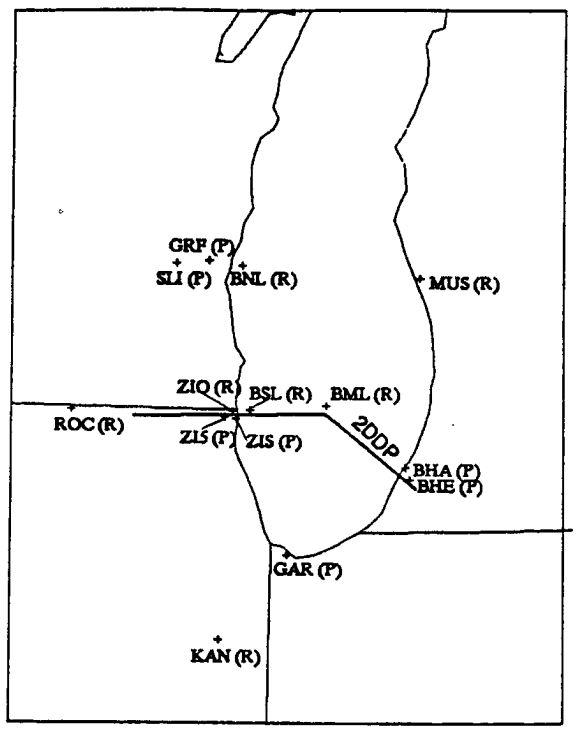

Figure 1.1: Location of various data collection sites.

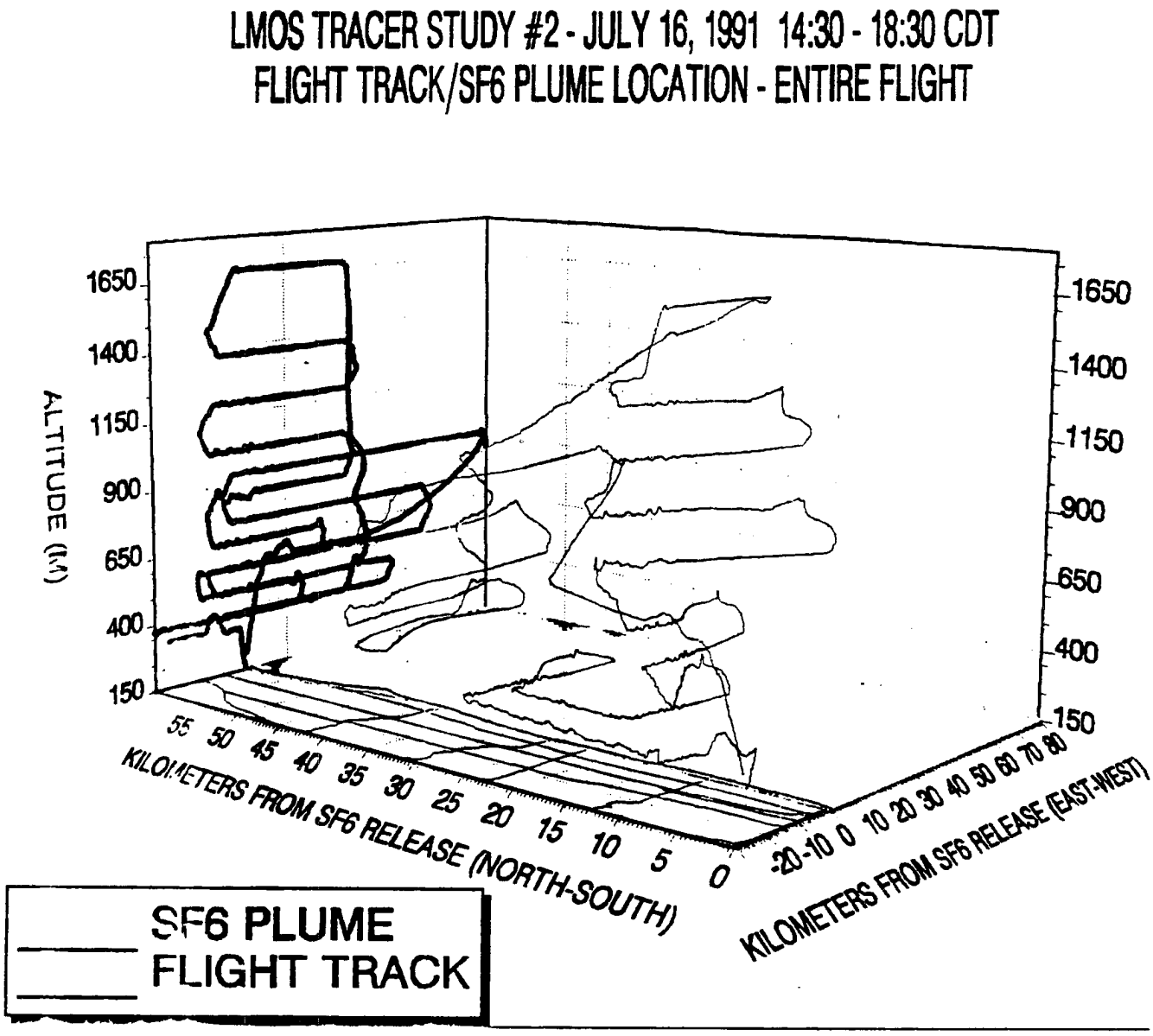

Figure 1.2: Paths taken by aircraft and van.

map of 7/16/1991. Notice the high pressure located to the southeast of the Lake Michigan area. Temperatures approached 30°C in most locations within the modeled area. Maximum ozone concentrations for 7/16/91 are shown in Figure 1.4. Note the numerous values greater than 100 ppb along the west coast of Lake Michigan. In addition, high values were noted along the east coast of the Lake in the state of Michigan. Figure 1.5 shows that the southern end of the lake is the major source of ozone precursors.

Given the locations of the highest O_3 values and the major source locations, the most plausible explanation is that some of the pollutants are channeled up the coast in a lake breeze, while others are injected into a return flow aloft and advected to the opposite shoreline where they undergo fumigation. This study intends to show that this phenomena can be modeled correctly using a Lagrangian Particle Dispersion Model (LPDM), while the Gaussian-plume based Industrial Source Complex Short Term (ISCST) model (Melli and Zannetti, 1992) has inherent difficulties in modeling this scenario.

A series of meteorological simulations were performed at a variety of grid spacings in 2 and 3 dimensions. The 16 km modeling domain and its topography are shown in Figure 1.6. The east-west line shows the slice used for the 2D simulations. A 3D simulation was also performed with water cells set to all land cells, in order to ascertain the impact of the Lake on dispersion. The simulations were used to drive the above mentioned dispersion models. All homogeneous simulations used the sounding shown in Figure 1.7 to initialize the model.

Non-homogeneous initialization was accomplished using an isentropic analysis package that utilized NMC 2.5° analyzed field data, surface observations, and upper air data. The different configurations for the meteorological modeling are summarized in Table 1.1.

The simulations were chosen in hopes of ascertaining the effects of grid spacing, dimension, and initialization characteristics on dispersion characteristics. Many of these are discussed in Moran (1992). In addition, land use characteristics have been shown to have an affect on atmospheric dispersion (Pielke et al., 1991). Computational constraints are imposed to some degree by these model characteristics and thus affect application of the model in an operational mode (Uliasz and Pielke, 1991).

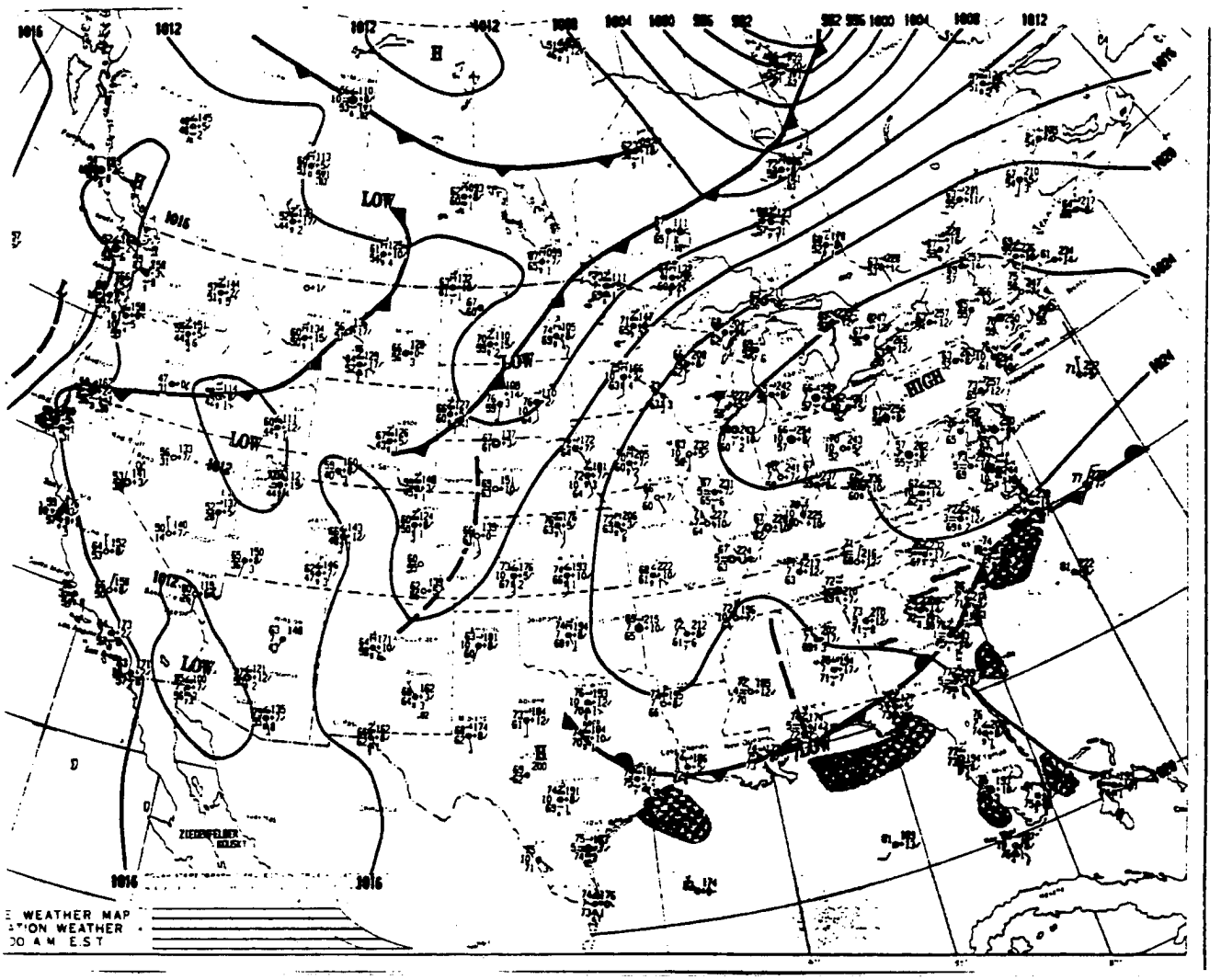

Figure 1.3: Surface map taken at 12 UTC on July 16, 1991.

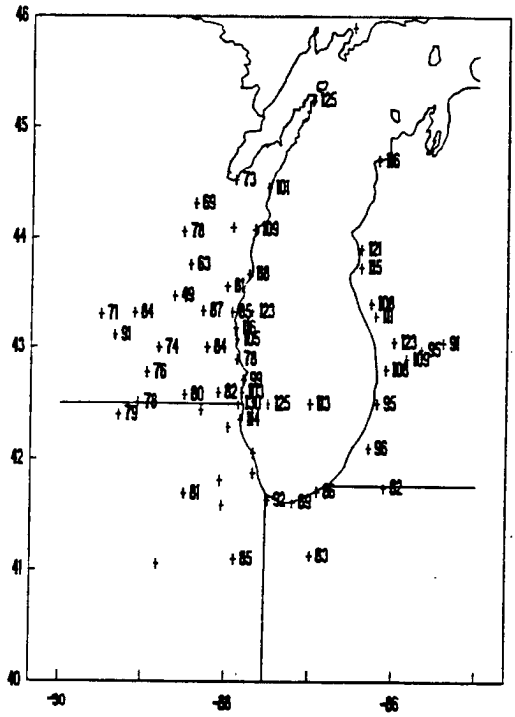

Figure 1.4: Maximum O_3 concentration (ppb) for July 16, 1991.

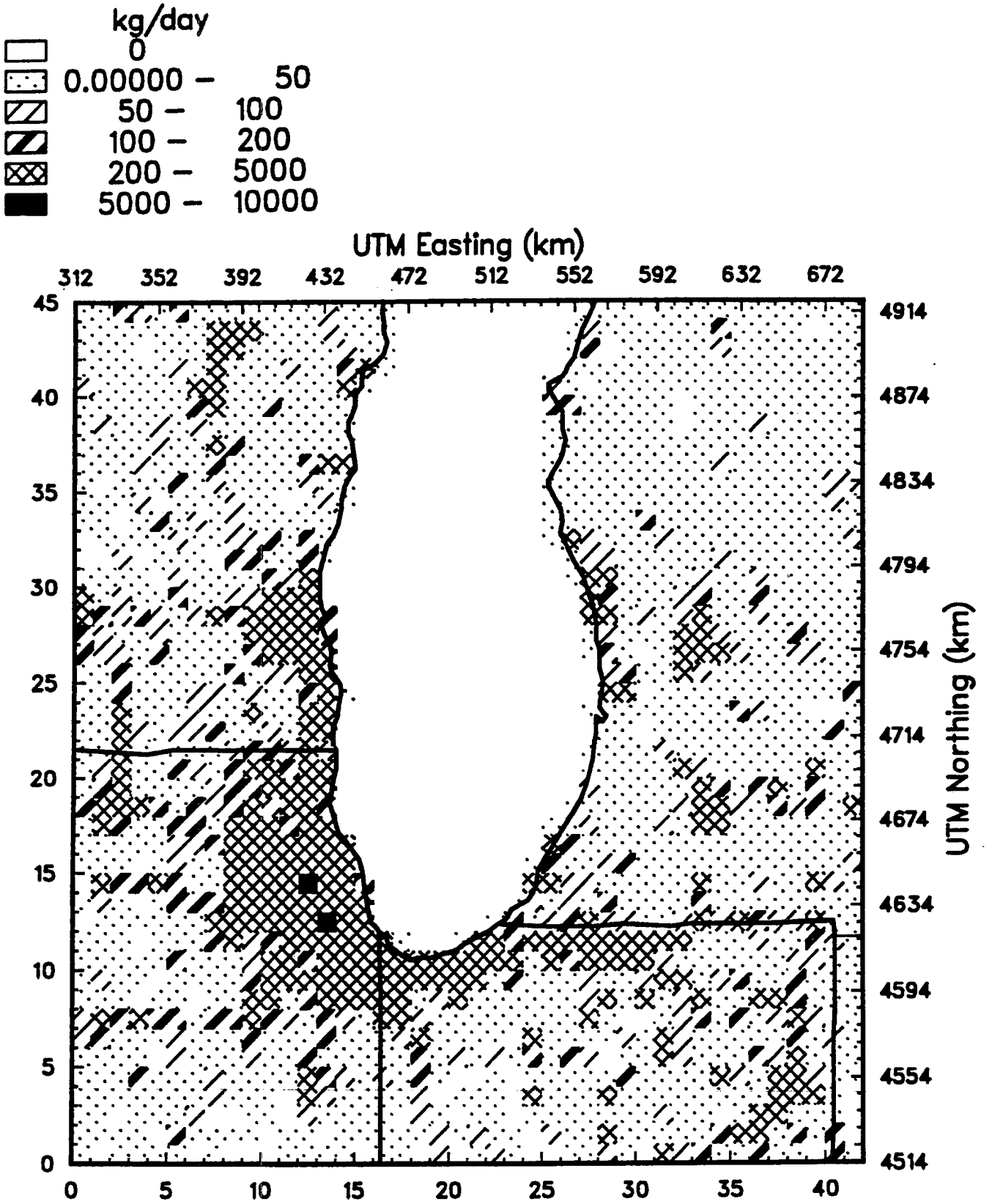

Figure 1.5: NAPAP emissions inventory of NO_x.

Figure 1.6: 16 km modeling domain and topography. The east-west line shows the approximate location of the 2D modeling plane.

Table 1.1: Summary of different configurations.

Run Name	Dimension	Nesting (Y/N)	Initialization	Grid Size(s) in km
2D16	2D	No	Homogeneous	16
2D4	2D	No	Homogeneous	4
2D2	2D	No	Homogeneous	2
3DH	3D	Yes	Homogeneous	16 and 4
3DV	3D	Yes	Variable	80, 16, and 4
NL	3D	No	Homogeneous No Water	16

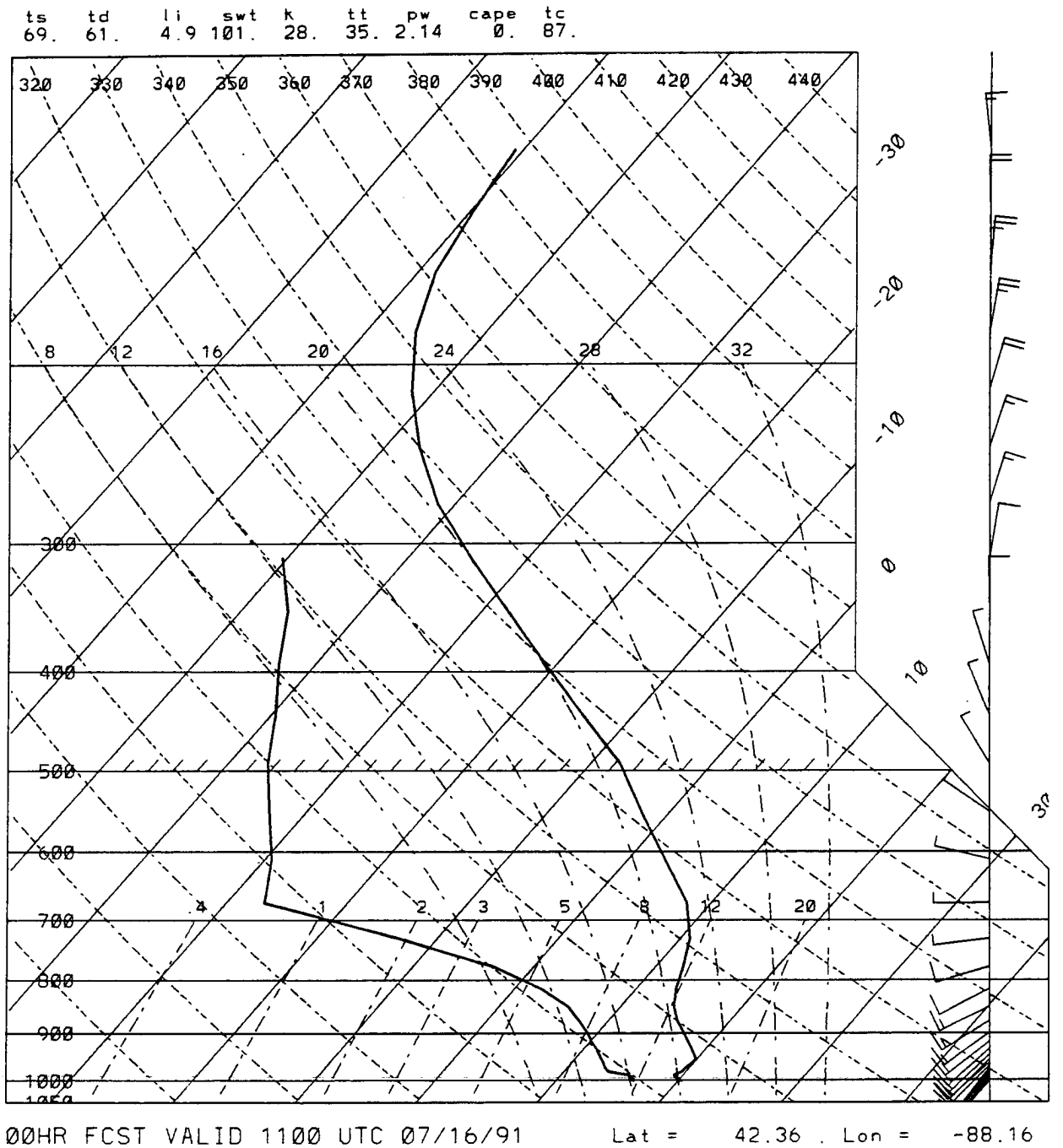

Figure 1.7: Sounding taken from Rockford, Illinois at 12 UTC on July 16, 1991.

The ISCST model was run off the meteorology of both RAMS and the sounding shown in Figure 1.7. Typically, even for short term applications of the ISCST, a sounding is used to asses daily impact. The RAMS meteorology was used to give the ISCST winds that roughly matched observations at hourly intervals, possibly enhancing the accuracy of the results.

Chapter 2

BACKGROUND

2.1 Mesoscale Dispersion Experiments

2.1.1 Previous Field Experiments

There are a multitude of gases available for tracer studies. The perfluorocarbons seem to be the most widely used followed by SF_6. When designing fields programs of this type consideration must be given to the properties of the tracer to be released. Of course it must be non-toxic, conserved, inexpensive to purchase, release, collect and analyze, easily detected, and have a low atmospheric background (Moran 1992). SF_6 meets most of these requirements, although the atmospheric background is near the detection limit.

Table 2.1 taken from Moran (1992), displays a summary of mesoscale dispersion experiments. To come up with this table of 25 experiments Moran specified that the releases were of fixed period, uniform over the release period, used one or more tracers, and the surface sampling network extended at least 25km downwind from the release site. The LMOS field study meets these requirements. Unfortunately the collection sites in LMOS were placed too far inland and none of the samplers detected any SF_6. The general design of the experiments reported in Moran (1992) was devised to look at a larger spatial scale than that of the LMOS experiment.

The RAMS/LPDM coupled model system (or their predecessors) was used to investigate 3 of the experiments listed in Table 2.1. The WHITEX field program was designed to ascertain the impact of the Navajo Generating Station on visibility in the Grand Canyon. It was found that the Navajo Generating Station was responsible for the majority of haze in the Grand Canyon. Moran (1992) also used this to study the 1980 Great Plains experiment and the Cross-Appalachian Tracer Experiment (CAPTEX) performed in 1983.

Table 2.1: Chronology of formal, surface-based, meso-β-scale and meso-α-scale tracer experiments (from Moran, 1992).

Experiment Name	Location	Period (mm/yy)	Tracers	Release Site(s)	Domain Size (km)	No. of Mon. Sites	Mobile Monitors	No. of Tracer Rels.	Release Time (h)	Sample Time (h)	References
Idaho–1	SE Idaho	??	^{131}I	INEL, Idaho Falls	100	36	no	1	3	dose	Lange (1978)
Solent	southern England	5/73	SF_6	Fawley PGS, Calshot	40	31	no	1	1	0.25	Emberlin (1981)
Idaho–2	SE Idaho	1/74–5/74	Kr-85, Me-21	INEL, Idaho Falls, Idaho	1500	13	no	int.*	2 m	10	Cowan et al. (1976) Ferber et al. (1977) Draxler (1982, 1983)
Oxnard Plain	southern California	9/75	SF_6	Ormond Beach PGS	80	8	yes	2	9–14	1	Lamb et al. (1978a)
Savannah River–1	South Carolina	12/75	SF_6, Kr-85 Me-21,	Savannah River Plant, Aiken	90	37	no	1	4	7	Bench et al. (1978) Draxler (1979)
California Delta	central California	9/76	SF_6, $CBrF_3$	Montezuma Hills; Martinez; Pinole	100	28	yes	8	2–9	1	Lamb et al. (1978b)
Idaho–3	SE Idaho	4/77,	Kr-85, PMCH PDCH, PDCB Me-20,21	INEL, Idaho Falls, Idaho	90	82	yes	1	3	6–7	Clements (1979) Draxler (1979)
LA Basin	southern California	7/77	SF_6	El Segundo PGS	150	24	yes	2	5	1	Shair et al. (1982) Sackinger et al. (1982)
Savannah River–2	South Carolina	3/75–9/77	Kr-85	Savannah River Plant, Aiken, SC	300	13	no	int.	0.5	10–168	Telegadas et al. (1978, 1980) Weber (1980) Pepper & Cooper (1983) Fields et al. (1984) Policastro et al. (1986a,b) Carhart et al. (1989)
PMVD–1	central Illinois	4–5/80, 7/80, 5/81	SF_6	Kincaid PGS	~50	~200	yes	375 h	~9	1	Bowne et al. (1983) Cher et al. (1984) Hanna (1986) Moore et al. (1988)
Great Plains	central U.S.	7/80	SF_6, PMCH, PDCH Me-20,21	NSSL, Norman, OK	600	55	yes	2	3	0.75–3	Ferber et al. (1981) Fowler & Barr (1983) (see also Section 3.1)
SEADEX	NE Wisconsin	5/82–6/82	SF_6	Kewaunee PGS	30	130	yes	9	5	4	Johnson et al. (1985) Lewellen et al. (1987)

*intermittent

Table 2.1 (cont'd): Chronology of formal, surface-based, meso-β-scale and meso-α-scale tracer experiments (from Moran, 1992).

Experiment Name	Location	Period (mm/yy)	Tracers	Release Site(s)	Domain Size (km)	No. of Mon. Sites	Mobile Monitors	No. of Tracer Rels.	Release Time (h)	Sample Time (h)	References
PMVD–2	eastern Tennessee	7–8/82, 9–10/82	SF_6	Bull Run PGS, Clinton	50	200	yes	326 h	~12	1	Bowne et al. (1985) Moore et al. (1988)
ACURATE	U.S. Atlantic coast	3/82–9/83	Kr-85	Savannah River Plant, Aiken, SC	1100	5	no	int.	0.32	12	Heffter et al. (1984) Policastro et al. (1986a,b)
CAPTEX	NE U.S., SE Canada	9/83, 10/83	PMCH	Dayton, OH Sudbury, ON	1100	86	yes	7	3	3–6	Ferber et al. (1986) (see also Section 3.2)
KfK/ TULLA	Upper Rhine Valley	4/83, 3/84, 3/85	SF_6	Karlsruhe, W. Germany	45 –60	50+	no	4	3–5	0.5	Thomas et al. (1986) Thomas & Vogt (1990)
METREX	metropolitan Washington, D.C.	11/83–11/84	PMCP, PMCH PDCH	Rockville, MD; Mt. Vernon, VA; Lorton, VA	90	93	yes	545	6	6 h – 1 mo	Draxler (1985)
Øresund	Denmark, Sweden	5/84, 6/84	SF_6	Barsebäck, S; Gladsaxe, DK	30	38	yes	9	3-5	1	Gryning (1985) Enger et al. (1985) Gryning et al. (1987) Andrén (1990b)
ASCOT '84	western Colorado	9/84–10/84	PMCH, PMCP PDCH	Brush Creek	25	100	no	5	9	0.25-1	Clements et al. (1989) Gudiksen & Shearer (1989)
Beijing	Beijing, P.R.C.	11/84	SF_6	Beijing	150	30	yes	4	2-4	$\leq$0.5	Lamb et al. (1990)
SCCCAMP	southern California	9/85–10/85	PMCH, PMCP PDCH	3 offshore, 2 onshore	200	50	yes	4	4	2, 24	Dabberdt & Viezee (1987) Dietz (1987)
SIESTA	Jura, NW Switzerland	11/85	SF_6	Gösgen NPP	90	100	yes	6	4–6	1	Gassmann & Bürki (1987)
DOPPTEX	San Luis Obispo, CA	8/86 9/86	SF_6 $CBrF_3$	Diablo Canyon NPP; Morrow Bay	50	150	no	8	2-8	1	PG&E (1988)
WHITEX	NE Arizona, SE Utah	1/87 2/87	Me-20	Navajo PGS, Page, AZ	250	8	yes	cont.	2 mo	6	SCENES (1987) Stocker & Pielke (1990) NRC (1990)
ANATEX	central, eastern NA	1/87 3/87	PMCH, PDCH PTCH	St. Cloud, MN; Glasgow, MT	3000	77	yes	66	3	6–24	Draxler & Heffter (1989) Clark & Cohn (1990) Haagenson et al. (1990) Draxler (1991)

These two experiments provided a broad contrast in terms of the land patterns investigated. The Great Plains experiment was conducted over gently sloping terrain, that could be considered nearly homogeneous, at least in terms of topographic variability, while the CAPTEX experiment was over complex terrain, with a large degree of heterogeneity. For each of these programs there were also several other models applied to these studies. Overall, Moran found that RAMS/LPDM produced the best correlations to the observed data. Again, it must be emphasized, these studies were on a larger spatial scale than what are investigated using the LMOS data set.

2.1.2 Lake Michigan Ozone Study

The Lake Michigan Ozone Study (LMOS) is a multi-state effort of Wisconsin, Illinois, Indiana, and Michigan, as well as the United States Environmental Protection Agency (EPA). One of the goals is to develop a photochemical model capable of predicting the transport and formation of ozone and its precursors (Gerritson, 1992). This effort was a response to the exceedingly high number of days in that area that were in violation of the 12 hour maximum ozone level set by the National Ambient Air Quality Standard (NAAQS). Many of these areas were in rural north central Wisconsin, far from major urban sources.

During the 1980's there were 213 days in which at least one monitoring station experienced ozone levels greater than 120 ppb (Lyons et al., 1992). Many of the highest levels were confined to a narrow band running roughly parallel to the Lake Michigan shoreline. Many ozone precursors,such as volatile organic compounds (VOC's) and nitrogen oxides (NO_x), originate from highly industrialized sources near the shoreline regions of northern Illinois and Indiana, and southern Wisconsin.

LMOS was coordinated to assist in developing modeling efforts. It is hoped that the model used here will help in assessing the impact of different sources on other areas within the LMOS domain. Besides RAMS and the LPDM, other models used for assessment include the Urban Airshed Model (UAM, Morris et al., 1992) and the use of the Empirical Kinetics Modeling Approach (EKMA, Melli and Zannetti, 1992). Indeed, much

of the preliminary design of the tracer study was accomplished through the RAMS-LPDM couplet (Lyons et al., 1992).

2.2 Model Description

2.2.1 The RAMS Model

The model used to create the meteorology was the RAMS model. The RAMS model is a primitive equation prognostic model. The model was run in a nonhydrostatic compressible mode for all simulations. The basic model equations can be found in Pielke et al. (1992). The model was run in both two and three dimensional modes.

The model was set up for each run with the following characteristics:

- Topography with a terrain-following σ_z coordinate system
- The horizontal domain was a stereographic tangent plane
- Arakawa C grid
- Second order leapfrog time differencing with time splitting (Tripoli and Cotton, 1982)
- Smagorinsky deformation K turbulence closure with a Richardson number enhancement (Tremback et al., 1987)
- Chen and Cotton (1983, 1987) shortwave and longwave radiation scheme
- Louis (1979) surface layer parameterization
- Multi-layer soil model based on Tremback and Kessler (1985)
- Vegetation based on Lee (1992)
- Rigid lid for the upper boundary
- Radiative lateral boundary based on Klemp and Wilhelmson (1978a, b)
- Water vapor was treated as a passive tracer

In the simulations water vapor was treated as a passive tracer, since convection was absent during the modeling period. There were some differences in model setup between the runs. In all runs, complete variable vegetation was employed. Also, in 3DV, variable water surface temperature files were used. Xian (1991) pointed out effects of water surface temperature on sea breeze characteristics. As a result of the variable initialization the soil moisture profiles were also set differently in the 3DV case.

2.2.2 4DDA and Nudging

In the 3DV simulation an isentropic analysis package is used. First, the NMC 2.5° analyzed field data is fed into a pressure analysis stage where it is put on a user defined grid that more than encompasses the area to be modeled. Next this pressure data is used as input to an isentropic analysis stage that interpolates the pressure data onto an isentropic grid. In addition, rawinsondes are objectively analyzed to the isentropic grid. Finally, surface data is objectively analyzed to the horizontal grid.

RAMS uses the files created by the isentropic analysis package to nudge the RAMS solution to the observations. The equation used is a tendency equation described by Wang and Warner (1988). The nudging is weighted at the five outermost grid points. Given the duration of the simulations (12 hrs) and the near homogeneous nature of the synoptic forcing (see Figure ??) it is probable that the variable initialization combined with nudging will have little impact on the solution obtained, but was used nevertheless to provide the most realistic synoptic forcing possible.

2.2.3 LPDM

The LPDM used in this study was modified to account for the shallow thermal internal boundary layer (TIBL). The main equations of the LPDM can be found in McNider et al. (1988). Unlike Gaussian plume and puff models, which generally assume a homogeneous, unchanging background flow, the LPDM incorporates RAMS generated mean flow fields as well as turbulent components parameterized from RAMS data. The particles then are advected using this information.

The LPDM accounts for effects of the TIBL by diagnosing boundary layer heights based on the Richardson number and the vertical profile of the momentum exchange coefficients. The Richardson number based height aids in defining the TIBL. The TIBL is characterized by extremely stable temperature profiles, and subsequently produces nearly no dispersion of an air mass contained within it.

The LPDM allows the user to pick multiple sources of point, line, area, or volume types. In addition, turbulence can be turned off to show the trajectory paths taken by a parcel. The LPDM also can take 2D meteorology and be run in a 3D mode for particle modeling. This feature was employed for the various 2D runs.

2.2.4 ISCST

The ISCST is an EPA approved Gaussian plume model (Melli and Zannetti, 1992). It can be run in a long term (LT) mode (multiple years) or a short term (ST) mode (days). For this particular application the ISCST was run in a short term mode. As Gaussian plume models generally do, ISCST uses a steady state synoptic background as forcing for dispersion. The model uses mixing depth, stability class, and wind information from a meteorological tower, as well as a sounding to supplement mixing depth information. Other features of the ISCST are:

- Specification of multiple sources and source types
- Deposition calculations
- User specification of the vertical temperature gradients and there subsequent assignment to Pasquill-Gifford classes
- User input topography and/or flagpole receptor heights
- Choice of a default EPA standard run or customized parameters
- Rural or Urban modes

A rigorous derivation of the Gaussian plume equation can be found in Pielke (1984). In addition, he points out several well known difficulties of these models when applied to complex mesoscale circulations. They are:

- Over simplification of fundamental conservation relationships
- Inability to represent recirculation, i.e., wind profiles are unidirectional in the vertical
- The use of a constant stability class, although the terrain may be heterogeneous

These limitations will be shown to be significant in the situation modeled in this study.

Chapter 3

METEOROLOGY

3.1 Observations

The surface map shown in Figure 1.3 illustrates a typical summertime pattern in the eastern United States. At 12 UTC the anticyclone was centered over central Pennsylvania as it moved off to the east. The resultant flow was southwesterly near western shore of the lake. Somewhat atypical of the flow was the magnitude of the surface winds. In the Lake Michigan area winds were roughly 10 m s^{-1}. Generally, winds are much lighter when the area is under the influence of a high pressure area. As a result of the strong flow the lake breeze was fairly weak, as the surface winds prevented the lake breeze from penetrating far inland. High temperatures in the Lake Michigan area ranged from 26°C in Escanaba, Michigan to 29°C in Grand Rapids, Michigan. The dewpoints on this day were also fairly high, ranging from 15°C to 22°C. Supplemental soundings taken over the lake illustrates its impact on the surface meteorology. Figure 3.1 exhibits a shallow inversion of roughly 200 m. The synoptic inversion also shows a height of 1700 m. It should be pointed on that the lake temperatures during the summer of 1992 were unusually high, roughly 23°C, which in turn decreased the magnitude of the conduction inversion present over the lake.

There was also a large amount of supplemental data taken on this day. Doppler sodar was deployed at Zion, Illinois. A time-height cross section shown in Figure 3.2 shows that there was a wind shift at about 11 LST, going from southwesterly to southeasterly. The doppler also provides information about the depth of the inflow, which was less than 200 m. The shallowness is directly related to the prevailing synoptic conditions. Since the surface winds were strong, the resultant lake breeze was relatively weak. Still the imposed mesoscale flow had an observable affect on the observed ozone measurements.

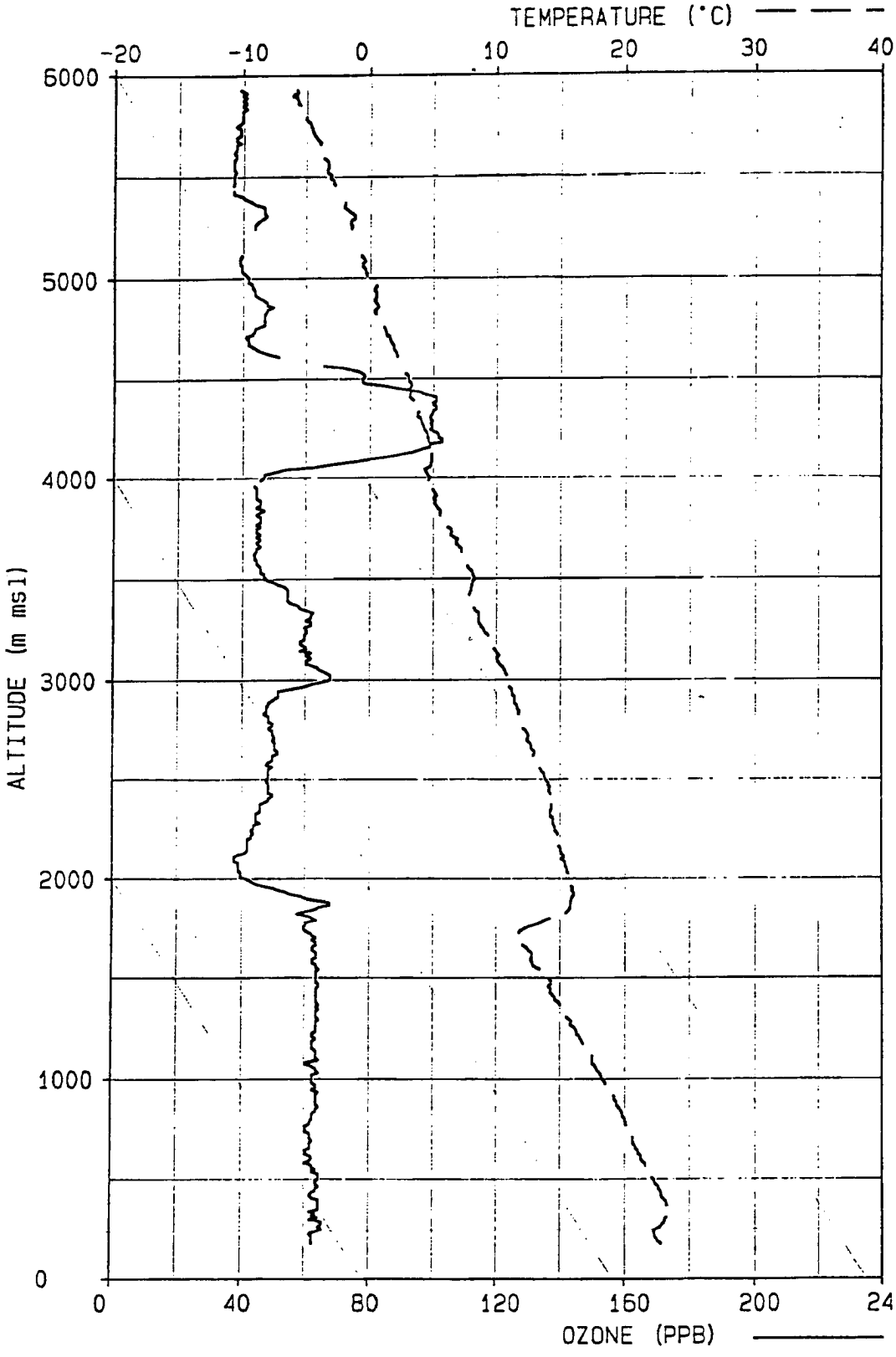

Figure 3.1: July 16, 1991 12 UTC sounding taken from a boat located near the center of the lake.

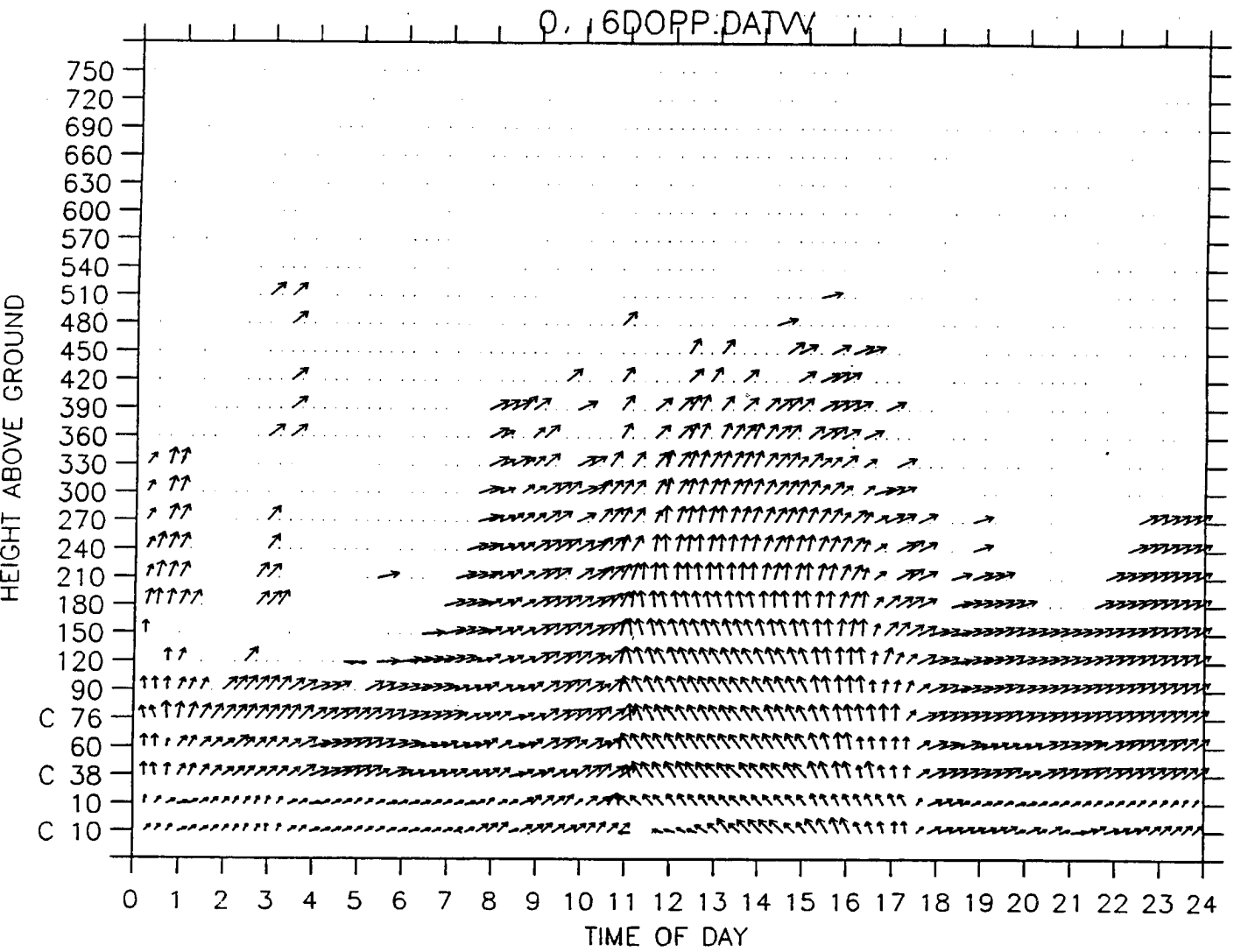

Figure 3.2: Doppler profiler data taken near the shore at the Zion site.

In addition to the doppler, Zion's meteorological towers were another source of information. They were located near the lakeshore, 3, 5, and 24 km inland. The wind measurements were made at 10 m AGL at 1 hour intervals, although the lakeshore site had information available at 30 and 70 m. Table 3.3 shows reversal in wind direction at the lakeshore site between 11 and 12 LST. Also notice the change in temperature and dewpoint. This airmass is quite stable with a Pasquill-Gifford classification of F. This in turn will be shown to impact the dispersion of SF6. A quantitative measure of the lake breeze penetration can be ascertained from inland tower data. The Figure shows that the wind direction changed between 12 and 13 LST at the 3 km site. Again the temperature drop is quite obvious as the stable airmass moves in. The 8 site shows no such change in direction, which indicated the lake breeze was between 3 and 8 km inland. It is presumable that these conditions were prevalent at Waukegan Harbor, the site of the SF6 release, since it is less than ten kilometers to the south of Zion.

ZION SITE Meteorological Tower data for July 16, 1991

CST	Wind Speed (mph)			Wind Direction			Temperature (F)
	2m	10m	78m	2m	10m	78m	2m
6	4.0	10.0	14.9	237	241	235	68.2
7	3.9	8.1	13.9	241	243	241	72.2
8	4.9	6.8	8.3	230	237	235	76.8
9	5.3	7.4	8.5	233	241	239	79.3
10	7.2	9.4	11.1	229	235	230	80.7
11	7.8	10.5	12.0	215	229	226	82.1
12	9.0	11.3	12.2	141	156	160	78.1
13	9.9	12.7	14.4	134	155	154	77.8
14	10.3	12.5	14.2	141	147	152	77.6
15	9.9	11.9	13.4	141	149	157	77.9
16	10.0	11.7	13.8	151	161	164	79.2
17	8.4	10.1	12.2	161	169	173	79.6
18	6.4	9.8	12.0	205	211	219	81.7

Figure 3.3: Time series of meteorological data taken from the Zion site at 10 m AGL.

3.2 Meteorological Simulations

3.2.1 Initial Conditions

As stated briefly in Section 1 there were a total of 6 simulations performed in hopes of ascertaining the effects of mesh size, dimensionality, and the lake on the meteorology and dispersion. A detailed discussion of initialization procedures aids in understanding the differences that developed between the simulation.

A lake breeze develops as a result of differential heating between the land and water. As the land heats up during the day a pressure gradient develops between the land/water boundaries, with lower pressure developing over the land relative to the water surface. Figure 3.4 shows a schematic of the diurnal evolution of the sea and land breeze in the absence of synoptic flow (from Pielke, 1981). The lowered pressure over the land results in an enhanced wind component blowing from lake to land. As the onshore winds approach zero inland, a convergence zone is formed. The convergence then forces upward motion, and an added component of velocity aloft, opposite in sign to the inflow off the lake at the surface. All of the perturbations in the wind field are relative to the prevailing synoptic wind. All simulations produced a lake breeze solenoid to varying degrees. This was related to the initial setup of the various runs.

The homogeneous simulations were initialized using the sounding shown in Figure 7. The sounding has a negative area of roughly 5600 J kg^{-1} with a heating of 396 J kg^{-1} to reach a convective temperature of 32°C. The convective condensation level was found to be 820 mb, the lifting condensation level 410 mb, and the K index was calculated to be 35. Total precipitable water was calculated as 2.14 cm. The sounding also possesses a mean directional wind shear of $23\frac{^{\circ}}{km}$ and a wind shear in magnitude of 4.1 m s^{-1} km^{-1} in the lowest 3 km.

The sounding was taken from the 3DV simulation at 6 LST from a cell located 32 km west of the Zion Nuclear Power Plant. The homogeneous simulations used the sounding altered in the following manner. An estimated planetary boundary layer (PBL) height was calculated from the 3DV run. The winds below this height were turned roughly 30°

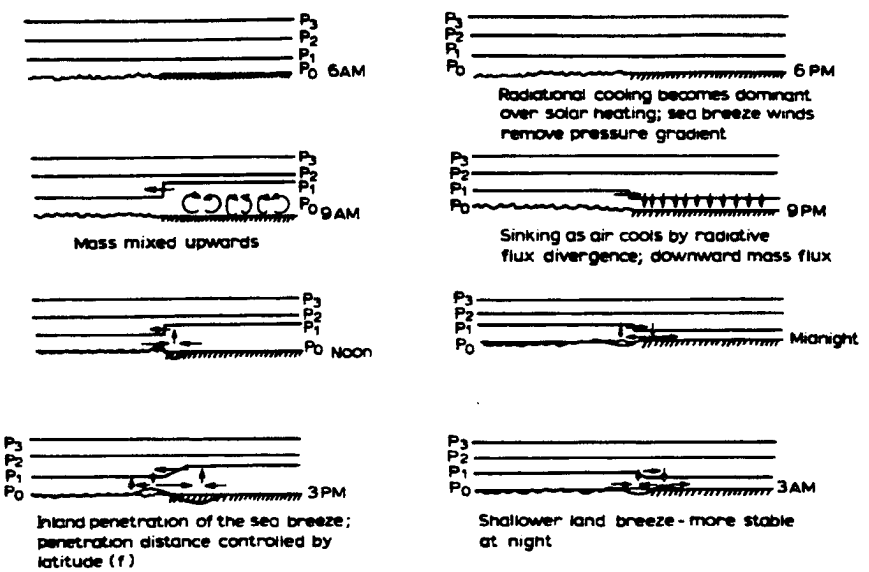

Figure 3.4: Schematic of the diurnal evolution of the sea and land breeze in the absence of synoptic flow (from Pielke, 1981).

clockwise. This was necessary because 2D simulations tend to strongly turn to lower pressure.

The presence of the nocturnal jet is evident in the sounding, as exemplified by the low level winds in excess of 10 m s^{-1}. The sounding displays dryness all the way up to the last level recorded by the sonde. This was the justification for treating water vapor as a passive tracer in the model.

Surface characteristics were initialized using a variety of data sets. For topography in the homogeneous simulations a 30 second topographical data set was used for all mesh sizes. The coarsest mesh in the 3DV run covered an area that was outside the areal coverage of the 30 second data set at some points, consequently, a 10-minute topographical data set was used.

The land percentage and vegetation for the simulations were derived from 30 second data supplied by the United States Geological Survey (USGS). Again, the coarse mesh for 3DV was initialized using a 10 minute data set. The USGS data contains 176 different vegetation classes. These classes were reduced to 18 total classes, which are then used by RAMS. Plots of the 16 km and 4 km grids and the vegetation assigned to them are shown in Figure 3.5. Notice the increase in detail as the mesh size is reduced. The variability in vegetation can produce solenoids in both the north/south and east/west directions, much like the quasi north/south orientation of the lake breeze. For transport on longer time scales this would invariably have a profound impact on dispersion (Lee, 1992, Pielke et al., 1991). The variable land percentages along the coast will have similar effects. In 2D the coastal variation in land percentage is not realized, since the land percentage is constant as one goes poleward or equatorward. The magnitude of these differences on the resultant dispersion will be ascertained in the next section.

One more surface characteristic, which was set differently for 3DV versus the other simulations, was sea surface temperature (SST). In the 3DV simulation the SST varied over the lake area, while in the other runs it was set to a constant. As pointed out earlier this has little impact on the meteorology of the lake breeze Xian (1991).

As mentioned earlier the 3DV run employed files that were used to nudge the entire domain towards an observed pattern. These files were spaced at 6 hour intervals, and

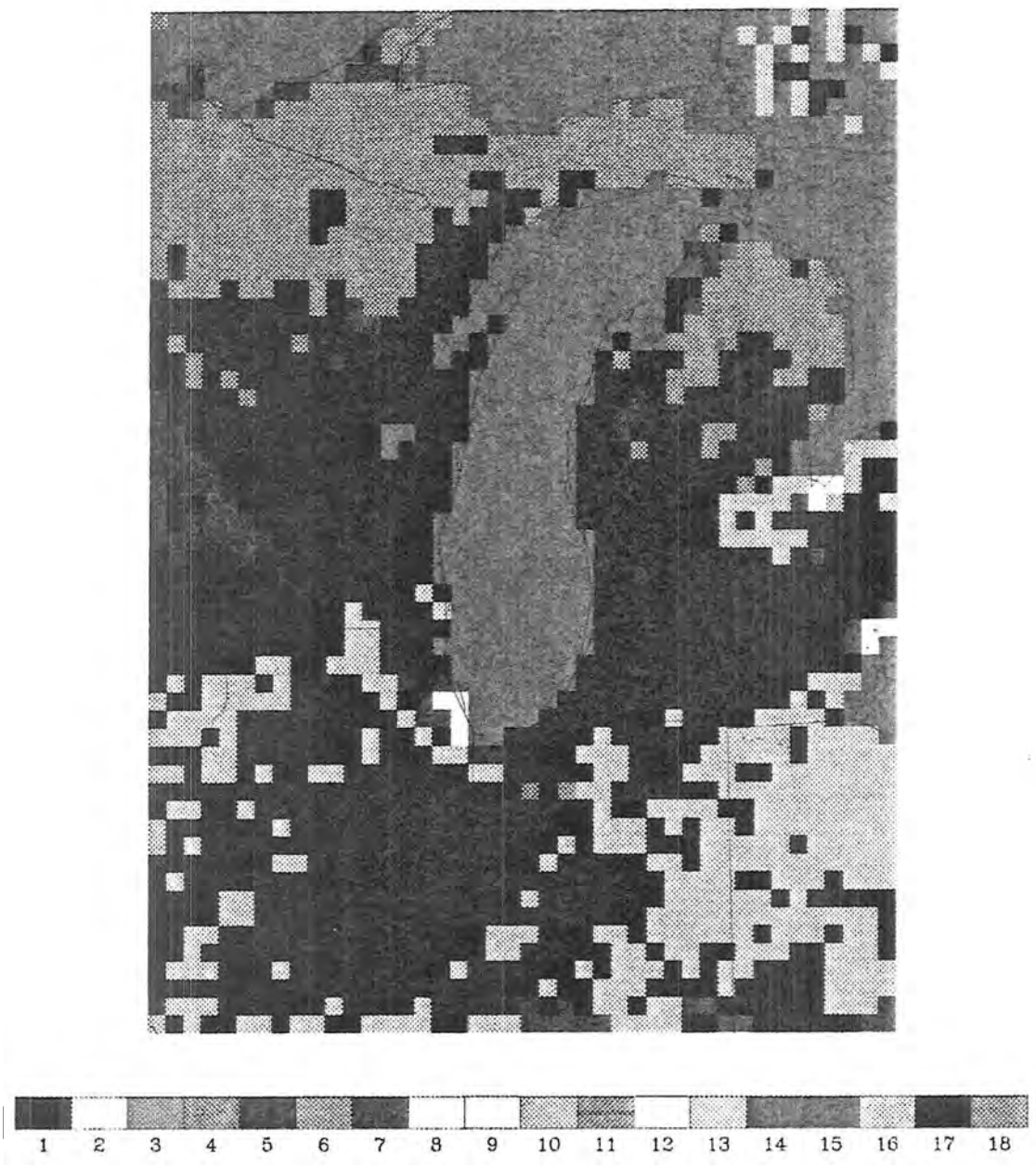

Figure 3.5: Plots of (a) 16 km and (b) 4 km grids land cover/vegetation type from the Biosphere-Atmosphere Transfer Scheme (BATS) (from NCAR/TN-275+ST, Dickinson et al., 19) 1-Crop/mixed farming, 2-Short grass, 3-Evergreen needleleaf tree, 4-Deciduous needleleaf tree, 5-Deciduous broadleaf tree, 6-Evergreen broadleaf tree, 7-Tall grass, 8-Desert, 9-Tundra, 10-Irrigated crop, 11-Semi-desert, 12-Ice cap/glacier, 13-Bog or marsh, 14-Inland water, 15-Ocean, 16-Evergreen shrub, 17-Deciduous shrub, 18-Mixed woodland.

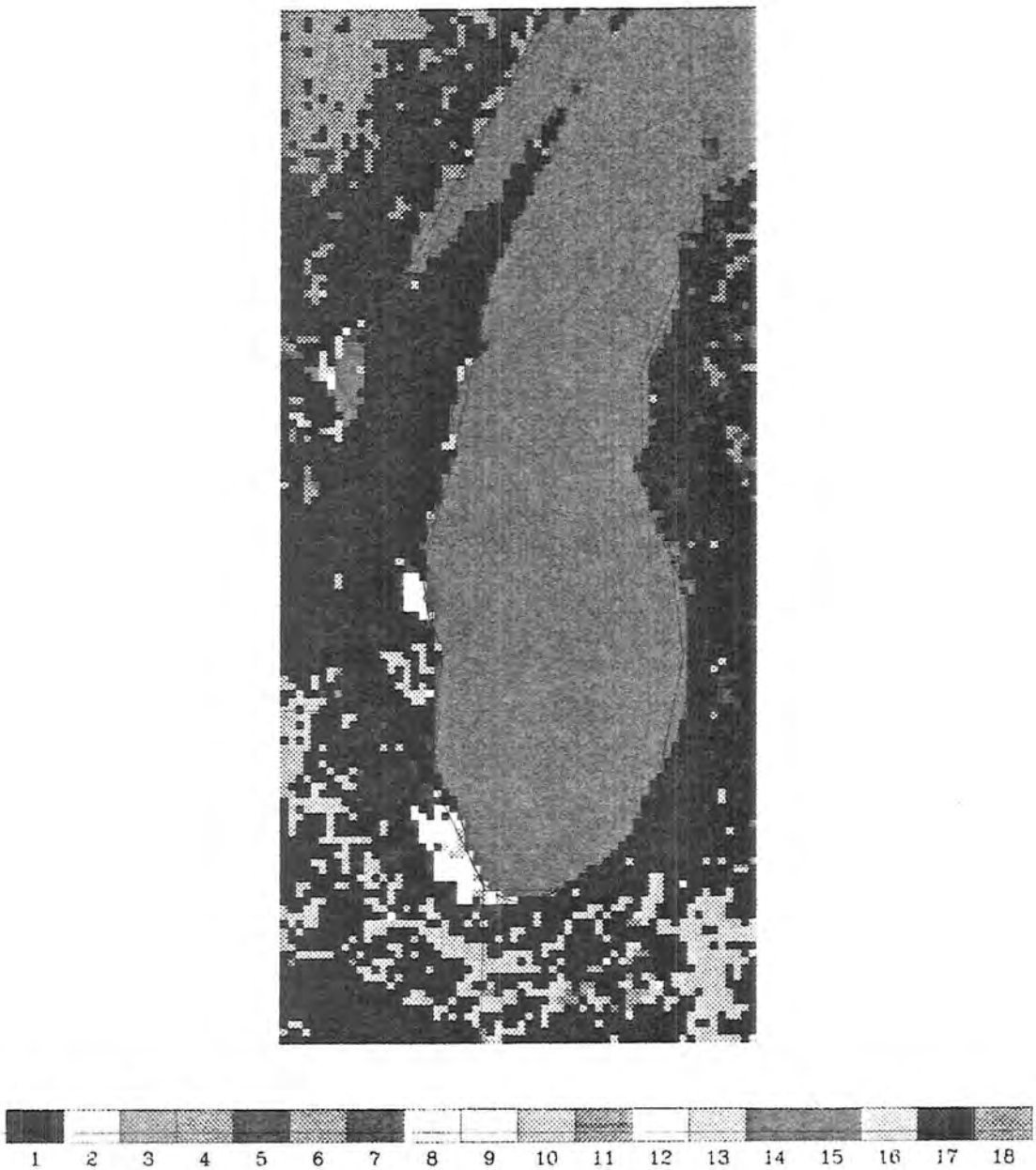

Figure 3.5: Continued.

created separately for each grid. This allowed finer details to be assimilated for finer mesh size. Previously it was mentioned that the synoptic forcing on the day was constant, and that this could minimize the effects of nudging on the final solutions. It is not too difficult to imagine a case where the nudging could be vital to the final solution, and the resultant dispersion patterns (a developing extratropical cyclone, for example).

Soil moisture was initialized using the U.S. Department of Agriculture's soil moisture survey. For 3DV this information was digitized to the coarsest mesh, then interpolated to the finer grids. An average of the 16 km 3DV grid values, at all soil grid levels, was computed and that value used to initialize the homogeneous runs at each corresponding level.

3.2.2 2D and 3D Comparisons of XZ Sections

This section will first present a series of meteorological plots in an XZ plane, through the Zion data plane, to demonstrate the differences between simulations. All output plots of meteorology that follow will be in the same format. Starting in the upper left and proceeding clockwise the first plot is 2D2, followed by 2D4, 2D16, NL, 3DV, and 3DH. In all plots the contours limits and intervals have been kept constant, and are listed in the captions.

The initial fields of U and θ are shown in Figures 3.6 and 3.7. The differences in the initial states are minimal, except in the 3DV case. This case exhibits lighter winds, and a slope to the θ isolines. In the heterogeneous case the variable nudging, and the fact the simulation has been integrated for the 36 hours model time, has resulted in the inhomogeneities present. Figures 3.8, 3.9, and 3.10, show the U, θ, and W after 4 hours of integration, 10 LST. The 3DV run exhibits a negative component of U indicating lake breeze onset has begun. This is due to the initial winds that were southerly,and to stronger thermal forcing already present in the 3DV case. This is apparent in Figure 3.9, which shows values roughly 1°C higher at the surface than the homogeneous case. The depth of the boundary layer also indicates more heating in the 3DV simulation. This is probably due to the soil moisture initialization, and will lead to a super-adiabatic layer in the homogeneous simulations that is somewhat stronger than is observed. Figure 3.10 shows

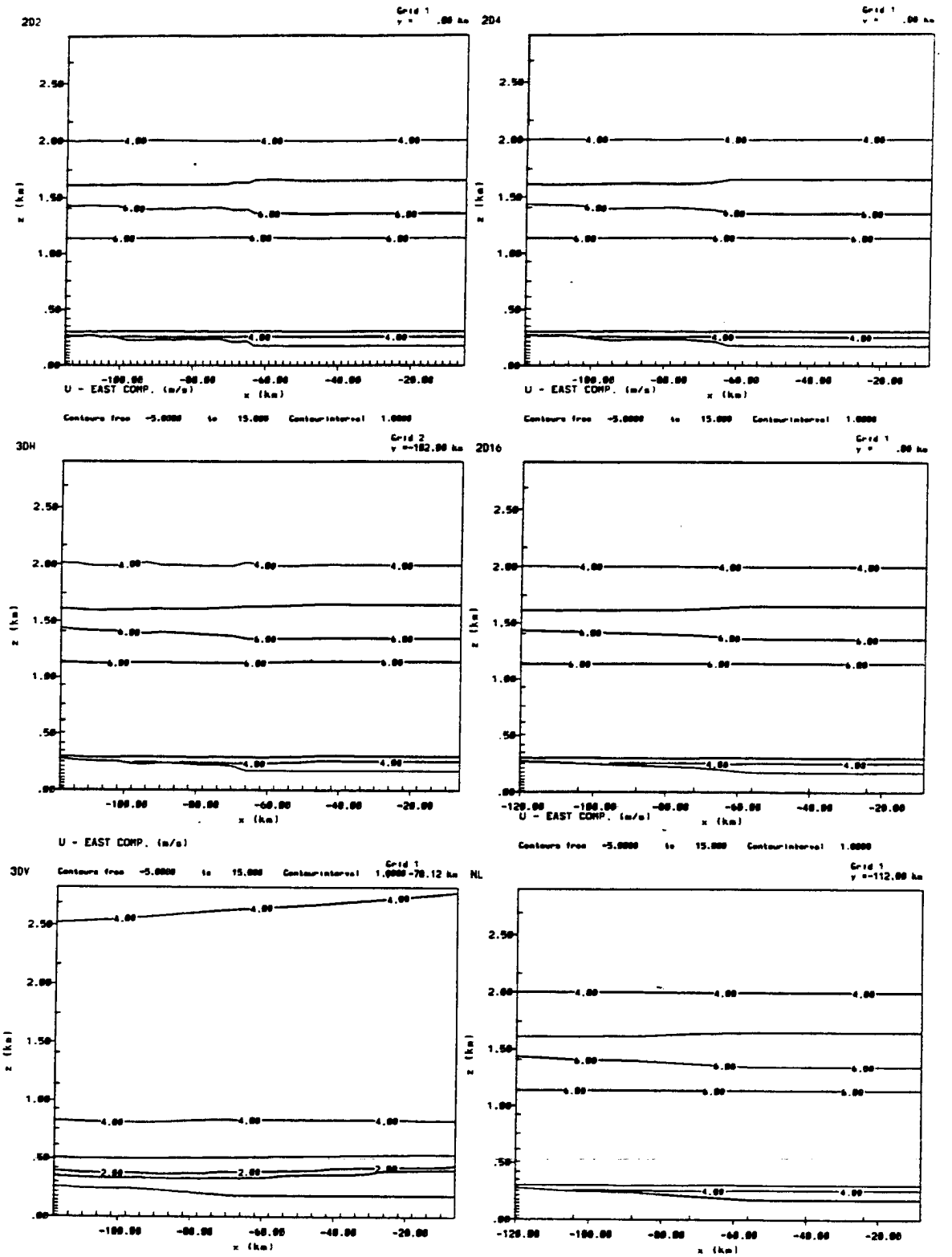

Figure 3.6: XZ plane of U component of velocity in m s^{-1} contoured from −5 to 15 in 1 m s^{-1} intervals at 6 LST.

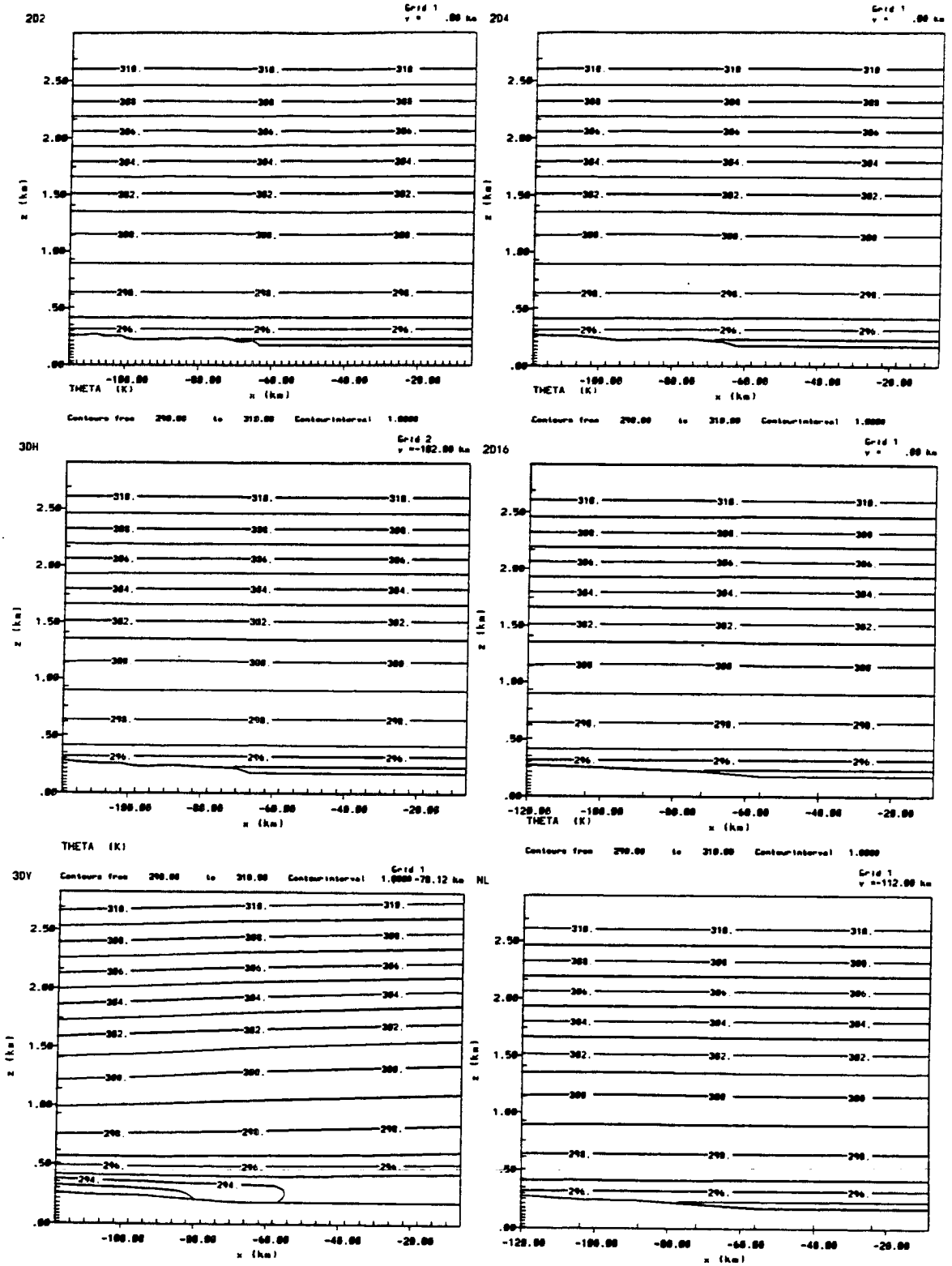

Figure 3.7: XZ plane of θ in K contoured from 297 to 314 by 1 K intervals at 6 LST.

the effects of the stronger heating on vertical motion. The homogeneous simulations show no vertical motion (at these contour intervals), while the 3DV run indicates the development of the up/downdraft couplet.

Figure 3.11 shows that by 11 LST 2D2, 2D4, 3DH, and 3DV all have developed a lake breeze circulation to varying degrees, while the other simulation with land water borders has not. This is expected because the 2D16 is not properly resolving the narrow lake breeze front. The results indicate a stronger convergence has developed in the 2D2 and 2D4 simulations than the 3DH run, bearing out the previous statement that 2D simulations tend to have stronger convergence. The structure of the inflow and return flow aloft are vastly different in the homogeneous and heterogeneous cases. Notice the confinement of these layers in the simulations. The homogeneous return flows are contained between a layer between 1 km and 1.5 km AGL, and are nearly parallel to the ground. The heterogeneous simulation has a broader vertical extent to the return flow aloft, and possesses a vertical tilt. It appears that the stronger heating, and resultant mixing have distributed the momentum more evenly across the boundary layer. The super adiabatic layer is readily apparent in Figure 3.12, for all simulations. It becomes clear that the surface layers and PBL have developed differently in the homogeneous simulations when compared to 3DV. Figure 3.13 shows the vertical motion at 11 LST. The updrafts are fairly weak at this time, since the lake breeze is at an early stage of growth and maximum surface temperatures will not be realized for nearly 3 hours. Notice the broad subsidence in 3DV. This seems to be the result of the large scale forcing in conjunction with the lake itself, and is partially responsible for the vertical tilt of the return flow aloft.

Figure 3.14, taken at 13 LST shows that all simulations with land water contrast have developed a lake breeze of varying degrees. The 2D2 and 2D4 runs show remarkable similarities. Both have an inflow depth of roughly 200 meters, and have penetrated inland about 4 km. In contrast the 3DH and 2D16 runs exhibit shallow inflows of about 125 meters. While 3DV has an inflow depth of around 200 m, it still possesses a unique structure to the solenoid. The vertical motion displayed in Figure 3.15 increase as Δx decreases, which is expected. Of course the increase has bounds, as several 500 m simulations showed the lake breeze updraft magnitude was nearly equivalent to that obtained

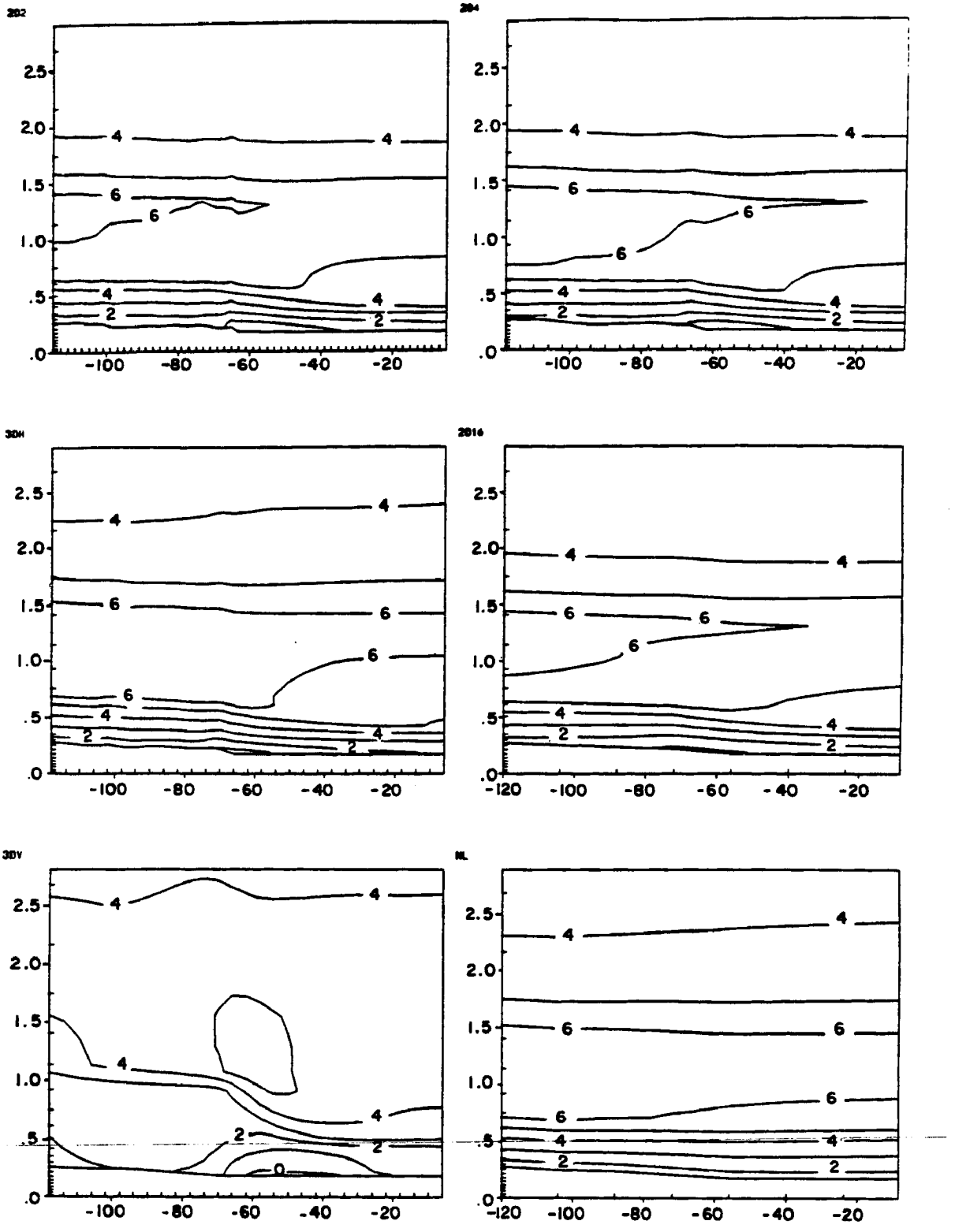

Figure 3.8: XZ plane of U component of velocity in m s^{-1} contoured from −5 to 15 in 1 m s^{-1} intervals at 10 LST.

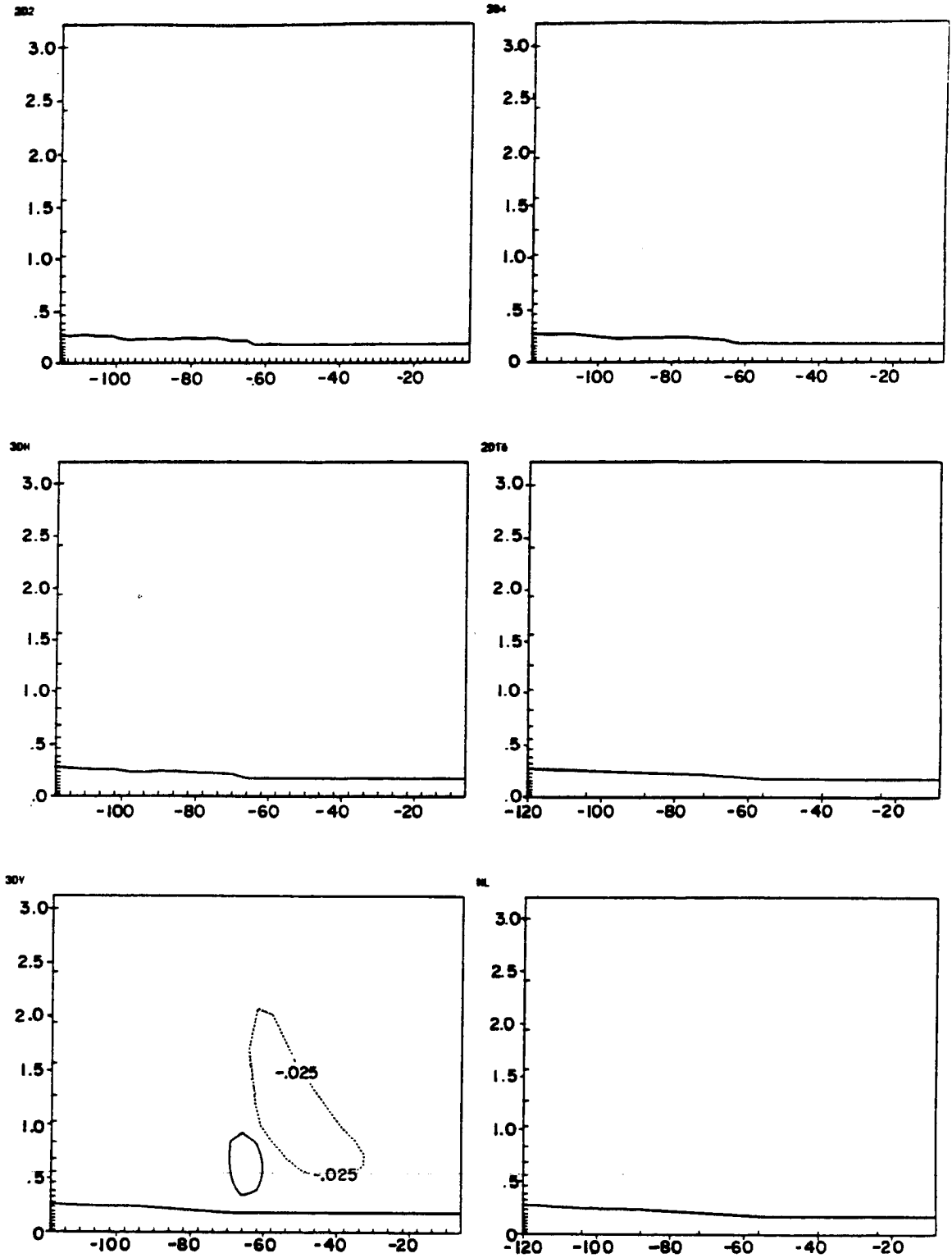

Figure 3.9: XZ plane of W component of velocity in m s^{-1} contoured from −.525 to .975 in .05 m s^{-1} intervals at 10 LST.

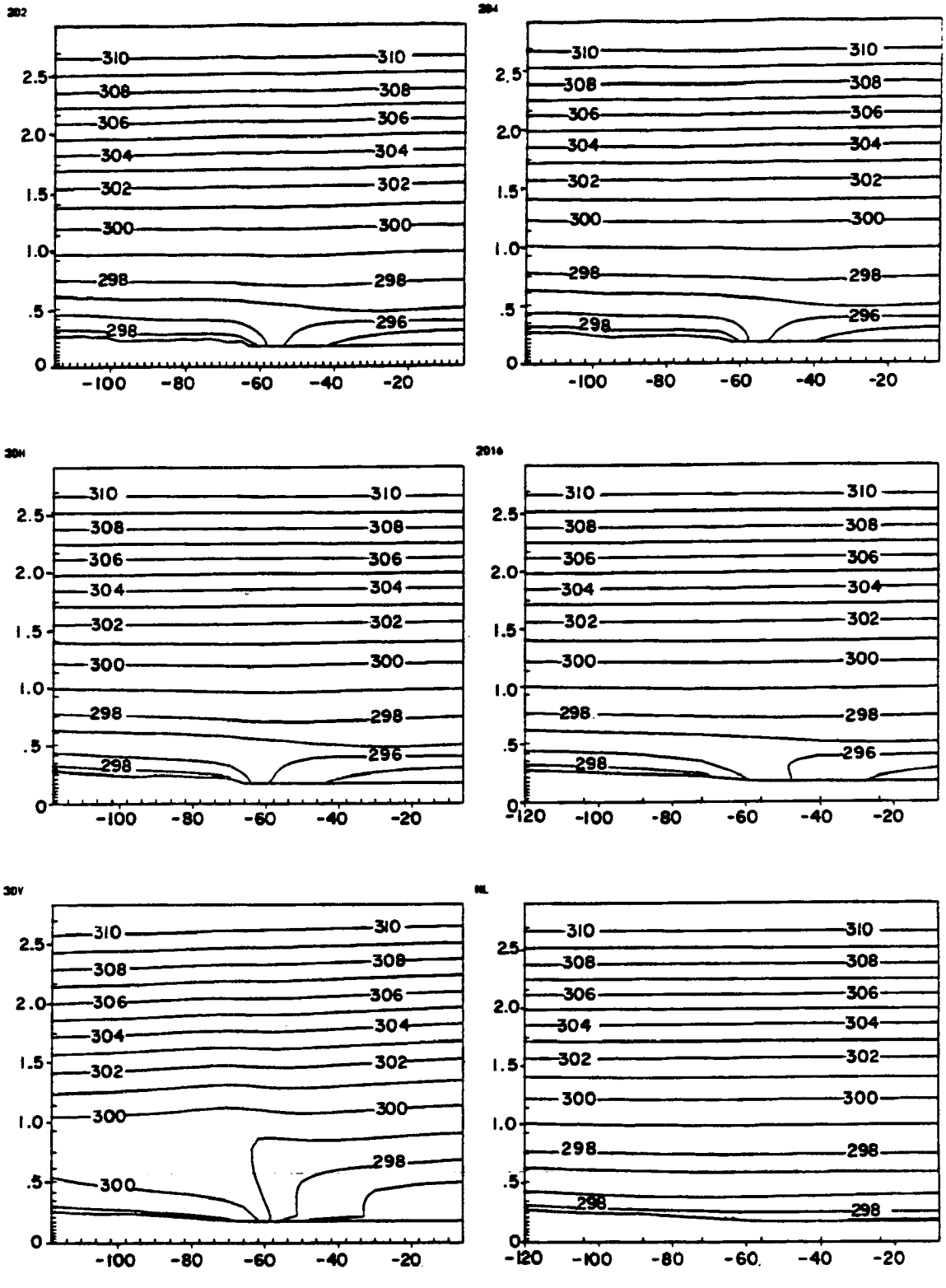

Figure 3.10: XZ plane of θ in K contoured from 297 to 314 by 1 K intervals at 10 LST.

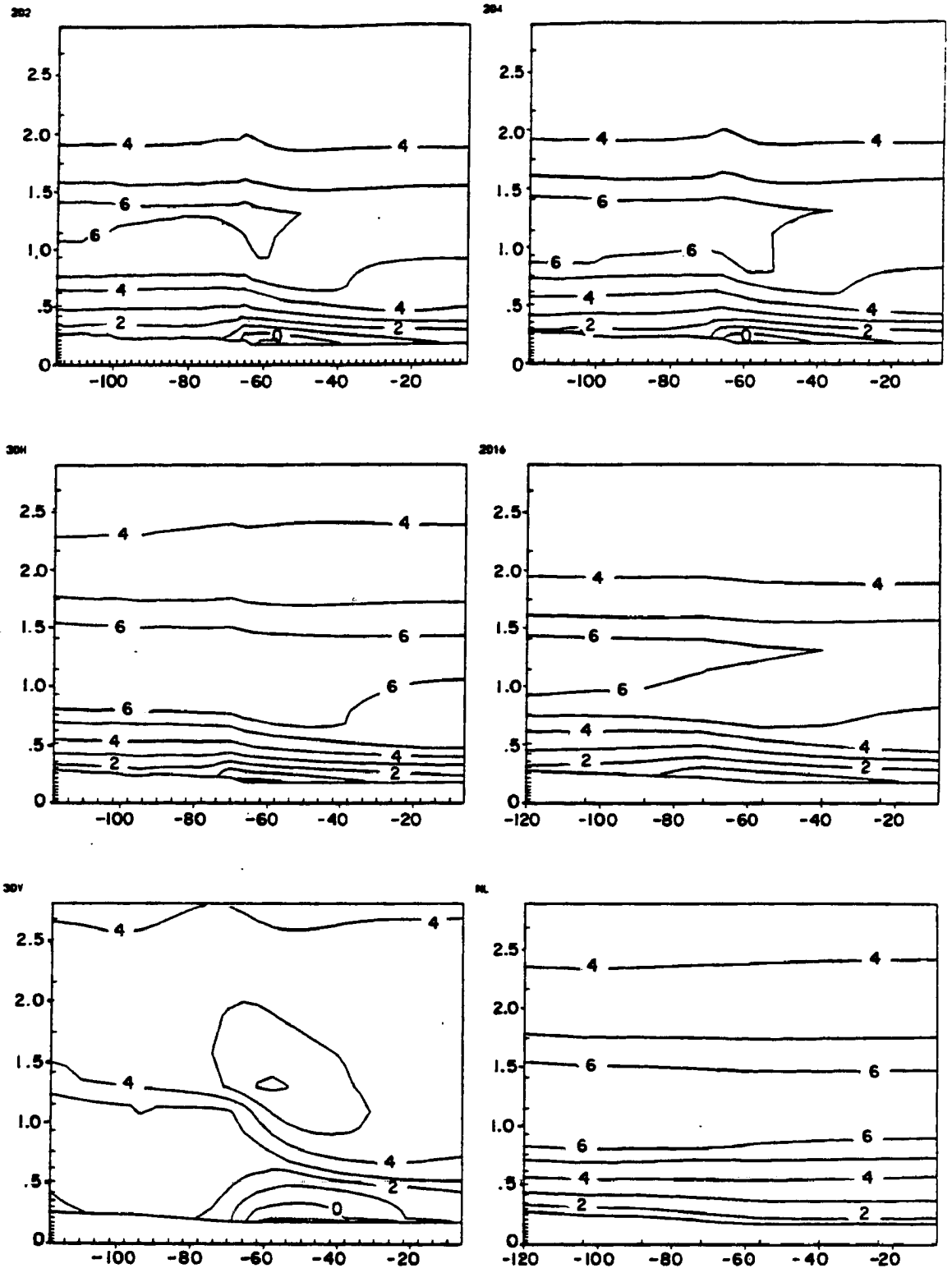

Figure 3.11: XZ plane of U component of velocity in m s^{-1} contoured from -5 to 14 in 1 m s^{-1} intervals at 11 LST.

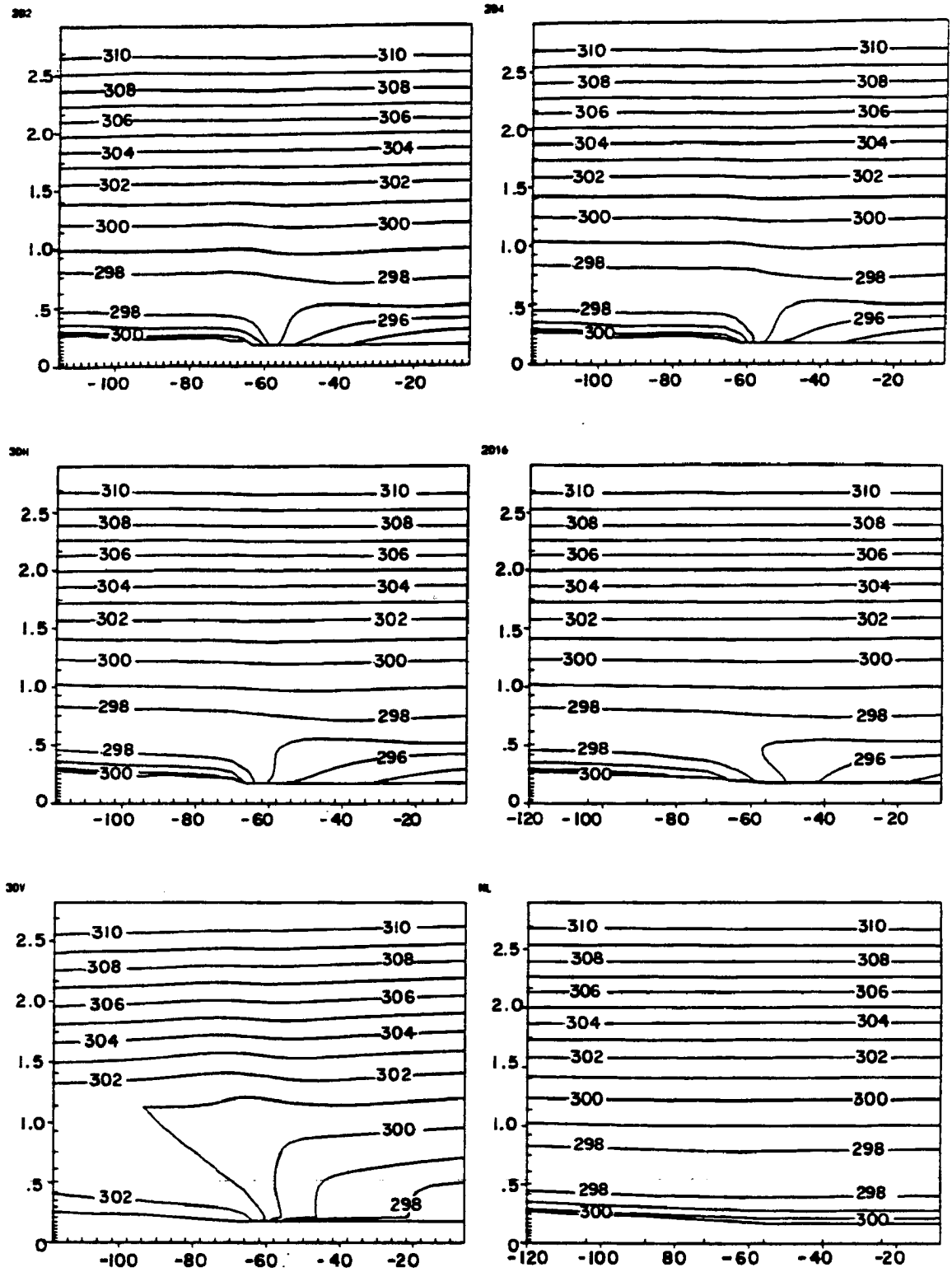

Figure 3.12: XZ plane of θ in K contoured from 297 to 314 by 1 K intervals at 11 LST.

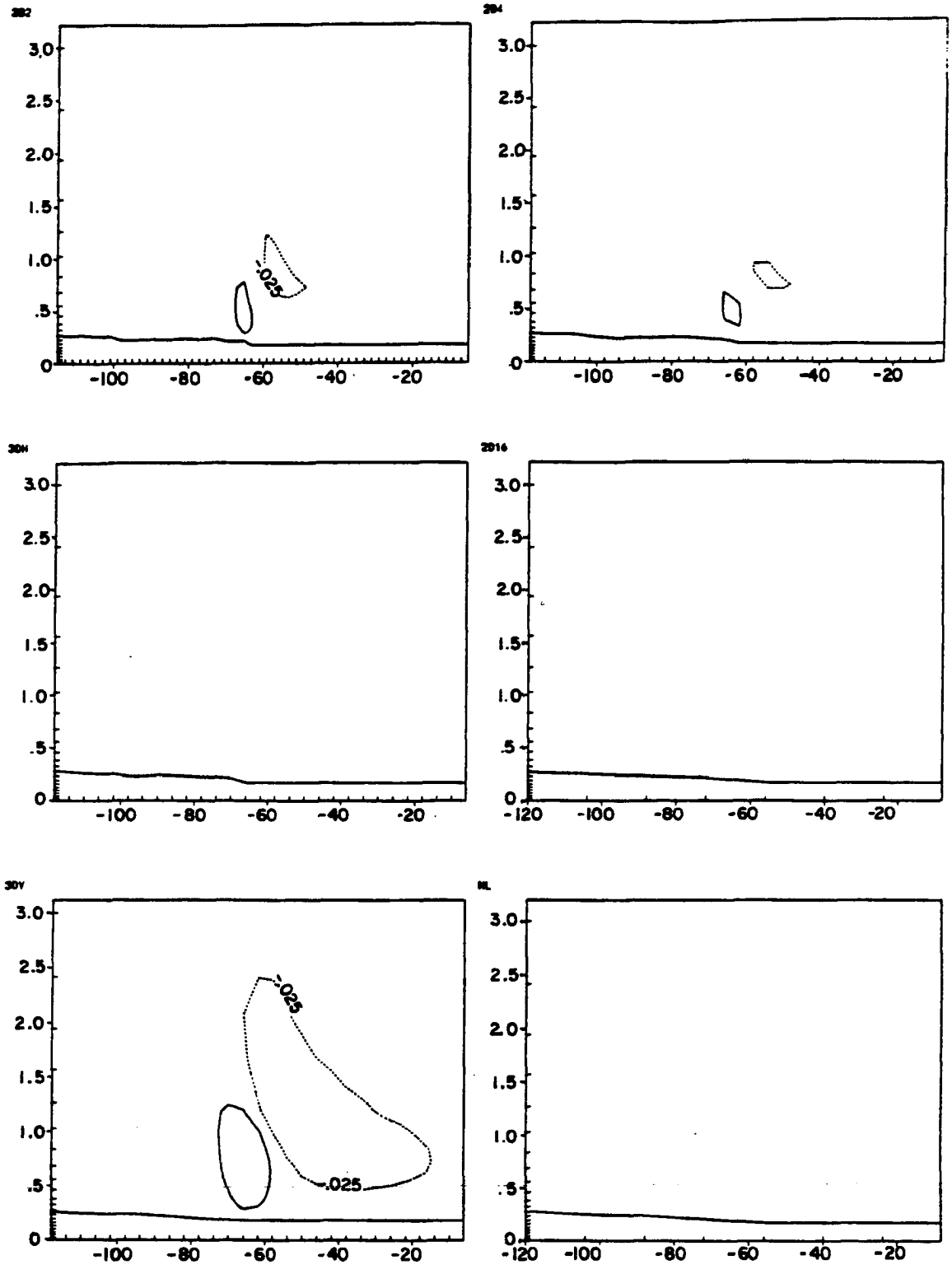

Figure 3.13: XZ plane of W component of velocity in m s^{-1} contoured from −.525 to .975 in .05 m s^{-1} intervals at 11 LST.

in the 2D2 simulation. 2D16 still does not register vertical motion of a magnitude greater than $\pm$ 2.5 cm s^{-1}, and will not until 14 LST.

By 16 LST the lake breeze circulations are near, or have peaked in the intensity of upward vertical motion. In the 3D simulations peak updrafts were not in excess of 15 cm s^{-1}, while 2D2 had peak updrafts of 35 cm s^{-1}. The 2D4 simulation had nearly the same updraft velocity as the 2D2 simulation (nearly 30 cm s^{-1}), indicating that the lake breeze is resolve properly with a 4 km mesh size in the x direction. This is an important result, since the 3D finest mesh sizes also used a 4 km Δx. This is important in terms of computational time, since the computational time roughly increases inversely proportional to the mesh size.

The final set of XZ figures show the lake breeze in a varying state of decay. Shown in Figure 3.16 is the U velocity component at 18 LST. The 3D simulations show that the lake breeze has nearly collapsed, while the 2D runs exhibit a slight weakening from the previous hours plots. This is clearly related to the extra degree of freedom inherent in the 3D simulations. The weakening lake breeze clearly shows up in the reduced potential temperature gradient plotted in Figure 3.17. The 2D simulations still display a TIBL, while in the 3D simulations the TIBL has collapsed. The vertical motions shown in Figure 3.18 are still greater than 10 cm s^{-1} in the 2D2 and 2D4 simulations, while in the other runs is less than 3 cm s^{-1}. Notice the enhanced subsidence over the lake has also decreased in the 3DV simulation, with the residual representing the synoptic and lake induced downward motion.

3.2.3 3D Comparisons of XY Sections

All XY plots in this section will be in the same format. The top 2 plots will be from NL, the middle 2 plots from 3DH, and the bottom 2 plots are from 3DV. Variables plotted, contour intervals, and limits are listed in the captions below the figures.

Figure 3.19 shows initial fields of U and temperature, in the left and right columns, respectively. The U field clearly details the previously mentioned initialization aspects. The 3DV simulation has nearly a zero field for U, while the other runs show values of U between 3 and 4 m s^{-1}. The temperature fields has no detail for 3DH and NL, which is

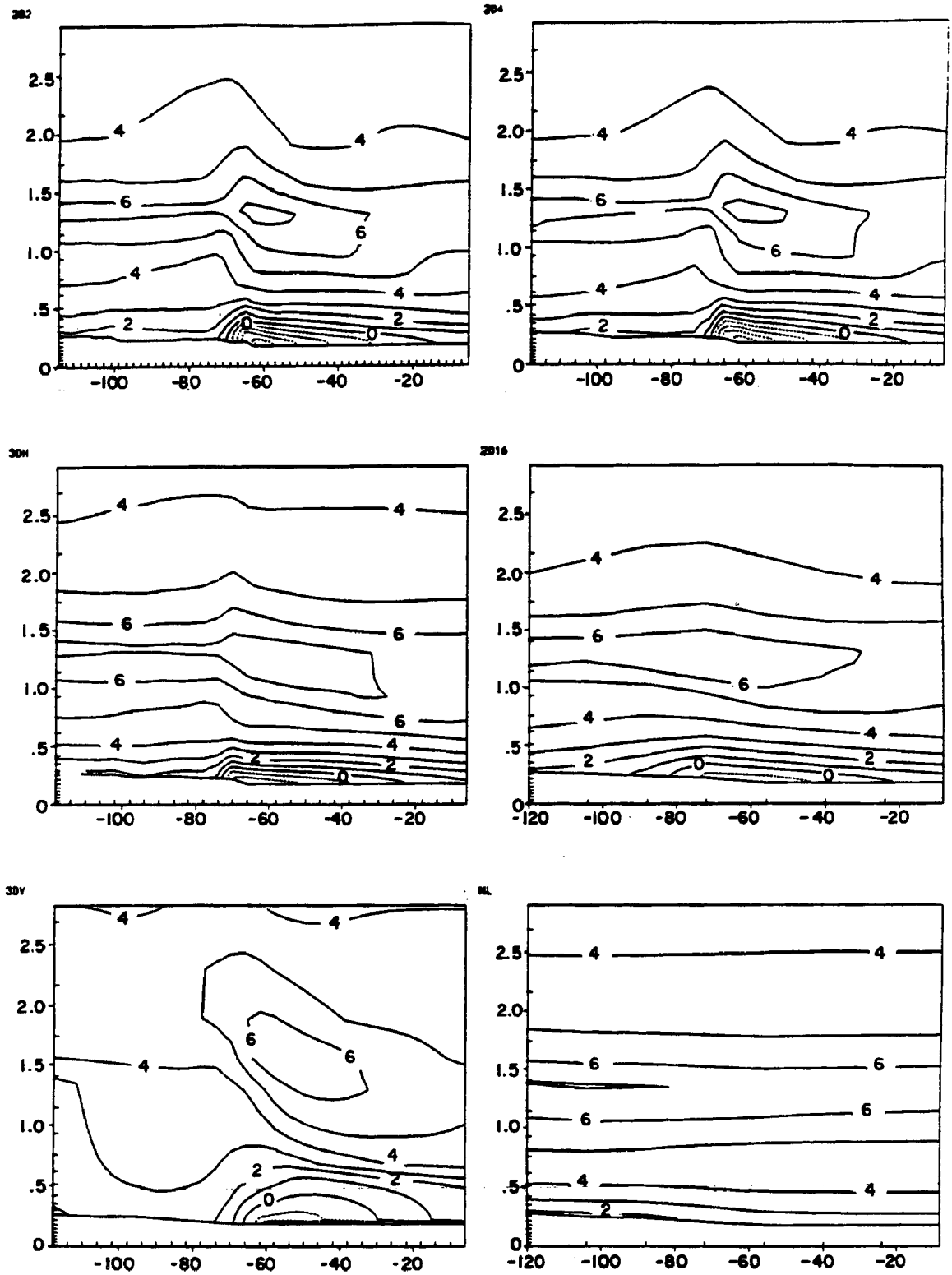

Figure 3.14: XZ plane of U component of velocity in m s^{-1} contoured from −5 to 15 in 1 m s^{-1} intervals at 13 LST.

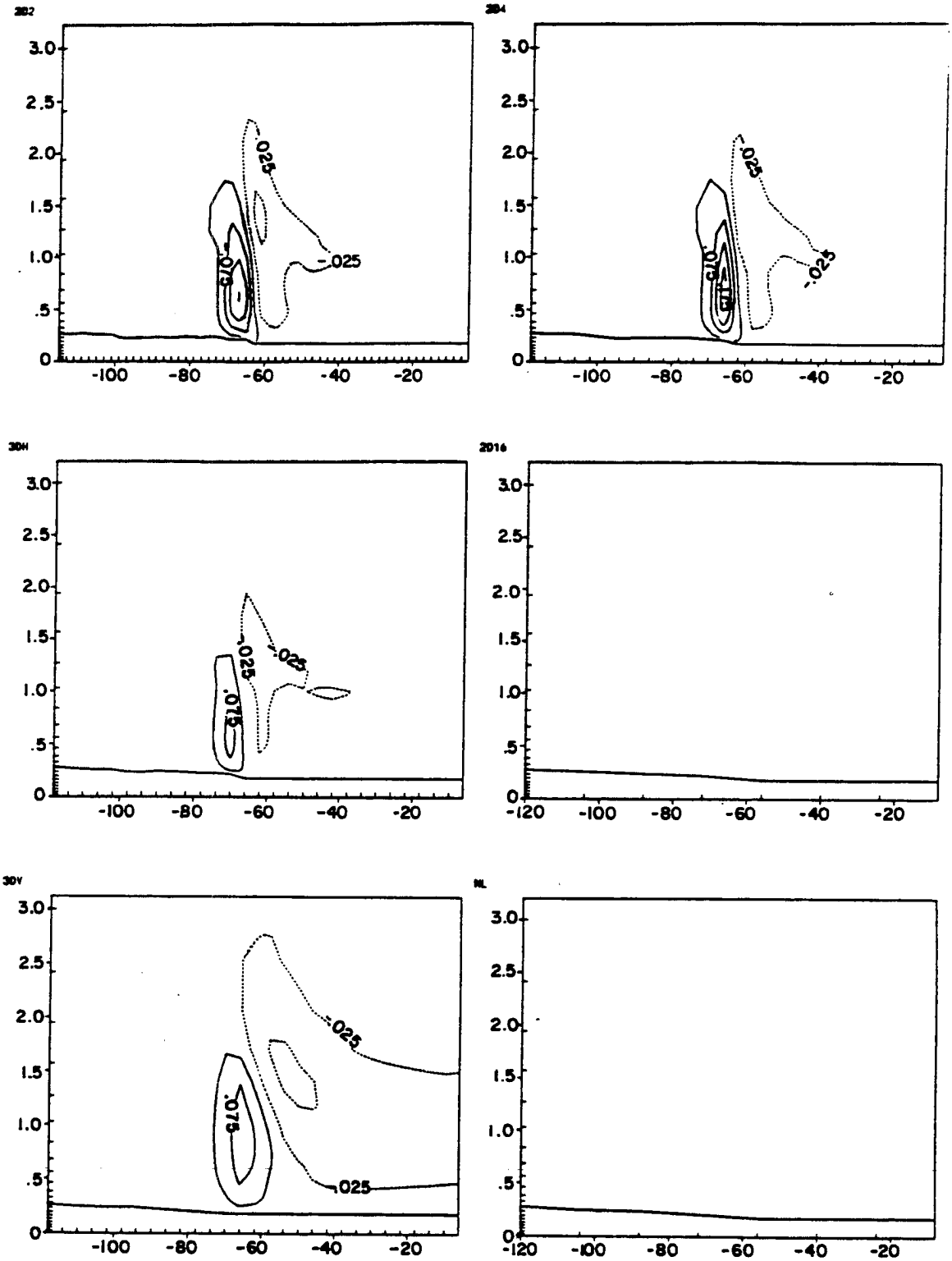

Figure 3.15: XZ plane of W component of velocity in m s^{-1} contoured from −.525 to .975 in .05 m s^{-1} intervals at 13 LST.

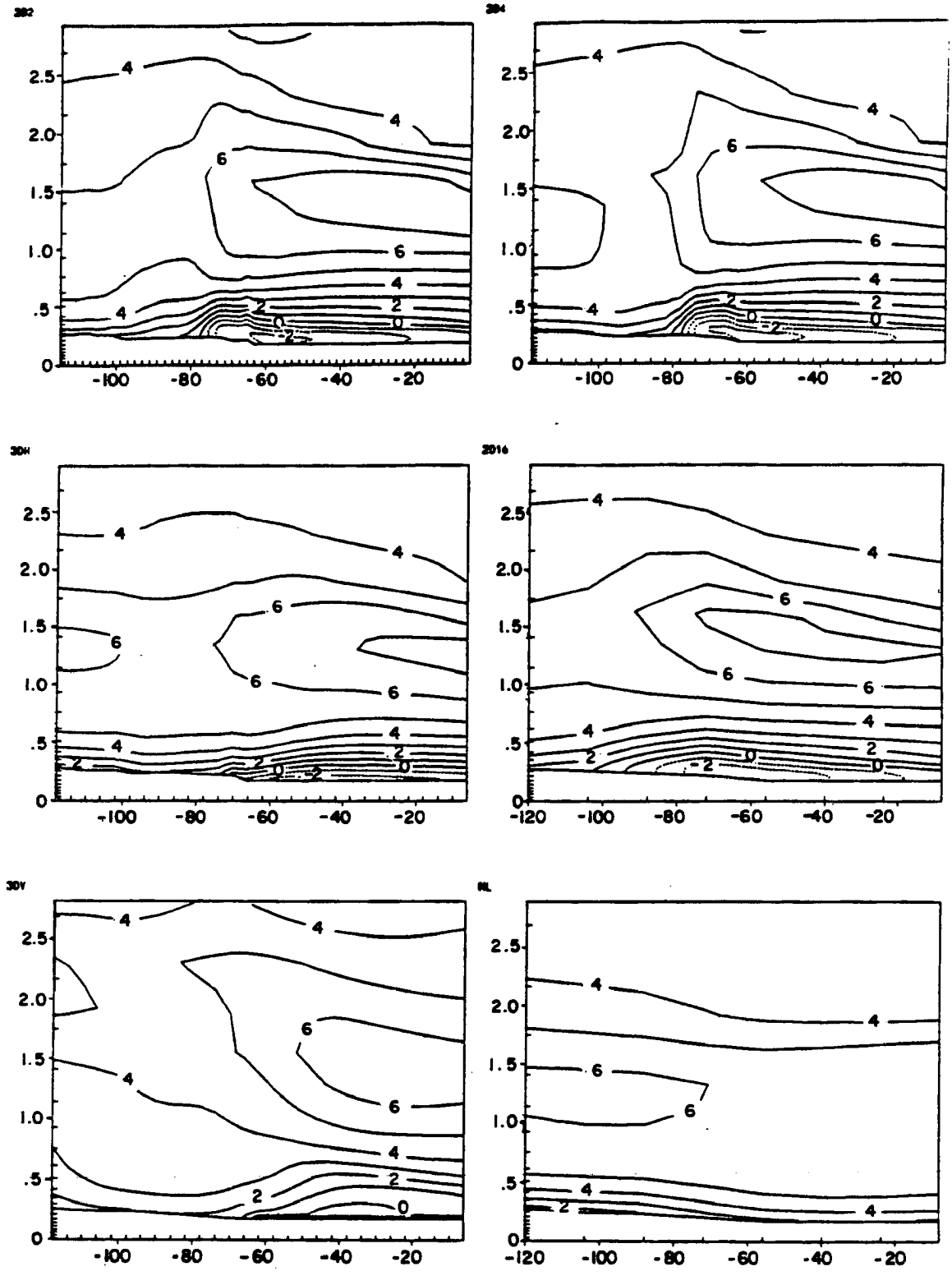

Figure 3.16: XZ plane of U component of velocity in m s^{-1} contoured from −5 to 15 in 1 m s^{-1} intervals at 18 LST.

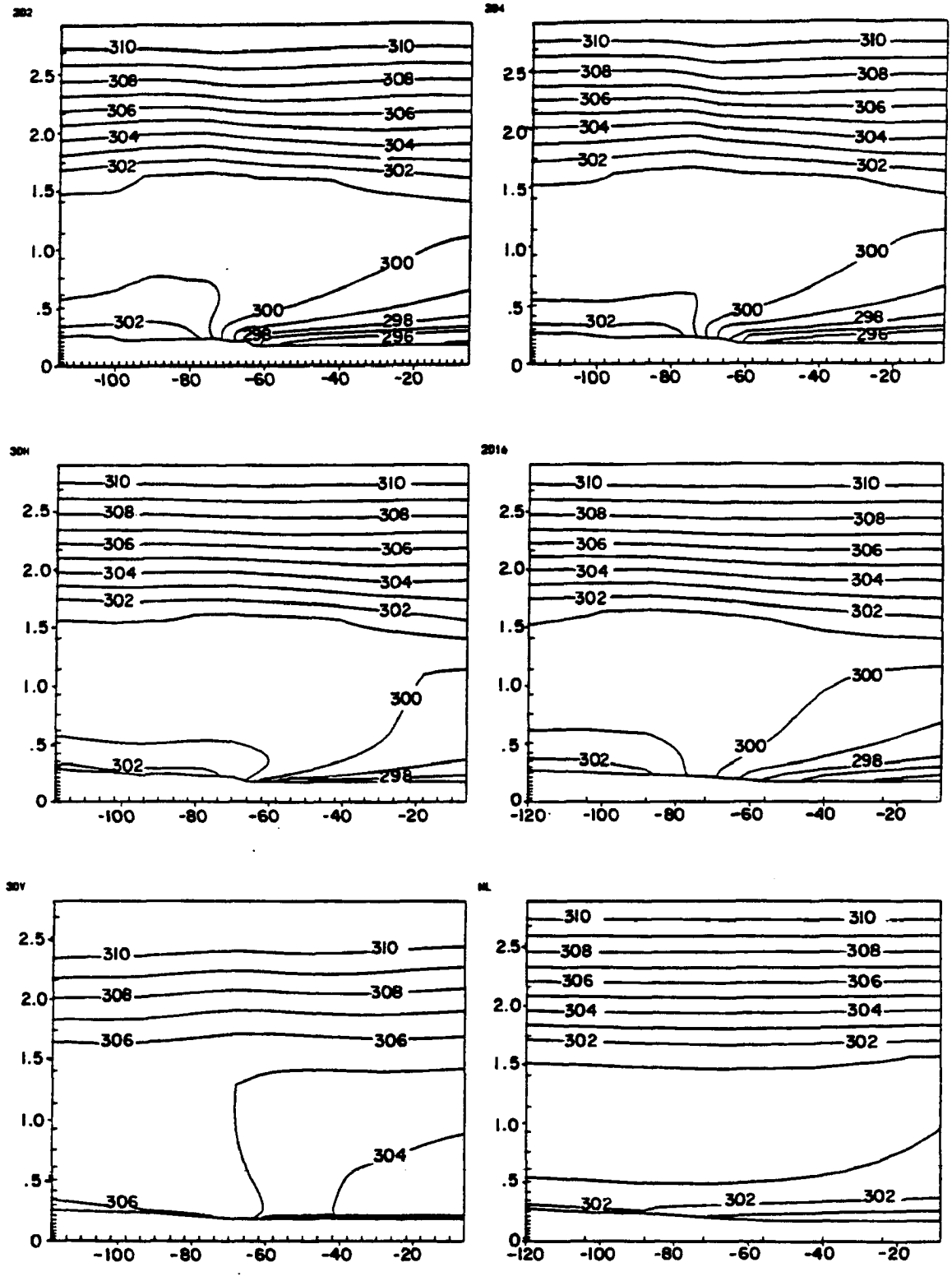

Figure 3.17: XZ plane of θ in K contoured from 297 to 314 by 1 K intervals at 18 LST.

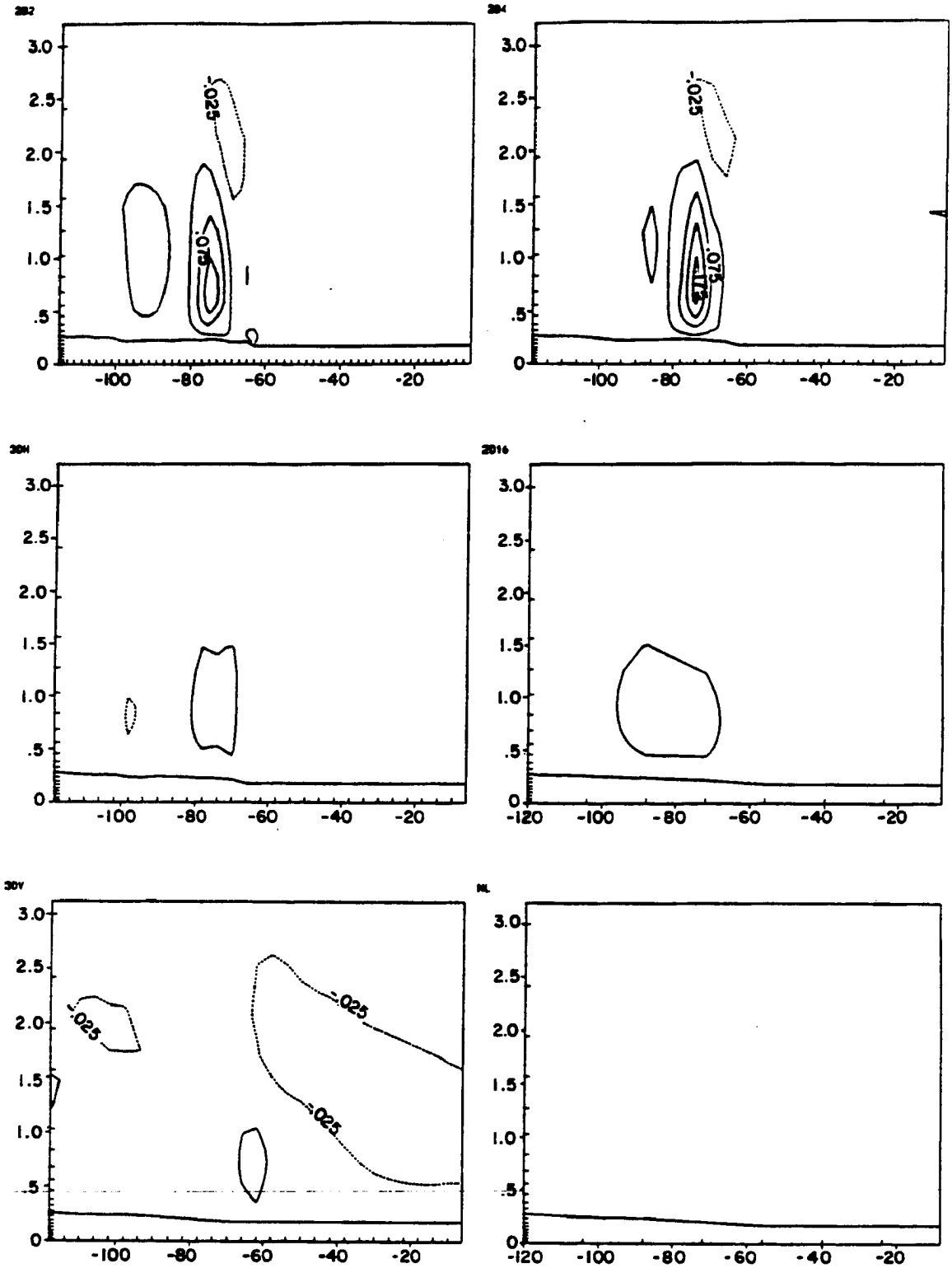

Figure 3.18: XZ plane of W component of velocity in m s^{-1} contoured from −.525 to .975 in .05 m s^{-1} intervals at 18 LST.

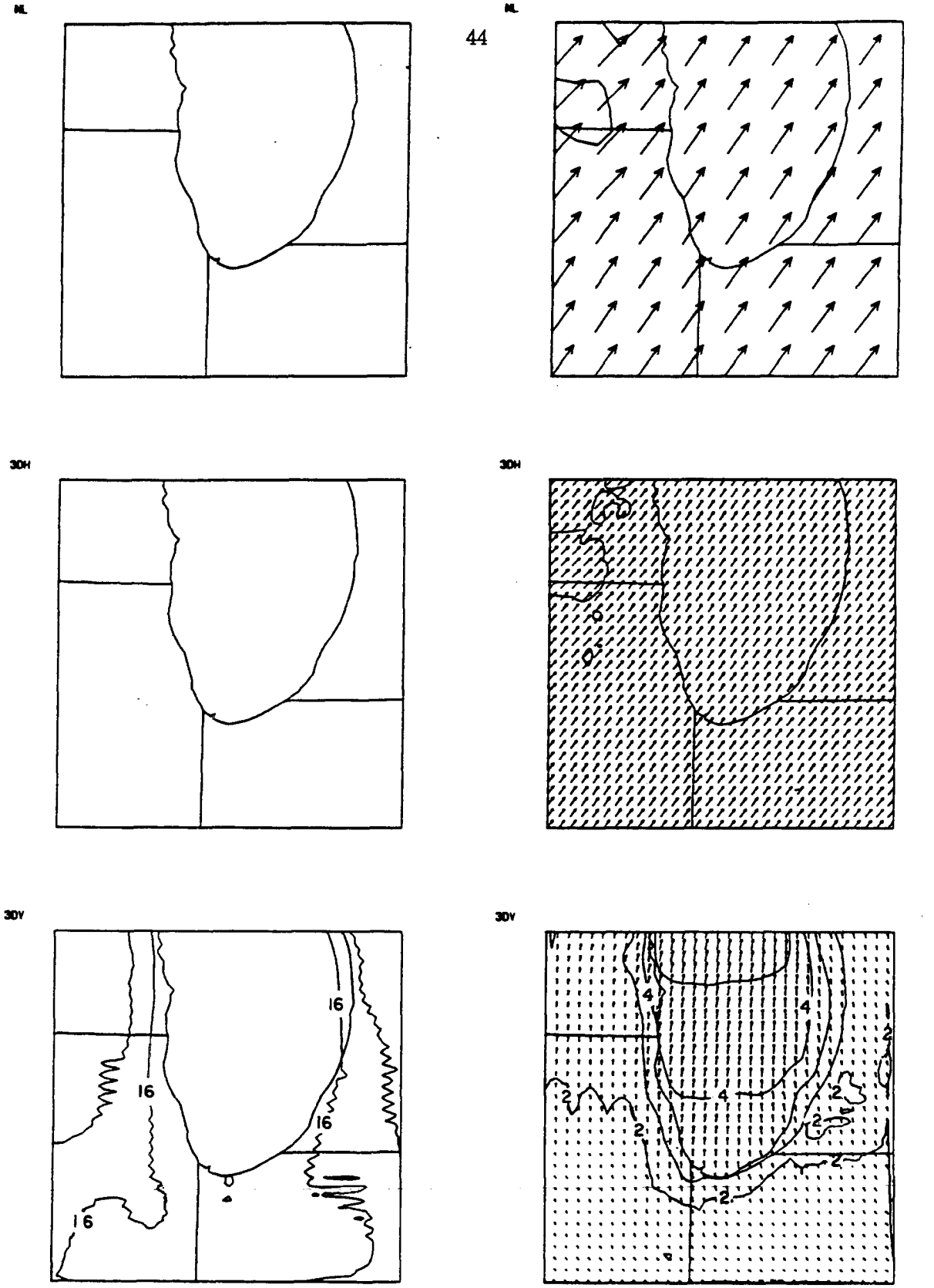

Figure 3.19: Left-hand column: XY dewpoint temperature from 15° to 30° in 1° intervals. Right-hand column: XY of component of velocity in m s^{-1} contoured from −5 to 15 in 1 m s^{-1} intervals at 6 LST.

expected for homogeneous initialization of the temperature fields. The 3DV simulation is actually 36 hours into integration, and shows some detail with a warm pool located over the south central portion of the lake, where the water temperature is warmest. The apparent noise present in the temperature field and U, is an attempt by RAMS to simulate buoyancy oscillations in the stable nocturnal atmosphere. At 10 LST inhomogeneities have developed to varying degrees in all 3D simulations as illustrated in Figure 3.20. The U field for 3DV has reversed in the vicinity of Zion, Illinois, and has slowed down considerably in 3DH. NL still shows no perturbations in U while some have developed in the temperature field. This is due to topographical and vegetative forcing. Notice that in the simulation with a lake, the isotherms are oriented in an east-west direction across the lake for 3DV, roughly following the temperature gradient of the sea surface temperature. The differences in heating rates between the homogeneous and heterogeneous simulations are discernible in the temperature plots. The homogeneous runs are about 2.5°C cooler than 3DV.

The lake breeze is fairly well developed by 13 LST. Figure 3.21 shows that the 3DH lake breeze has penetrated further inland than the 3DV counterpart, as indicated by the dashed line on the U plot. An interesting feature unique to the 3D lake simulations is observable near Milwaukee, where the land water boundary forms a peninsula. There is an obvious splitting of the magnitude of the lake breeze at this point, where it is weakened by the lake breezes north and south of the convergence, as well as the orientation of the direction of the prevailing wind to the shore.

Figure 3.22 shows features that are also observable in the 3D lake breeze simulations. The right hand column has wind speed vectors plotted over contours of wind speed and the plot is taken at 14 LST. Over the southeastern portion of the lake a mesohigh has developed to varying strengths in 3DH and 3DV. It is clear that air advecting from the Chicago metro area could take a multitude of paths in virtually any direction. Some could go up the Illinois-Wisconsin coastline, or end up in Indian or Michigan. The mesohigh predicted by RAMS also leads to a convergence line oriented emanating from the southern portion of the lake and extending in a northeasterly direction.

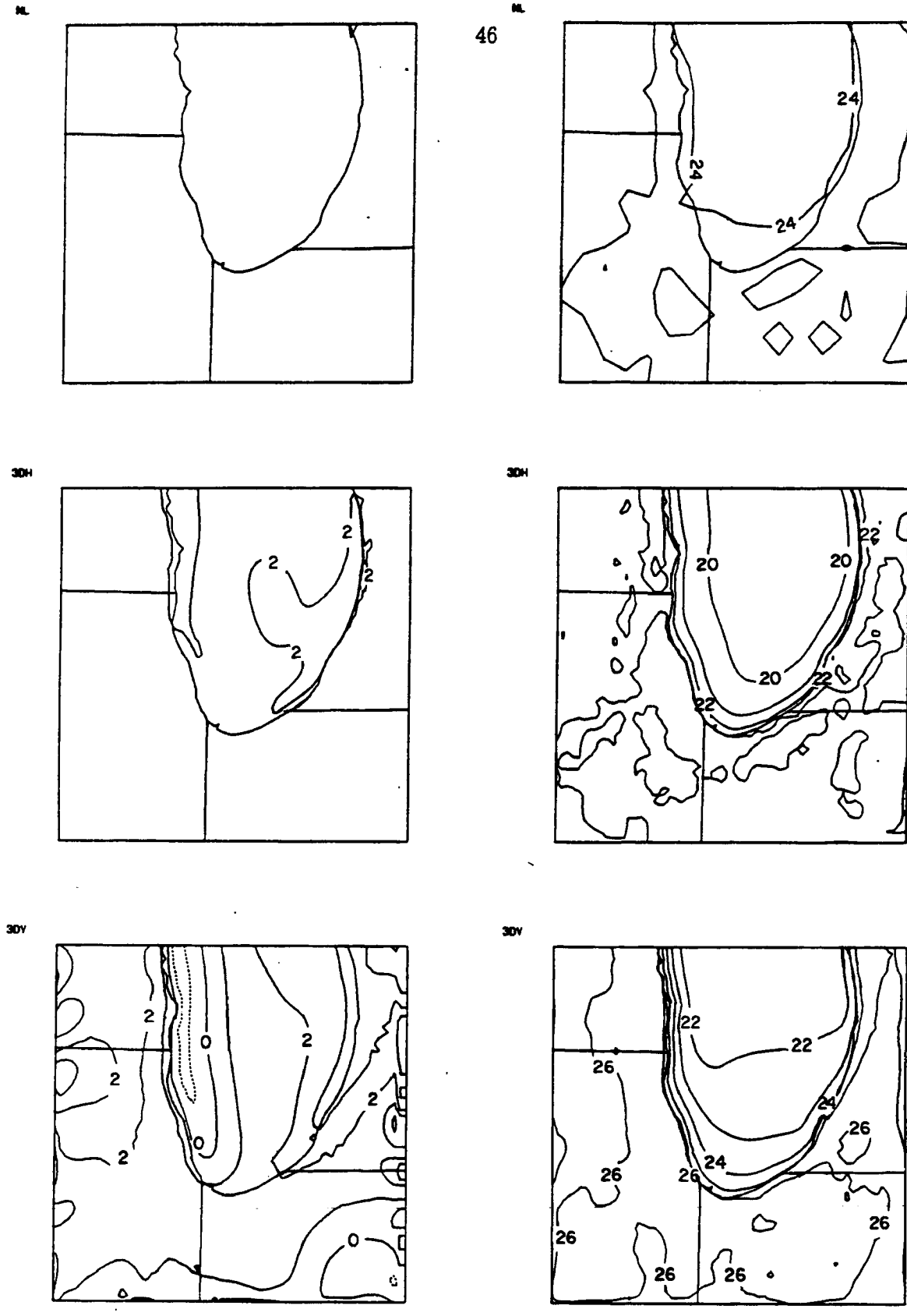

Figure 3.20: Left-hand column: XY of U component of velocity in m s^{-1} contoured from −5 to 15 in 1 m s^{-1} intervals. Right-hand column: XY temperature from 15° to 30° in 1° intervals at 10 LST.

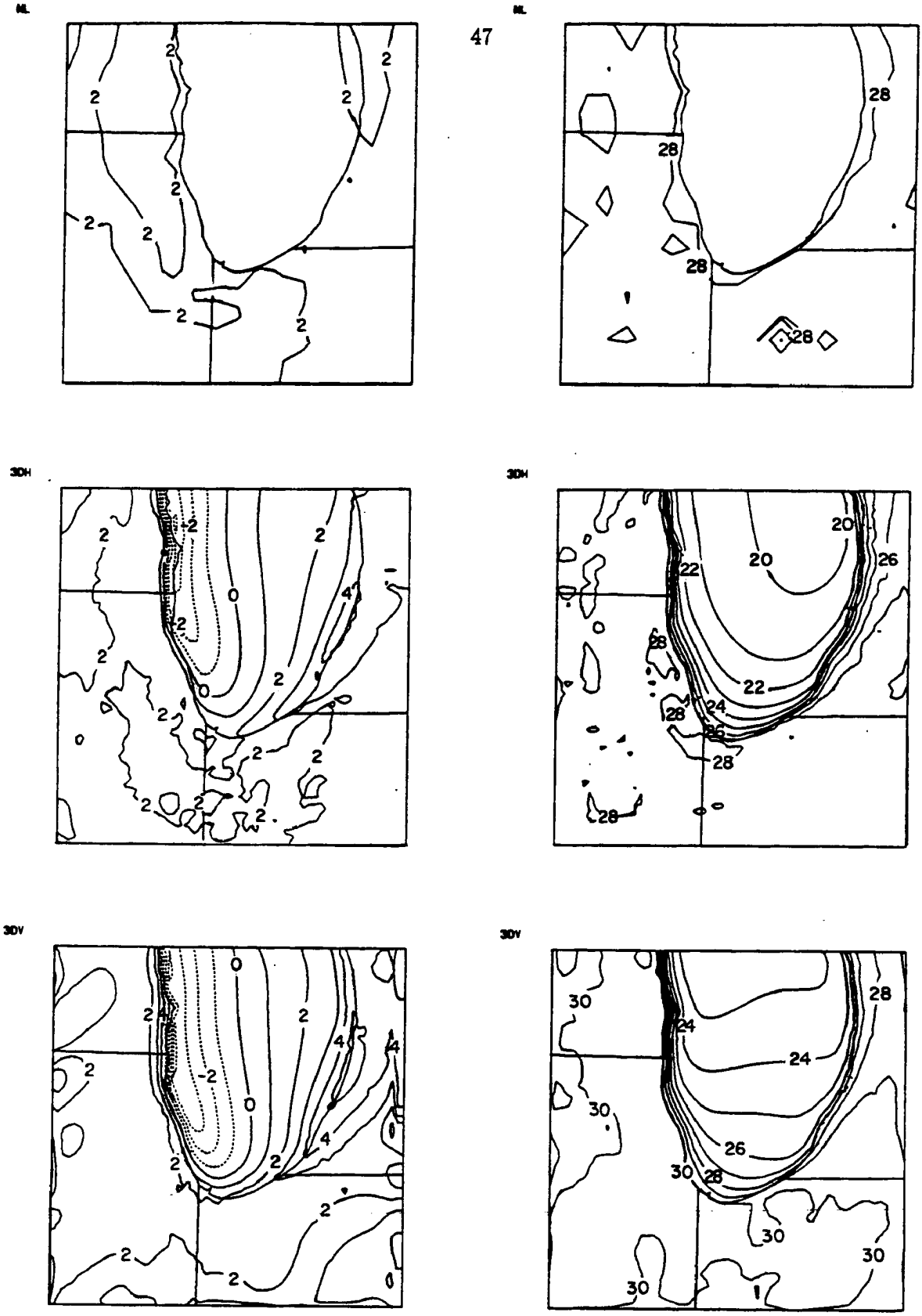

Figure 3.21: Left-hand column: XY of U component of velocity in m s^{-1} contoured from −5 to 15 in 1 m s^{-1} intervals. Right-hand column: XY temperature from 15° to 30° in 1° intervals at 13 LST.

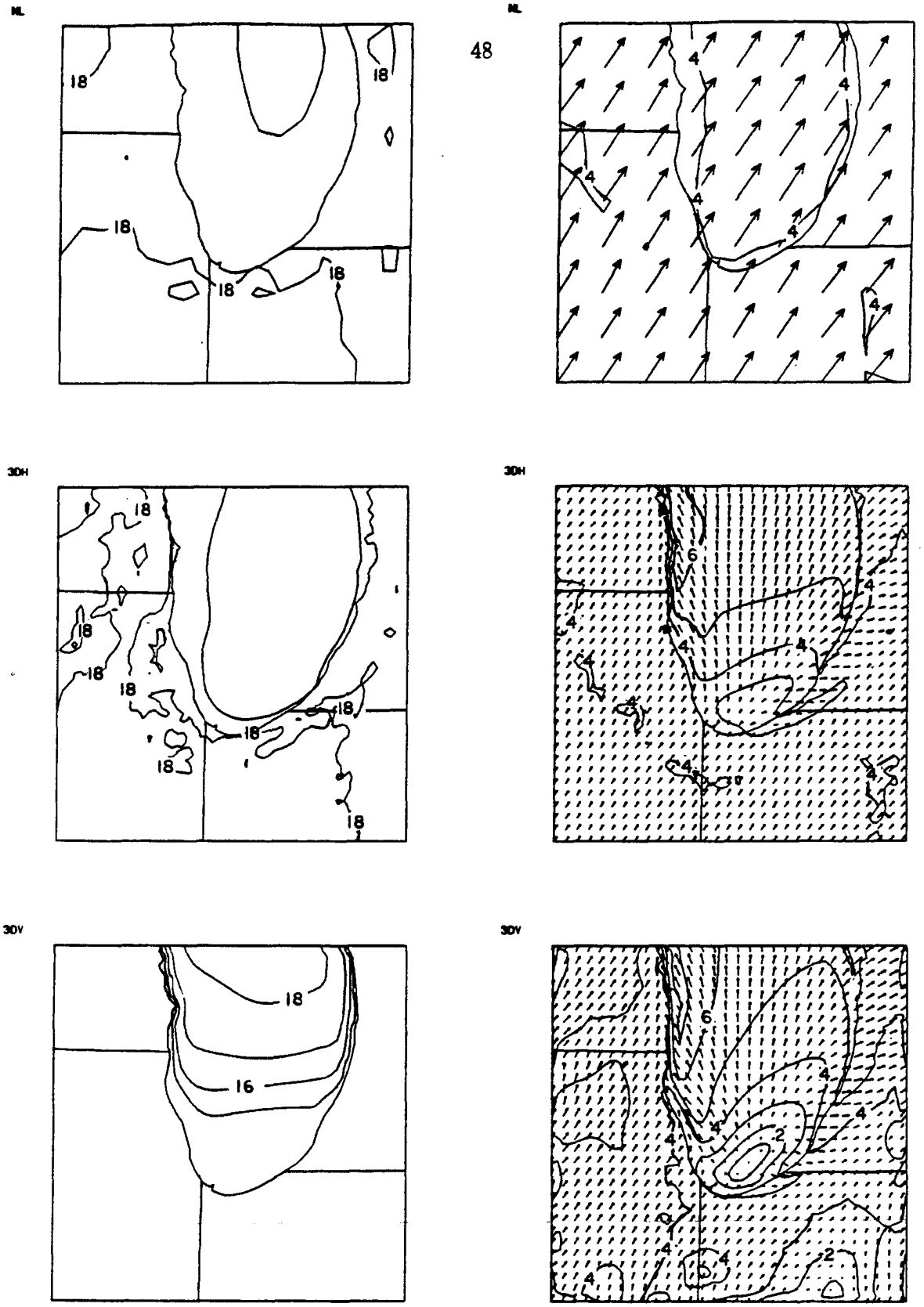

Figure 3.22: Left-hand column: XY dewpoint temperature from 15° to 30° in 1° intervals. Right-hand column: XY of component of velocity in m s^{-1} contoured from –5 to 15 in 1 m s^{-1} intervals at 14 LST.

Figure 3.23 shows the decaying stages of the lake breeze at 18 LST. The plots of U shows that the negative component is nearly offshore in the Zion area for the 3DV simulation, while the 3DH run indicates the flow is still onshore in the area. The temperature fields are still cooler than those in the 3DV simulation by nearly $3°C$.

3.2.4 Observations and Model Comparison

The Zion tower data was used to compare the output from the RAMS model. A synthetic tower was created from the RAMS data by linearly interpolating between grid points to the corresponding location of the towers near Zion. This was done in both the horizontal and vertical directions. This comparison provides information about model performance and bias by performing correlations at each of the 4 meteorological towers located onshore, 3 km inland, 8 km inland, and 24 km inland from Zion.

Figure 3.24 shows plots of time series for wind direction. The 180° line has been darkened to indicate lake breeze onset. The upper left panel is the time series at the Zion shoreline site. The diagram shows that the observed wind begins to turn around slightly after 11 LST. The 2D2 runs is the only simulation that predicts the turn around within a few minutes of its occurrence. The other simulations have the lake breeze coming ashore between 10 and 11 LST. These results are all acceptable, since the temporal resolution of the observations is only 1 hour. Referring back to Figure 3.2 shows that 2D2, 2D4, 3DH, and 3DV also made accurate predictions of the depth of the inflow layer, which was about 210 to 240 meters.

The other sites are valuable for comparing the total inland penetration of the lake breeze. The upper right panel shows that all simulations predict that the front reached the 3 km site, which agrees with the observations. Notice that the 3DV simulation barely reaches the 3 km site. Further inland, at the 8 km location, the data implies that the 2D2, 2D4, and 2D16 simulations all have reached the tower. This is in disagreement with the observations, which show wind directions from 200° to 240°. None of the 3D simulations (of course, the NL run would not, because it never produces a lake breeze) reach the 8 km tower. Again this is related to stronger convergence generally predicted in the 2D simulations. This does have an impact on the dispersion results, as will be explained in

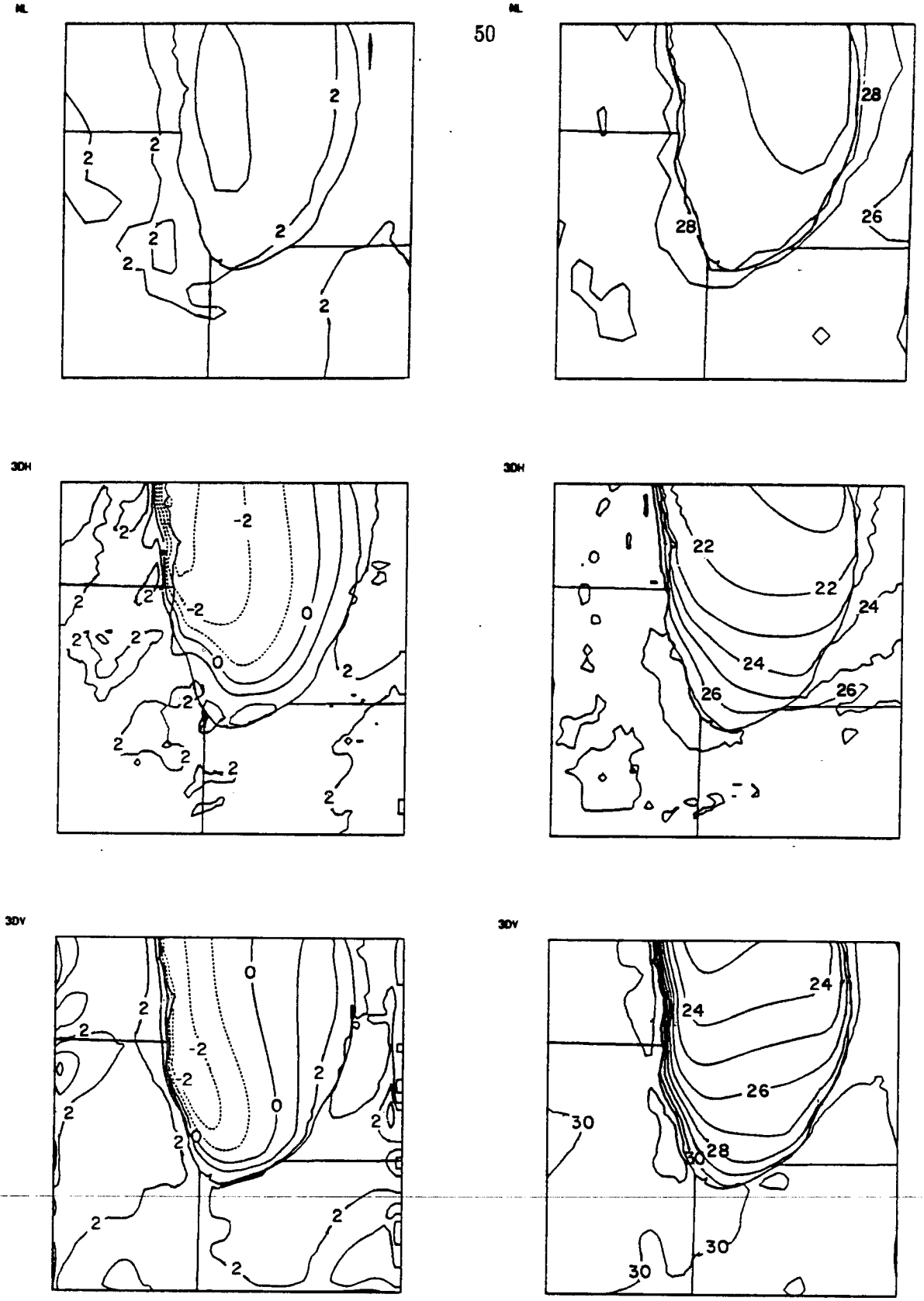

Figure 3.23: Left-hand column: XY of U component of velocity in m s^{-1} contoured from −5 to 15 in 1 m s^{-1} intervals. Right-hand column: XY temperature from 15° to 30° in 1° intervals at 18 LST.

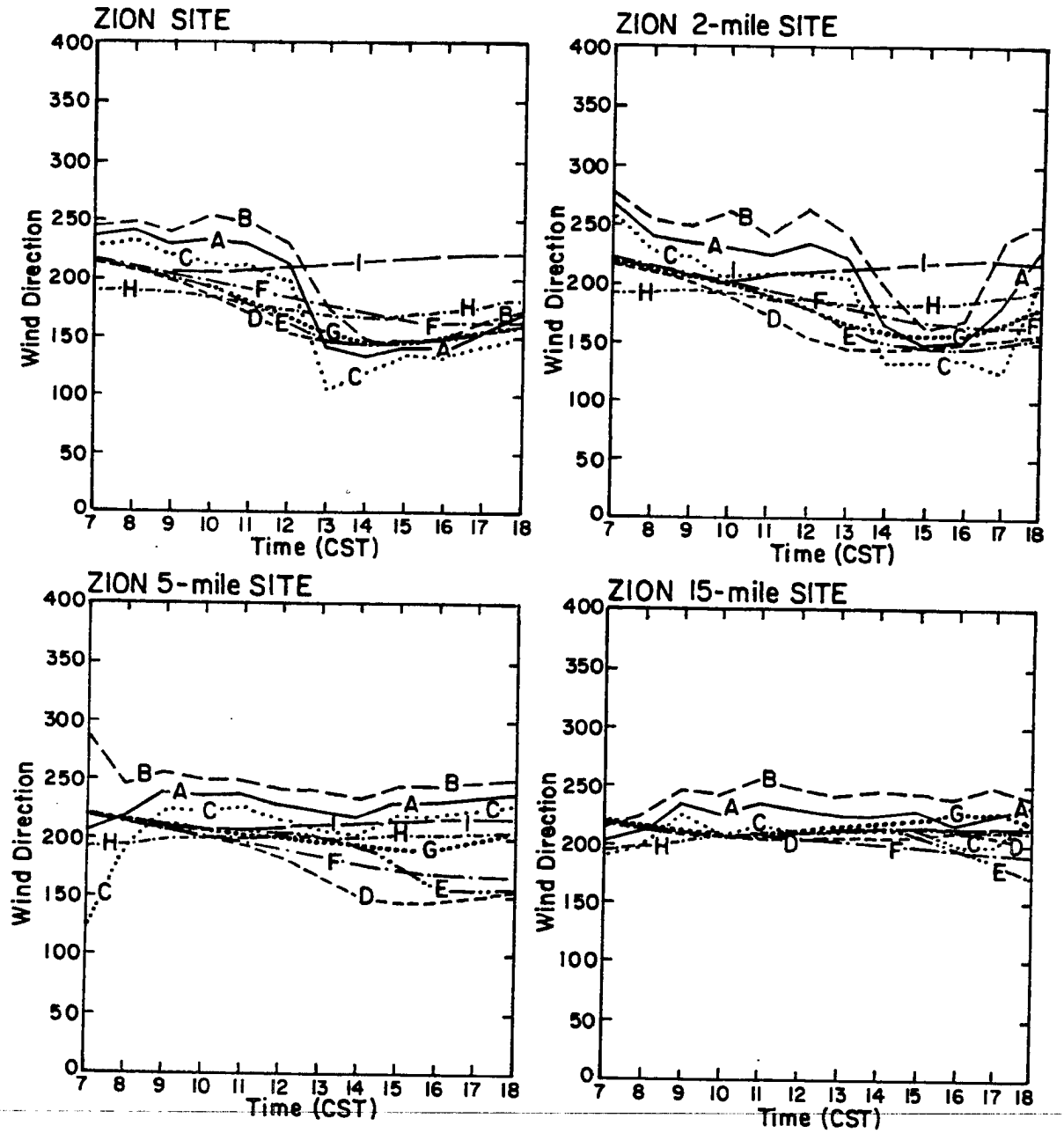

Figure 3.24: Time series of wind direction for: A – specified site; B – Site $+\sigma_\theta$, C – site $-\sigma_\theta$; D – 2D2; E – 2D4; F – 2D16; G – 3DH; H – 3DV; and I – NL.

the next section. The upper left panel of Figure 3.25 is a plot of wind directional bias by site number. Site 1 corresponds to the shoreline, site 2 is the 2 km location, site 3 the 8 km location, and site 4 is the 24 km location. As expected, NL has a bias of $-23°$ at site 1, simply because it does not predict a sea breeze. The other simulations tend to overpredict the turnaround, although this comparison does not take into account σ_θ. The 2D nature of 2D2, and 2D4, is evident as the curves show they overpredict the extent of turn-around the most. The other panels will be explained shortly.

The other quantitative measure of the wind compared was the total wind speed. Figure 3.26 shows the total wind speed at the different tower locales. Again, the 2D2 and 2D4 simulations overpredict near the convergence zone. Moving inland, the curves begin to approach the observations. The bias for total wind speed is shown in the previous figure, in the upper right panel. The magnitude of the bias is the least in the NL case, simply because it makes no lake breeze prediction. The model still does a good job in predicting the magnitudes, with the largest departure being slightly more than 2 m s^{-1} in the 2D2 run, and this only occurs near the frontal boundary.

Finally temperature and dew point were compared to the Zion tower observations. The temperature is particularly important since some of the quantities diagnosed in the LPDM are dependent on the surface temperature. Dewpoint is included in the bias plots, despite the seemingly inconsistent observed data, where there were several large jumps from hour to hour at inland sites, and its relatively unimportant contribution for the day modeled.

The temperature curves displayed in Figure 3.27 bear out what was seen in the previous meteorological cross sections, that the temperature was generally a couple of degrees warmer in 3DV. At the Zion site, shown in the upper left, the drop in temperature as the front passes, is fairly evident in all cases except NL and 3DV, although the 3DV curve does level off. The temperature drop shows the same trends in each model run except none of the runs predicts the temperature increase when the front moves back offshore. The 8 km site shows fairly good agreement except the 2D2 and 2D4 runs that penetrated too far inland, bringing in the cooler air. Finally, the 24 km site shows similar

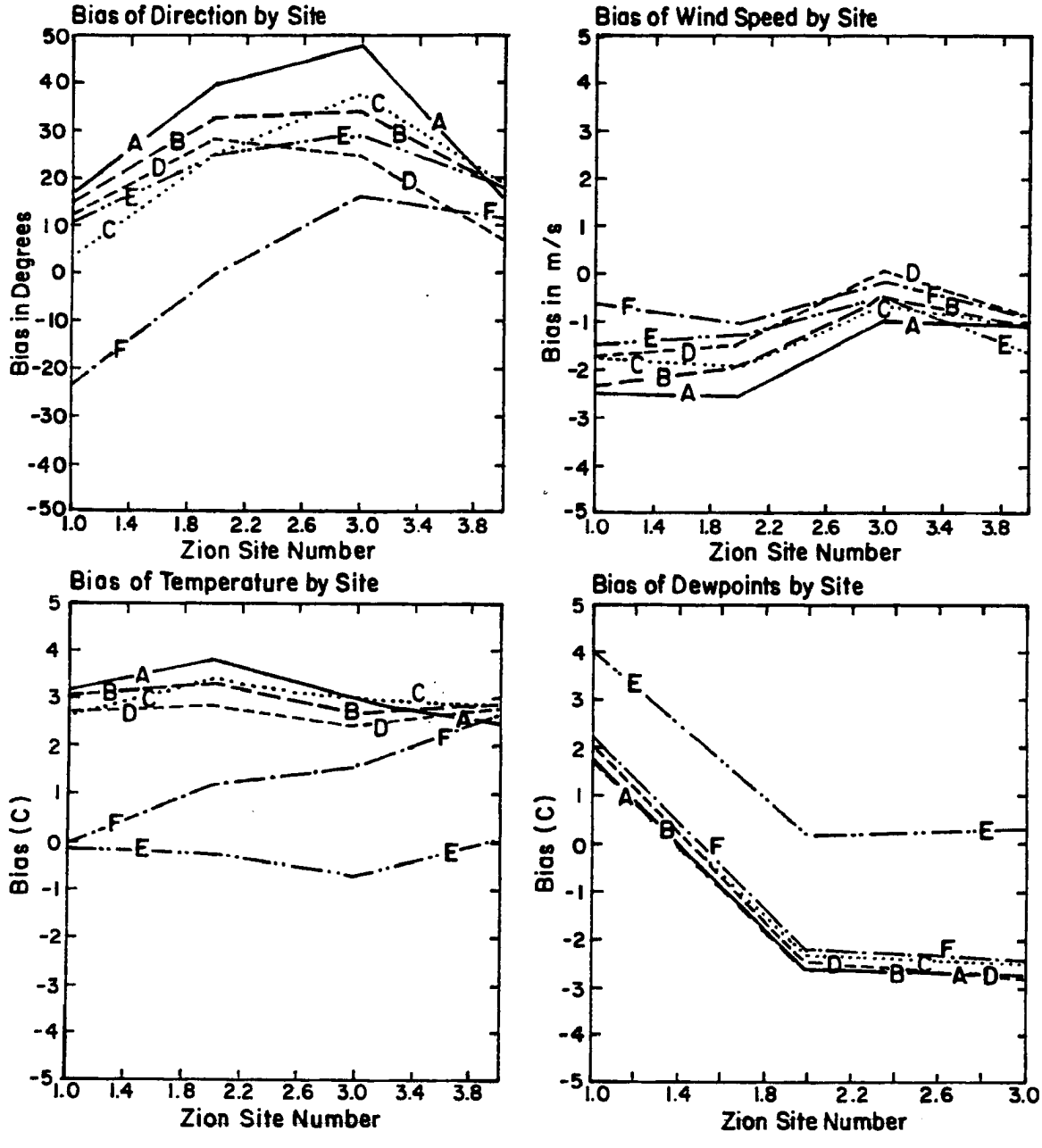

Figure 3.25: Bias for wind direction, wind speed, temperature, and dewpoint at A – 2D2; B – 2D4; C – 2D16; D – 3DH; E – 3DV; and F – NL.

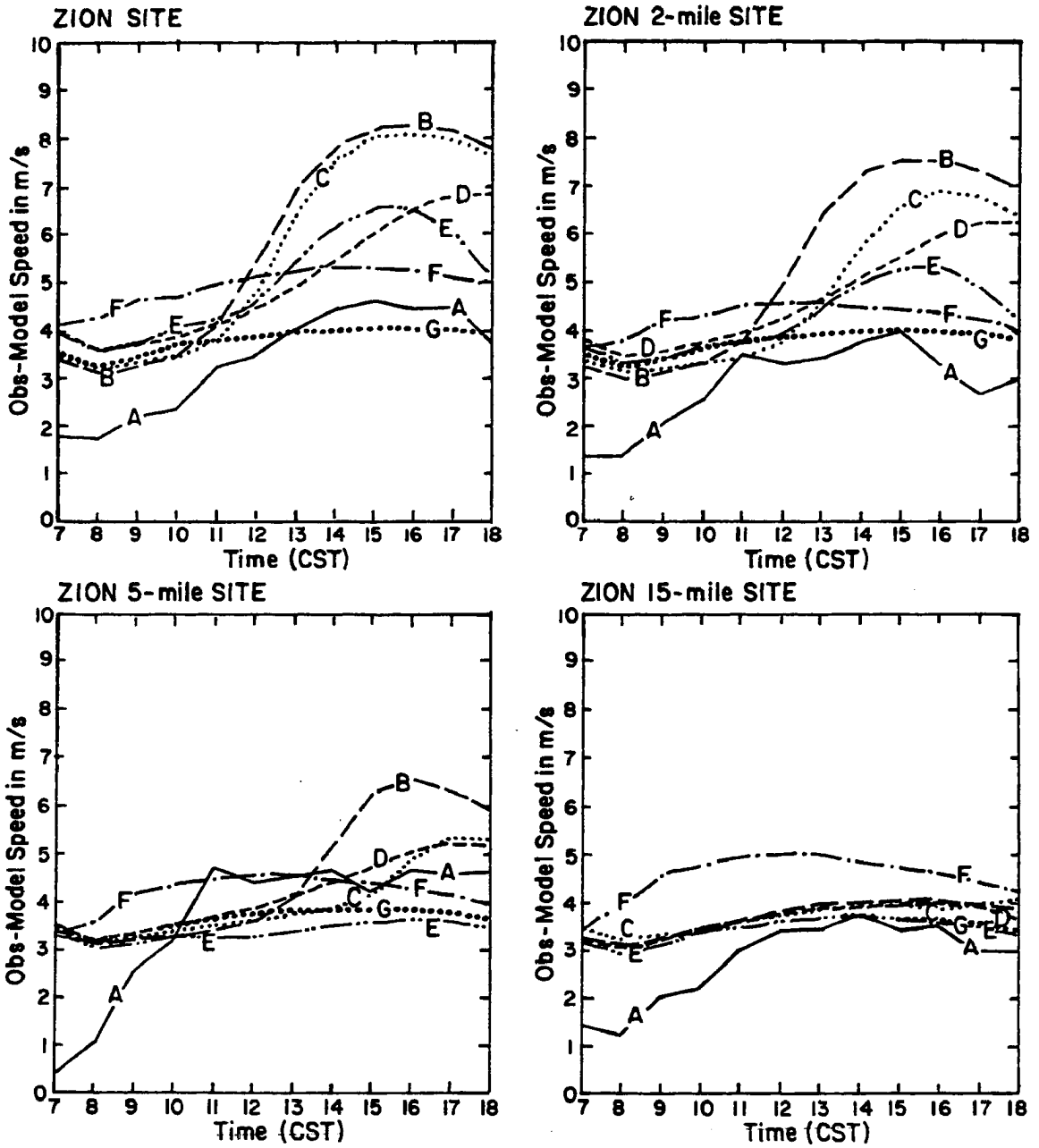

Figure 3.26: Time series of wind speeds for A – specified site; B – 2D2; C – 2D4; D – 2D16; E – 3DH; F – 3DV; G – NL.

curves for all simulations. The 3DV simulation appears to perform the best, and this could be a benefit of the added information from the nudging.

In order to quantify this information in a more detailed manner, correlation coefficients, r, were computed at the selected sites, for the previously mentioned variables. The results are contained in Figure 3.28. The site numbers are identified as before, with the furthest inland tower being dropped from the dewpoint evaluation due to reasons mentioned above. In the upper left panel, correlations for wind direction are displayed. As expected, the NL simulation has a negative correlation. The best performance appears to be the 3DV simulation, which has correlations ranging from .95 at the shoreline site to .66 at the inland site. This could be attributed to the enhancement due to nudging. The rest of the simulations appear to be quite similar. Moving to the upper right hand panel, correlations for total wind speed, the 3DV simulation shows remarkable correlation. The effects of the frontal boundary passing, or being in close proximity to the 8 km site seems to degrade the correlations for the other simulations that form a lake breeze. The nudging is again the most plausible explanation for the 3DV results. Finally the lower left panel shows correlations for temperature. The results are quite similar in all cases. The most difficult temperature prediction should occur where frontal boundaries are observed, and this is born out by the results. Notice the correlations all increase as one proceeds inland, further away from the convergence zone. The NL simulation performs better than others at the shoreline and 3 km sites, because it is the shape of the curve that matters most when computing correlation. A quick glance back at the bias plots shows that, not only did the 3DV simulation obtain the correct magnitude, it also predicting the correct curve, as evidenced by the correlation.

We have seen several trends in the results of the meteorological simulations. As expected, the 2D2 and 2D4 simulations shows enhanced convergence over their 3D counterparts. This resulted in stronger vertical motion, as well as further inland penetration. In addition, the homogeneous runs appear to be running a few degrees cooler than observed, as demonstrated by the bias curves. As for overall performance in terms of observational agreement, the 3DV simulation clearly coincides the most with observations. The impact

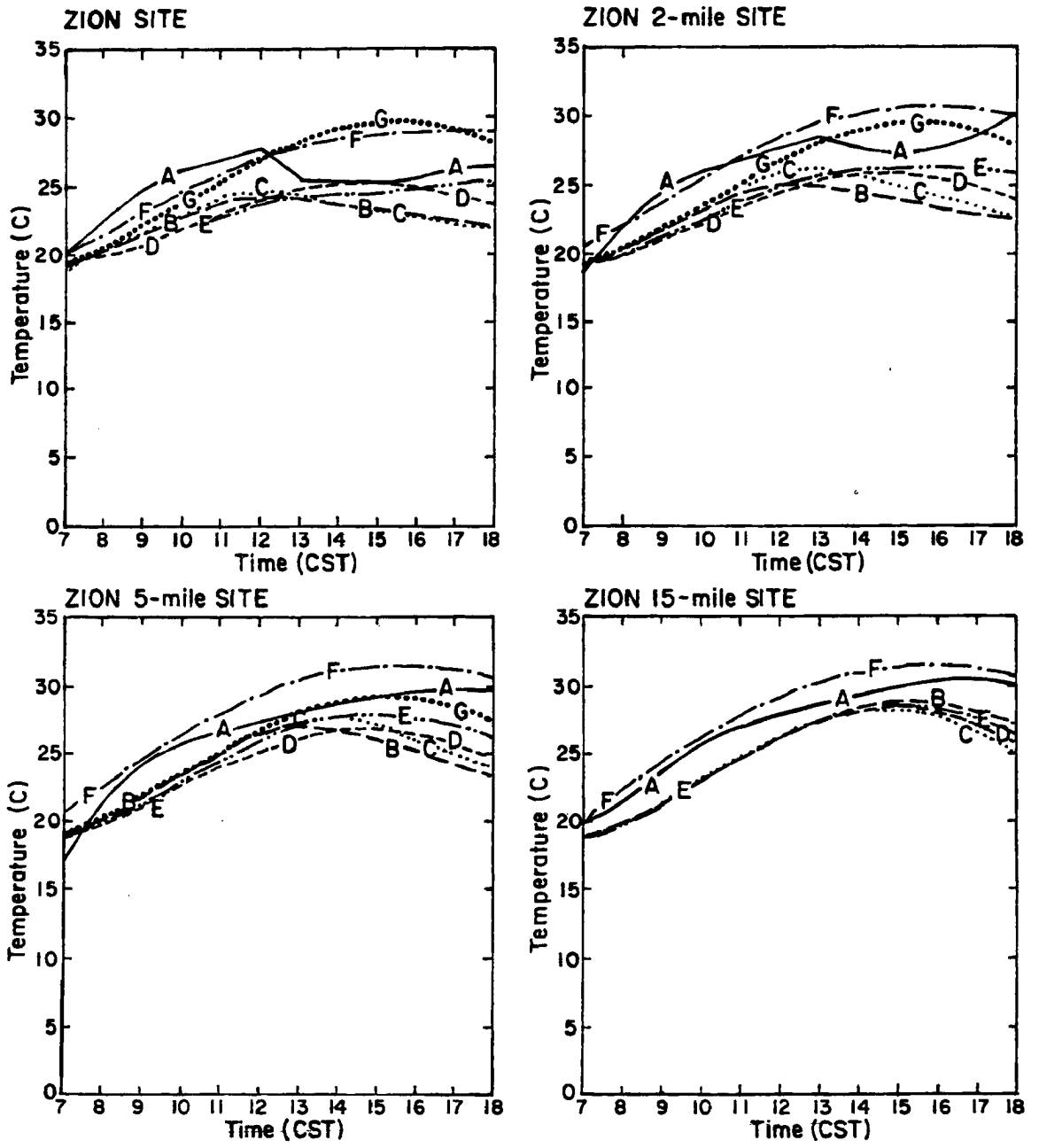

Figure 3.27: Time series of temperature for: A – specified site; B – 2D2; C – 2D4; D – 2D16; E – 3DH; F – 3DV; and G – NL.

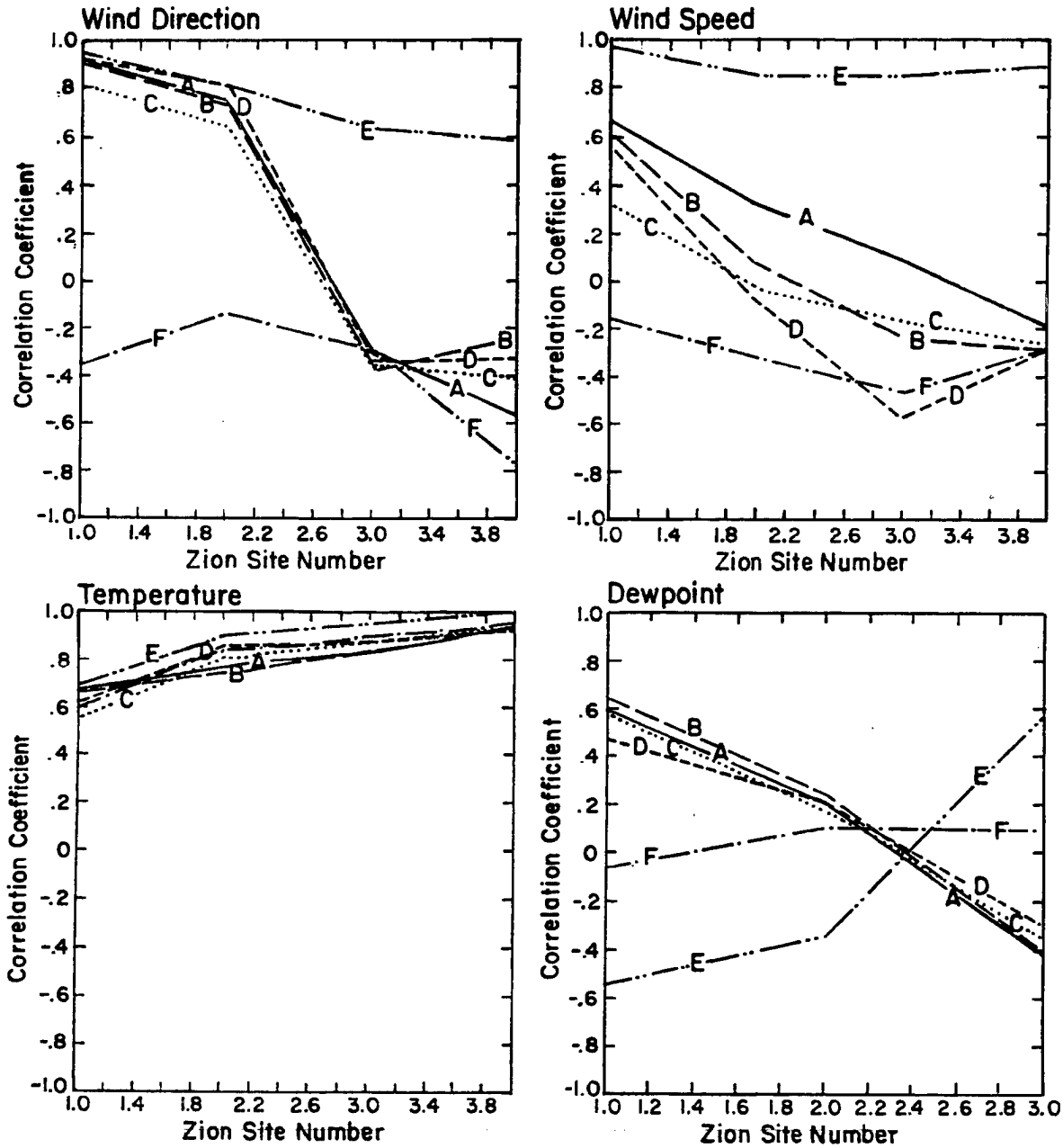

Figure 3.28: Correlation coefficient for wind direction, wind speed, temperature, and dewpoint at A – 2D2; B – 2D4; C – 2D16; D – 3DH; E – 3DV; and F – NL.

of the accuracy of the simulations should translate into similar results for the dispersion modeling.

Chapter 4

DISPERSION MODELING

4.1 LPDM Description

The Lagrangian Particle Dispersion Model (LPDM) is based on the work of McNider et al. (1988). The LPDM uses the RAMS model output to advect and diffuse the particles. Several quantities are diagnosed in order to compute a turbulent component to the mean wind fields. These turbulent components have basis in the work of Smith (1968). There are several different regimes that are determined through the calculation of boundary layer height, Richardson number, and Monin-Obukhov length.

The particles are first classified according to the sign of the Monin-Obukhov length. A negative Monin-Obukhov length indicates a convectively unstable situation. The values of the PBL and mixing coefficients, which are interpolated in time and space to the particle position, as all variables are, are then used to diagnose sigmas in the horizontal and vertical directions. This information is also used to determine a Lagrangian time scale. The time scale is used to retain some component of the previous turbulent fluctuation, thus giving the particle memory. A complete set of the equations and parameterization relating these quantities can be found in McNider et al. (1988).

If the Monin-Obukhov length is positive then the LPDM evaluates the sign of the Richardson number and compares it to the critical Richardson number. When the Richardson number is positive then the fluid is stably stratified; a Richardson number of zero indicates neutral stratification; and a negative Richardson number implies an unstable stratification. The critical Richardson is calculated from the vertical grid spacing. It is based on theory that indicates when the Richardson number is greater than 0.25, even in the presence of a wind shear, the flow becomes laminar. Thus, if the Richardson number

is greater than zero, but less than the critical Richardson number, vertical sigmas are calculated based on a relationship between the deformation and mixing length, while the horizontal sigmas are based on the surface friction velocity. If the Richardson number is greater than the critical Richardson number, the flow is laminar, and the turbulent components are set to a minimum threshold.

Not all situations are covered by the previous two regimes, and this is even more prevalent in the case where internal boundary layers are present. Internal boundary layers present a difficult problem and can lead to a contradictory situation. This occurs when the Monin-Obukhov length is positive, indicating a stable layer, and the Richardson number is negative, indicating an unstable layer. The Monin-Obukhov length is diagnosed based on surface values, while the Richardson is calculated at the particle position. The contradictory situation can occur quite frequently in the thermal internal boundary layer. This is handled by looking at a PBL height based on Richardson number, and one based on the mixing coefficients. The position of the particle relative to these heights is used in conjunction with the difference in these values to parameterize the wavelength of the maximum in the vertical velocity spectra. The wavelength is then used as before in determining the Lagrangian time scales and turbulent velocity fluctuations.

4.2 Comparison of LPDM Simulations

The SF_6 was released at 1241 LST on July 16, 1992. A total of 600 kg were released in four hours, corresponding a release rate of 150 kg hr^{-1}. Fans were deployed to vent the SF_6 from the release site, which was at 2 meters above lake level in Waukegan Harbor. Roughly an hour after the release began, aircraft flights begun. The aircraft made multiple transects at a variety of heights, ranging from 100 m AGL to 1600 m AGL. The aircraft also varied distance from the release site, reaching a maximum distance of 50 km from the harbor (Bowne et al., 1991).

The LPDM was run off the meteorology of the six simulations. Based on the release data the LPDM was configured to use an effective release height of 5 m AGL. The release was started at 1241 LST and continued for 4 hours. Locations of the particles were

tabulated every fifteen minutes of simulation time. A total of 20000 particles were released at a rate of $1.33 \frac{particles}{s}$. The 20000 figure was arrived at after several sensitivity runs were completed. It was found that results improved steadily as the number of particles was increased from 1000 to 20000 particles, at which point the improvement was no longer perceptible. Up to 100000 particles were released for this sensitivity comparison, and no appreciable difference was noted above 20,000.

Figure 4.1 shows an XY cross section of the simulated particle plume after 1 hour of simulation time. The order of the plots as follows. Moving clockwise and starting in the upper left hand panel, is the 2D2, followed by 2D4, 2D16, NL, 3DV, and 3DH. Only the 2D2 and 2D4 plumes show similarity. Inspection of the plots close to the source, shows that the plume in these 2 runs moves inland further than any of the other simulations. Notice the narrowness of the plume as it moves inland in the extremely stable lake air. The air changed from a Pasquill-Gifford class of A to an F when the front passed. In the case of the 2D2 and 2D4 simulations the front has moved further inland. The 3D plumes are quite different. The 3DH plume appears to reach the frontal boundary rather quickly. Once the plume reaches the front it is quickly injected upwards by the updraft into the return flow aloft. In the 3DV simulation it appear that the plume slides up the coast more before it is transported aloft. The NL plume appears to be Gaussian in shape, as it should be when minimal shear is present. An XZ cross section of the particles is shown in Figure 4.2. The time and order is the same as the previous Figure. The base of the plumes show considerable divergence from one another. The 2D2 and 2D4 plumes are the widest, because there is greater inland transport in these simulations. The NL simulation appears to have an unrealistic bias towards the lowest levels, despite the presence of the superadiabatic layer in the homogeneous runs. Further investigation is continuing into the cause of this accumulation. The 3DV plume is the narrowest, probably a result of more southerly flow in this simulation. The LPDM parameterization appears to have reasonable results even in the 2D16 run, where vertical motions were less than 2.5 cm s^{-1}. Despite the weakness of the updraft the particles still get transported aloft.

After two hours of simulation time the plumes in the lake breeze simulations have become highly non-Gaussian in structure. Figure 4.3 shows an XY cross section at this

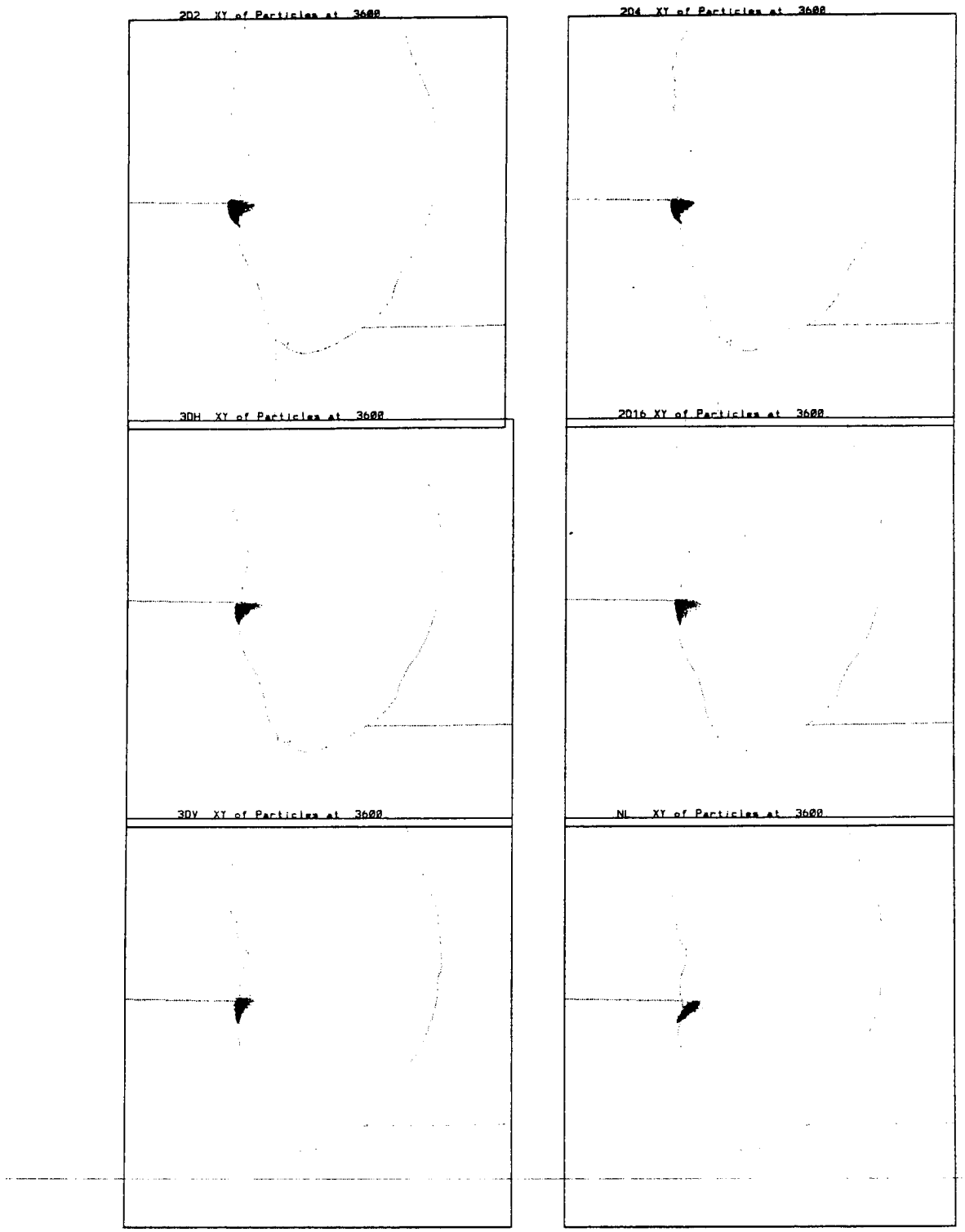

Figure 4.1: XY of LPDM plume. Time is time from release (1214 LST).

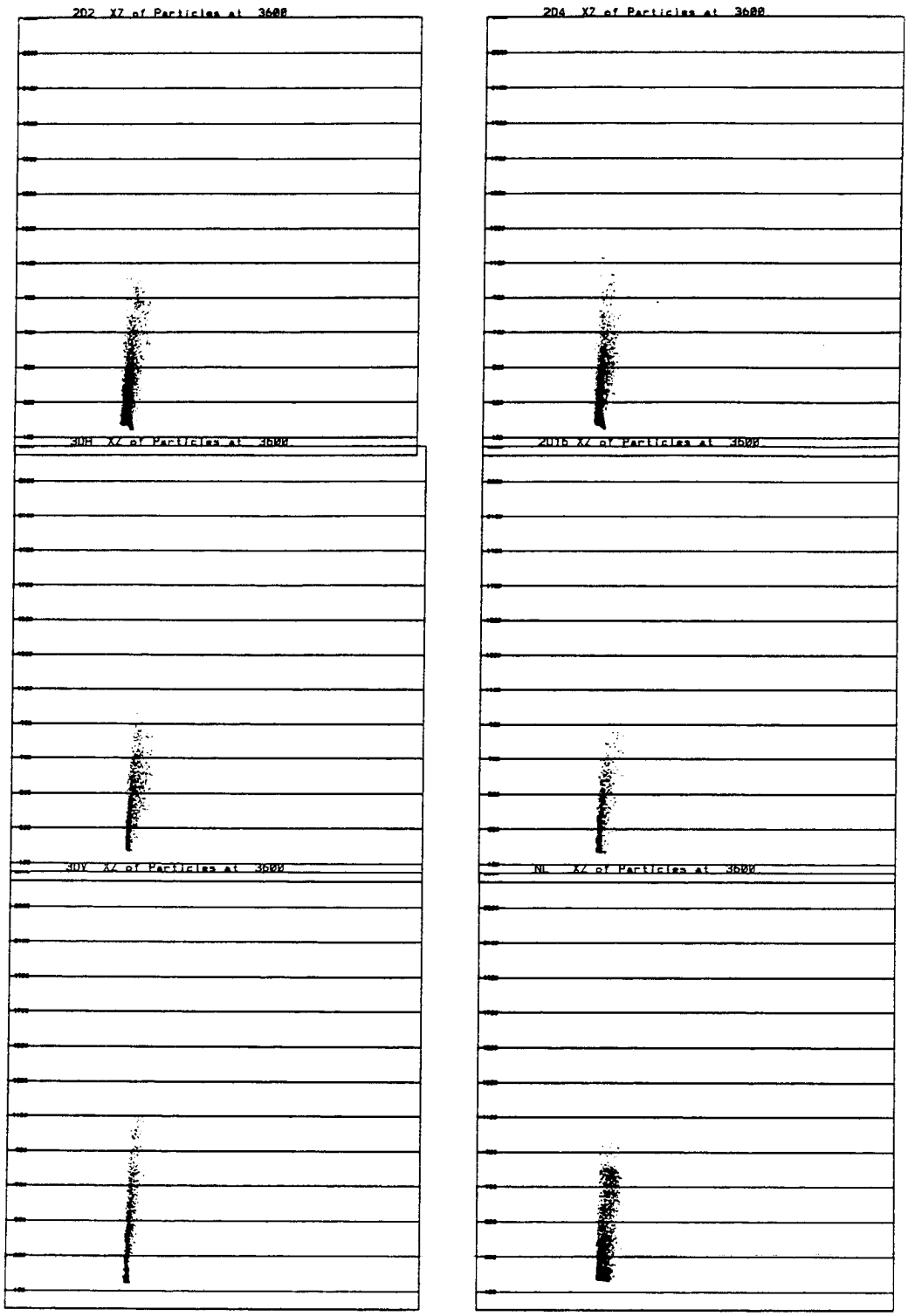

Figure 4.2: XZ of LPDM plume. Time is time from release (1241 LST).

time. The 2D2 and 2D4 plumes are being transported even further inland at this time. Thus the particles aloft are translocated roughly 10 km north of the release point, while in the 3DH, 3DV and 2D16 simulations there are particles aloft in close proximity of the source. The XZ section taken at this time shows the effects of the stable lake air. In Figure 4.4 the plume is nearly solid black until the particles are injected aloft. Also, notice that particles that subside after undergoing transport aloft, although they do not reach the surface. This result stems from the fact that the lowest 200 meters of air above the lake is extremely stable, prohibiting particles from penetrating into air below this level.

Particle positions in an XY plane after five hours of simulation exhibit several similarities in spatial extent for the lake breeze simulations, as displayed in Figure 4.5. Notice the NL plume has no similarity to the others. The 3DH, and to a lesser degree the 3DV, simulations show the 3D nature of the coast line, while the 2D runs exhibit a straight line to the left edge of the plume. Because of more southerly flow in the 3DV case, the 3DV plume is further north than any of the other plumes, while the homogeneous simulations show more particles to the east northeast of the release site.

Overall, it appears that the homogeneous runs produced quite similar results. All homogeneous plumes appear to have the same spatial extent in the horizontal direction. Analysis of Figure 4.6 shows a different result for the vertical distribution of particles. The 2D2 and 2D4 runs appear nearly identical. This, and the previously mentioned similarities support the decision to use a 4 km mesh for the 3D simulations. The 3DV plume does not have the vertical extent of the other plumes, however. This is related to the vertical motion realized in the simulation. Notice the 2D16 plume also shows a vertical distribution of lesser magnitude. Outside of the NL plume, which was mixed by a convective boundary layer, the 3DV and 2D16 realized the smallest magnitude of vertical motion. The subsidence over the lake is evident in all the lake breeze simulations. There is a downward slope to the particles distribution as one moves eastward across the lake. When animation is used this becomes even more noticeable.

The main focus of this research was to ascertain the impact of the lake on dispersion. That was one reason the NL simulation was performed. Another way of quantifying the

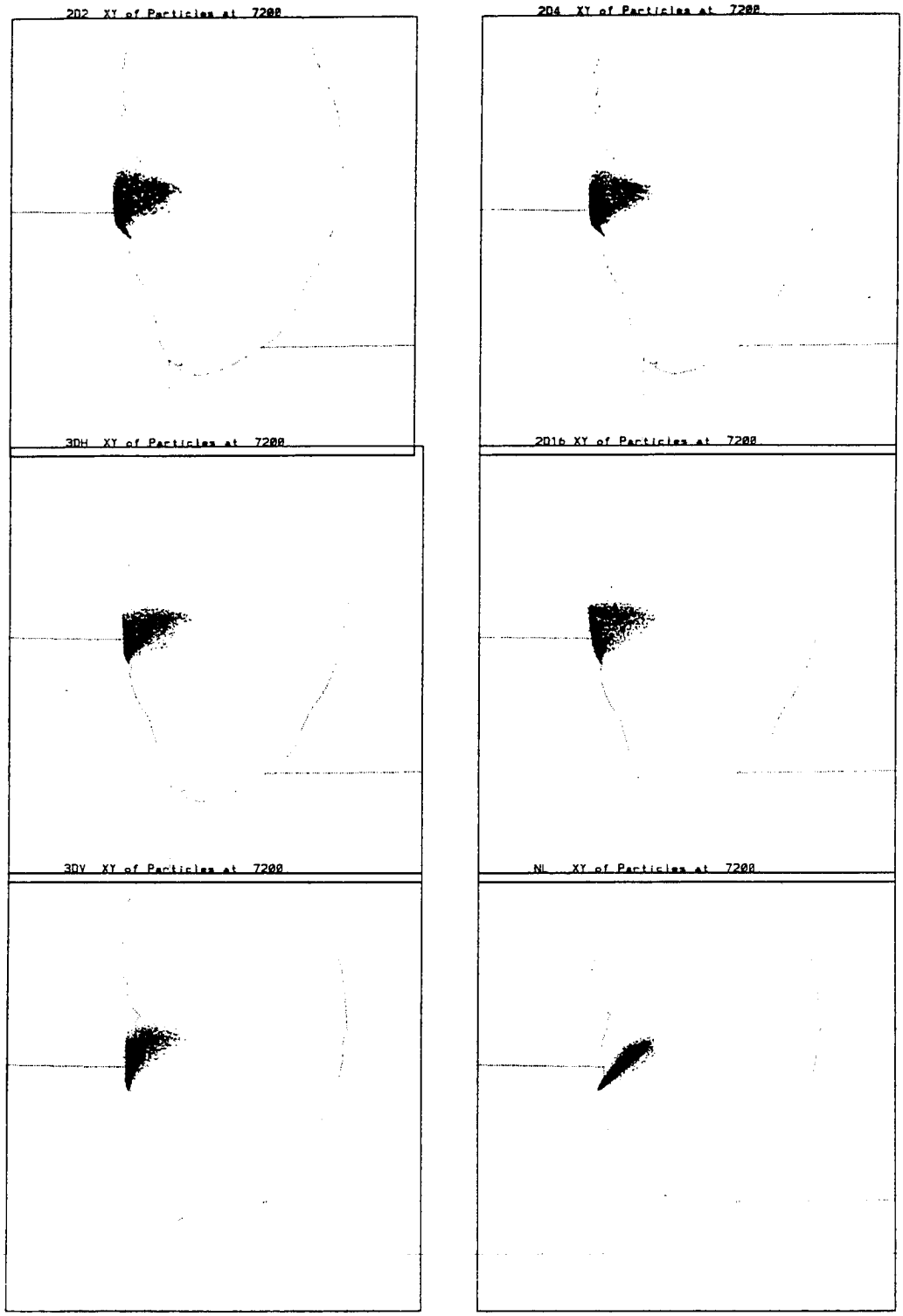

Figure 4.3: XY of LPDM plume. Time is time from release (1241 LST).

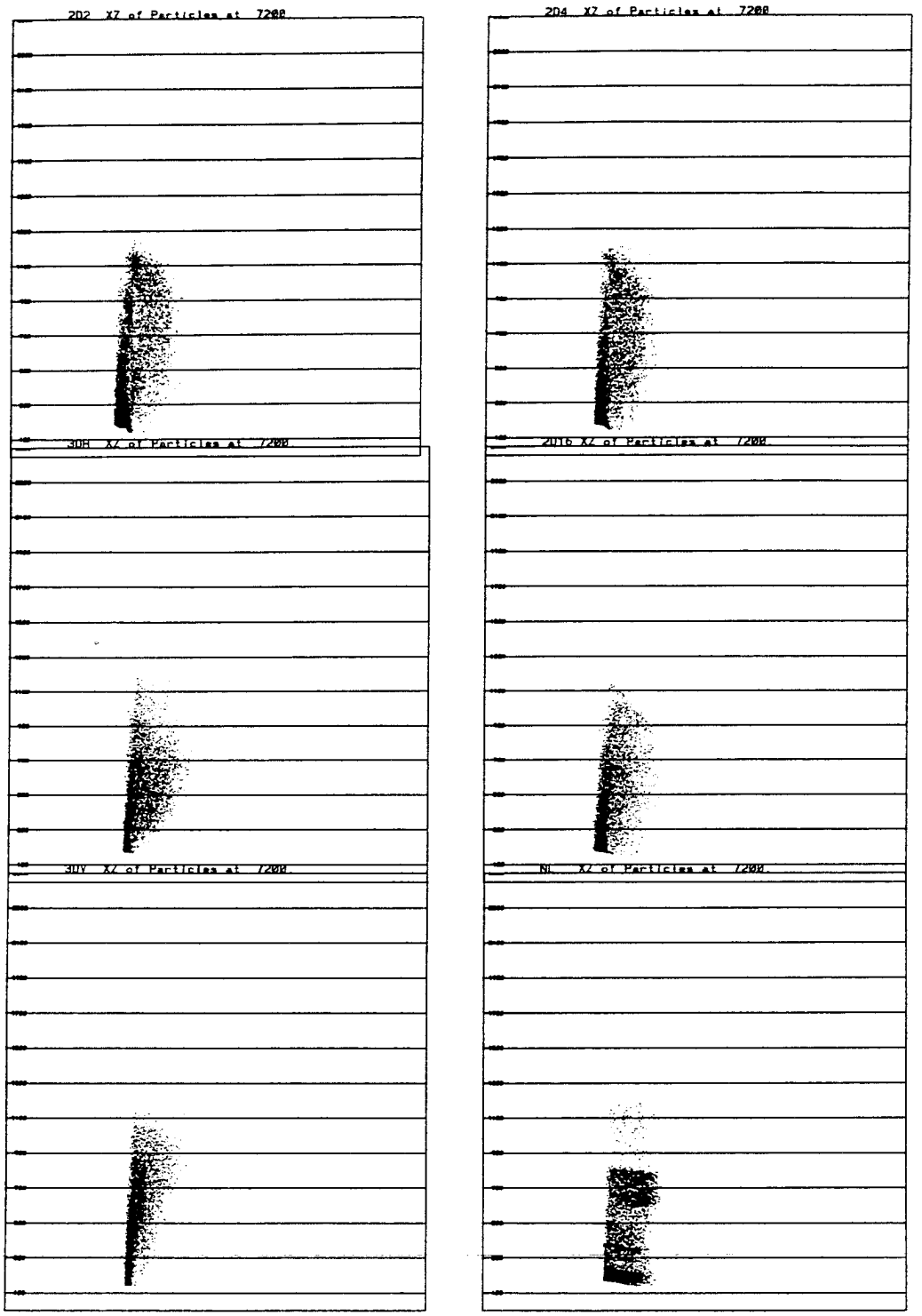

Figure 4.4: XZ of LPDM plume. Time is time from release (1241 LST).

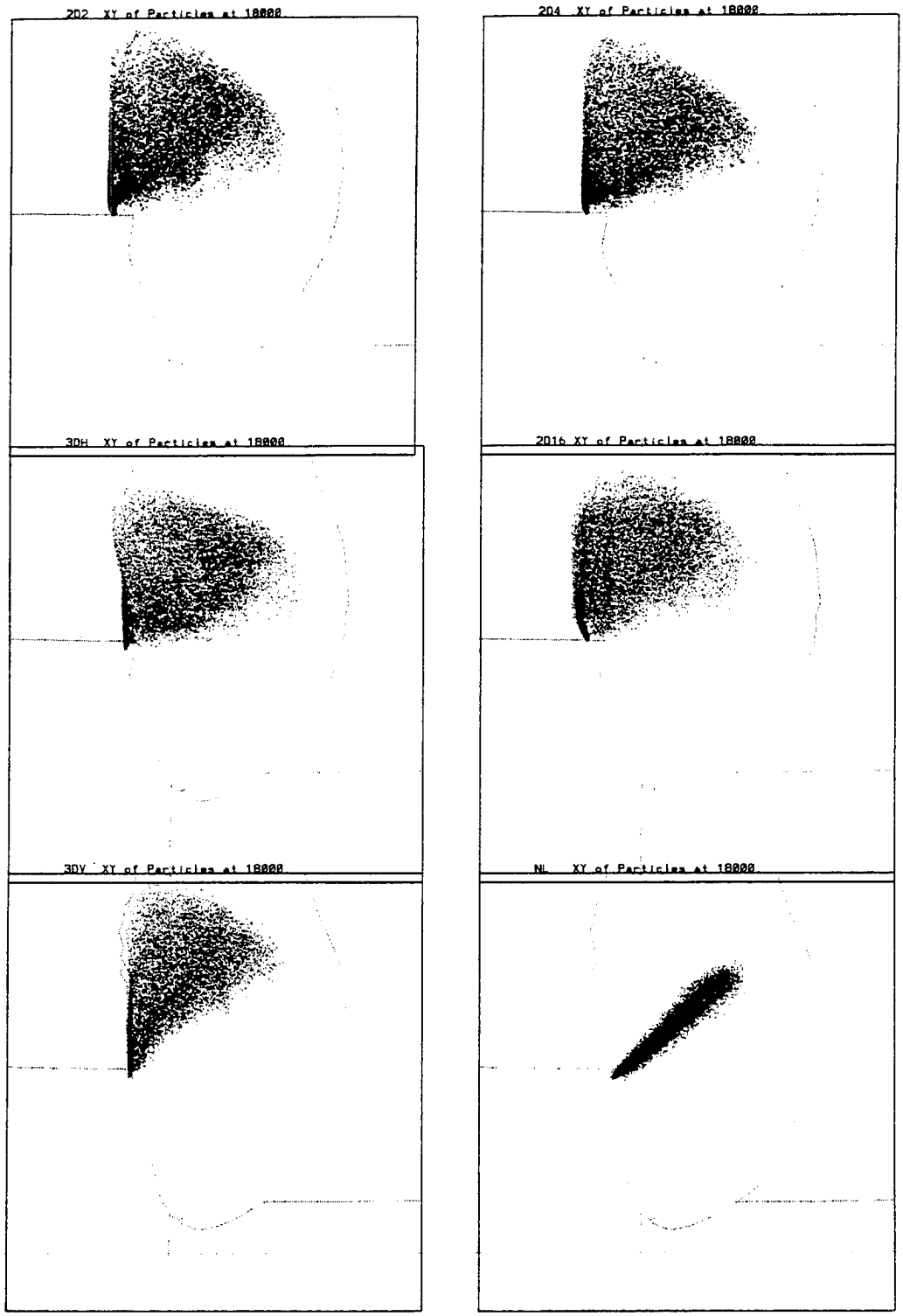

Figure 4.5: XY of LPDM plume. Time is time from release (1241 LST).

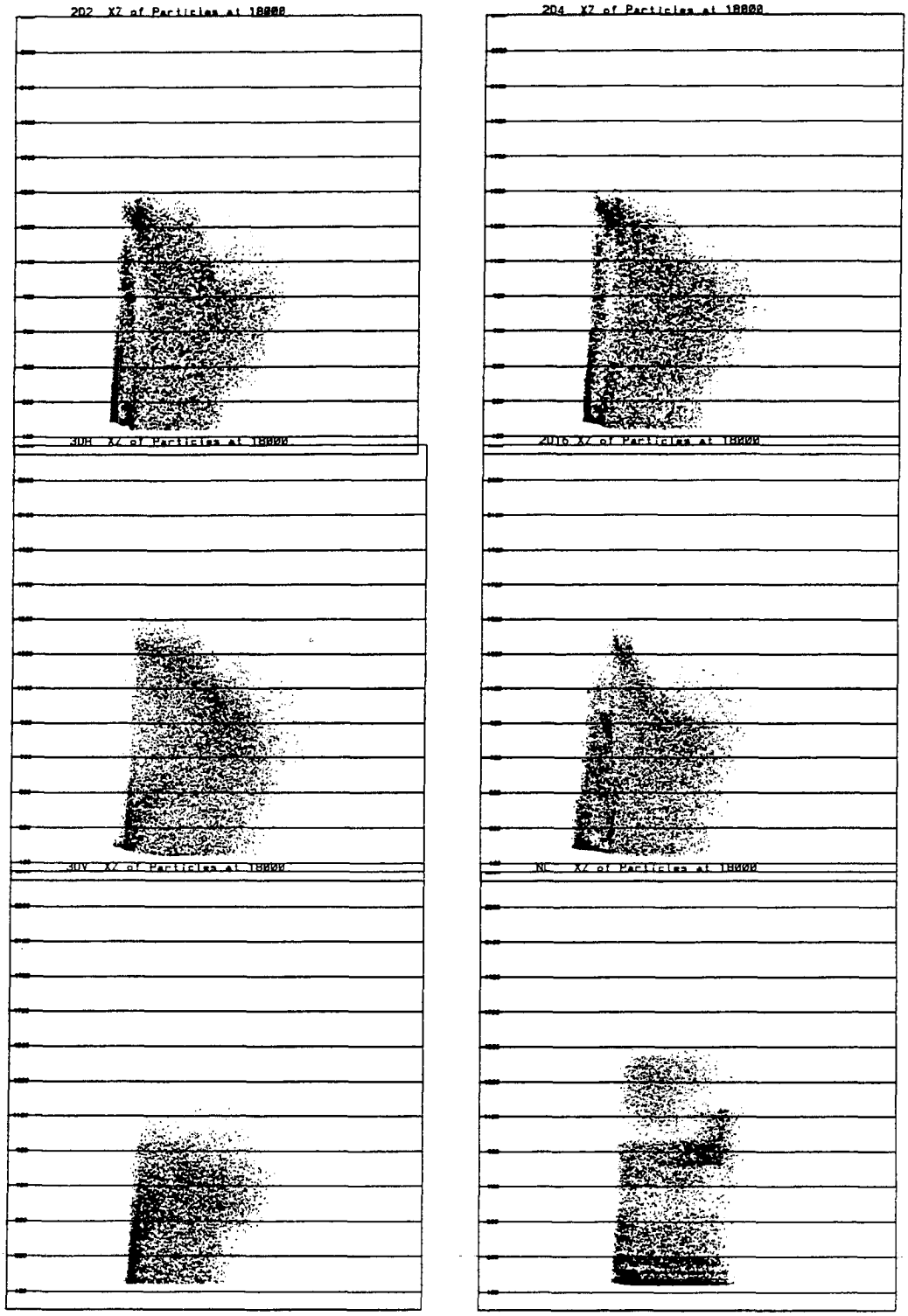

Figure 4.6: XZ of LPDM plume. Time is time from release (1241 LST).

Table 4.1: Summary of LPDM recirculation data.

Run Name	Ratio of Recirculations to Total Particles	% Particles Undergoing Recirculation	Maximum Number Recirculations
2D16	.88	70	4
2D4	1.0	80	5
2D2	1.05	82	4
3DH	1.05	76	5
3DV	1.00	67	5
NL	0	0	0

lake effect was to calculate the percent of particles recirculated from the beginning of the simulations. Table 4.1 provides a summary of this data. The second from left column lists the ratio of particle recirculations to total particles released, followed by percent of particles undergoing recirculation. The last column shows the maximum number of recirculations. The impact of the lake is obvious. From 70 to 80 percent of the particles are transported in a solenoidal circulation. This number appears to be fairly consistent throughout the entire set of lake breeze simulation. If this number were realized for the entire urban corridor along the west side of the lake, the potential impact to Wisconsin could be enormous. Of course, this number is meaningless unless the tracer data verifies the LPDM results.

4.3 Observational LPDM Evaluation

The tracer data collected on July 16, 1992 was used to verify the results of the LPDM simulations. The spatial position, observed concentration as well as time of day were recorded for later analysis. Software was developed to use this information by flying a hypothetical, numerical plane through the LPDM created plume and calculating an LPDM concentration. Each particle in the LPDM represents a certain mass of SF_6. By counting the number of particles in a volume along the flight path, the concentration was ascertained. Considerable amounts of testing went into the determination of a grid volume to use for the calculation. It was found that the results were optimized when the volume used was 250 m perpendicular to the flight path and 100 m for ΔZ. The third dimension was the distance between consecutive measurements, typically 100 to 150 m.

The plane lifted off at 1341 LST. For the first half hour of flight the plane detected no SF_6, at which point it made a low transect just north of the harbor. Shown in Figure 4.7 is an XY cross section of the flight path after 5 hours. The flight path is shown in red. Figure 4.8 shows an XZ cross section at the same time. In these figures the alternate bands of blue and yellow represent 100 m intervals of height, thus the plane made measurements up to 1500 m AGL. The first part of the flight concentrated on measurements near the release point at a variety of heights, while the last couple of hours were flown at distances of 20 to 50 km to the north and east of Waukegan harbor.

A series of plots showing concentration verses time are shown in Figures 4.9 through 4.20. The Figures are arranged in the same order as the LPDM plots. The plots have different ranges, because the peak concentrations vary from simulation to simulation. The time is listed along the bottom and is the time from plane takeoff. The ordinate is the concentration in part per trillion (ppt). The first figure starts at 30 minutes after liftoff and lasts 15 minutes. The best performance during this interval is the 3DH run. The LPDM detections nearly coincide perfectly throughout the entire interval, while the other simulations exhibit about a 100 to 200 second delay between observations and LPDM. The peak values of the LPDM range from nearly 1200 ppt in the NL and 3DV simulations to nearly 2600 ppt in the 2D16 run. The values are considerably larger during the first parts of the flight because the plane is flying very near the source of the SF_6. The 3DH continues to excel over the duration of the flight. Notice there are several panels were NL displays no values. It was no surprise that the NL simulation produces some acceptable values. Inspection of the flight and a knowledge of the synoptic scale winds suggest that the NL simulation should agree with the part of the plume that coincides with the direction of the synoptic wind.

Correlations were calculated for each simulation based on the aircraft data. There is a question that comes to mind when calculating the correlation values. Since the LPDM output is produced at a frequency of 15 minutes, and the aircraft data is at 1-2 second intervals, what averaging time should be used for determining the correlations? Instead of trying to answer this question the correlations were calculated over a spectrum of averaging

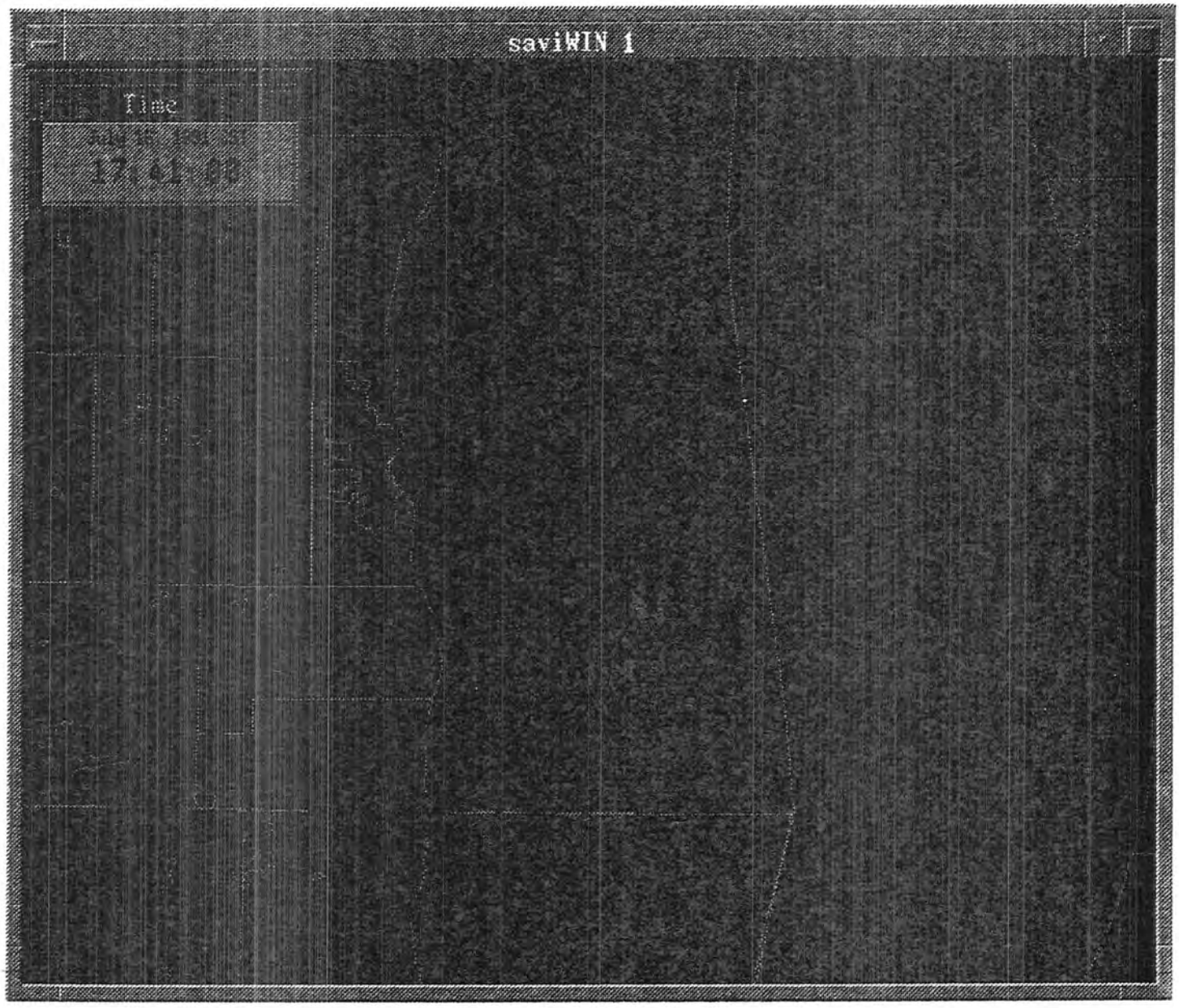

Figure 4.7: XY Cross section of the flight path (in red). Time of takeoff was 1341 LST and the final time was 1741 LST.

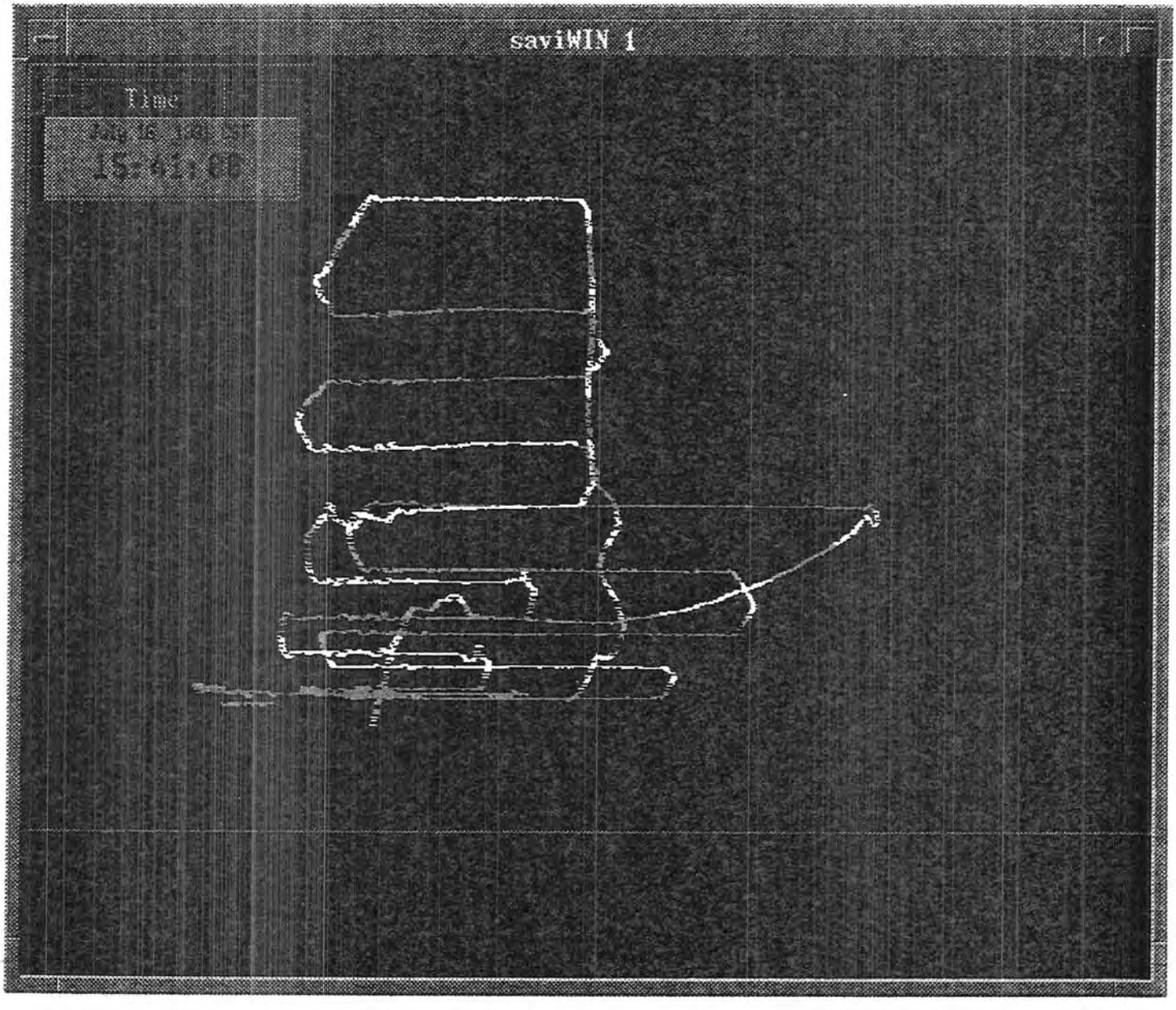

Figure 4.8: XZ Cross section of the flight path from 1341 to 1741 LST. The alternating blue yellow represents 100 meter intervals of height.

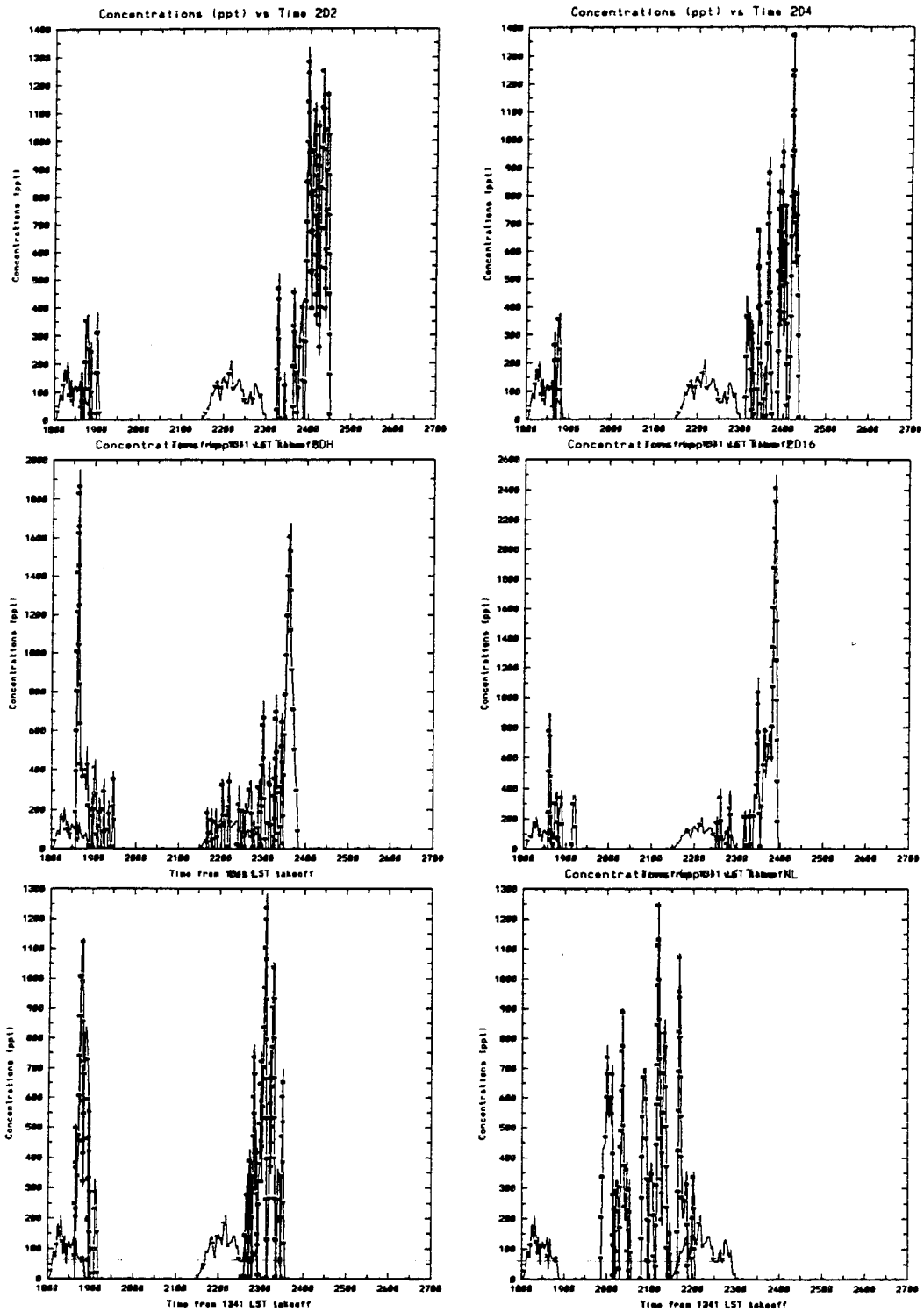

Figure 4.9: Concentration vs. time: A – observations; B – LPDM.

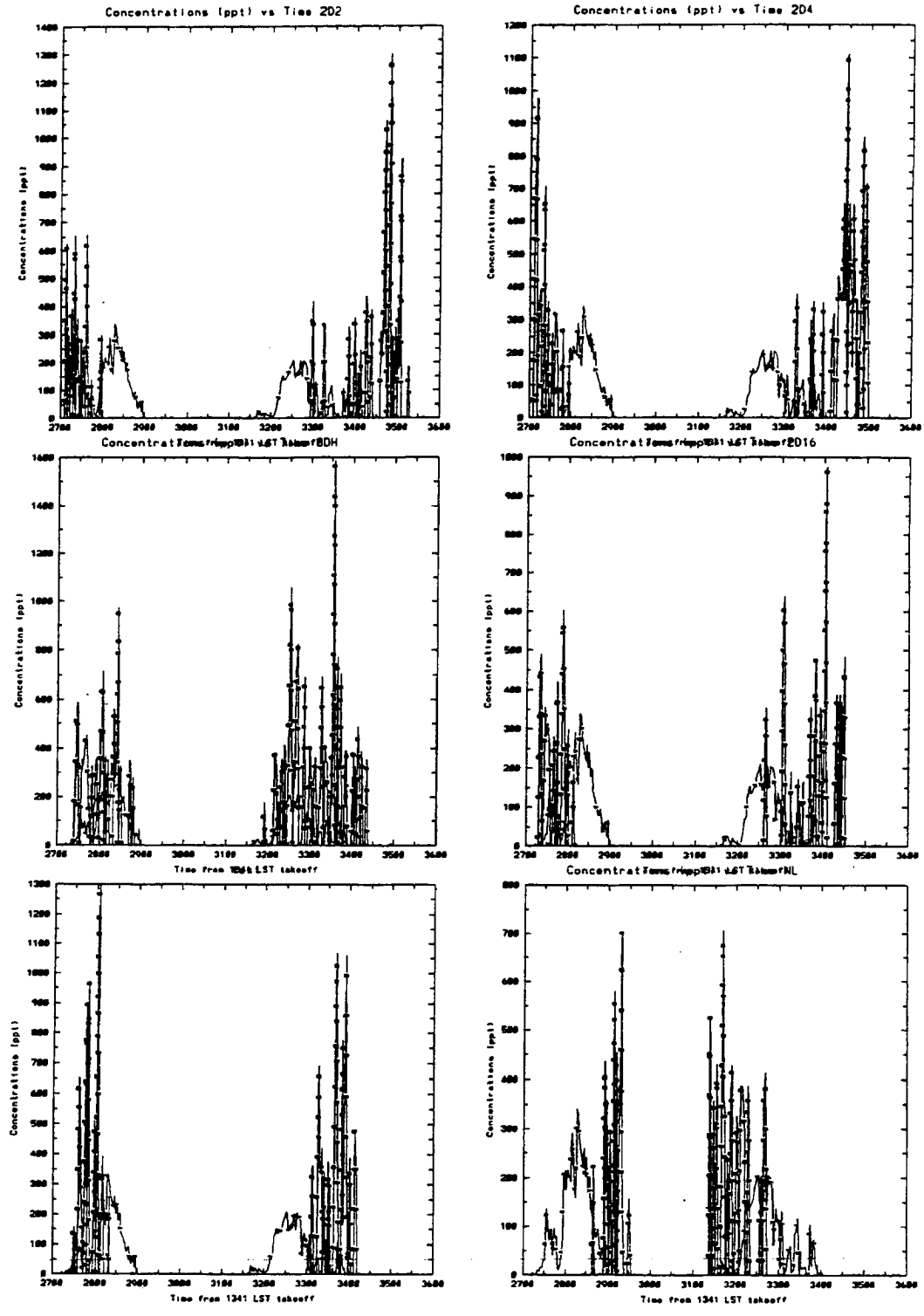

Figure 4.10: Concentration vs. time: A – observations; B – LPDM.

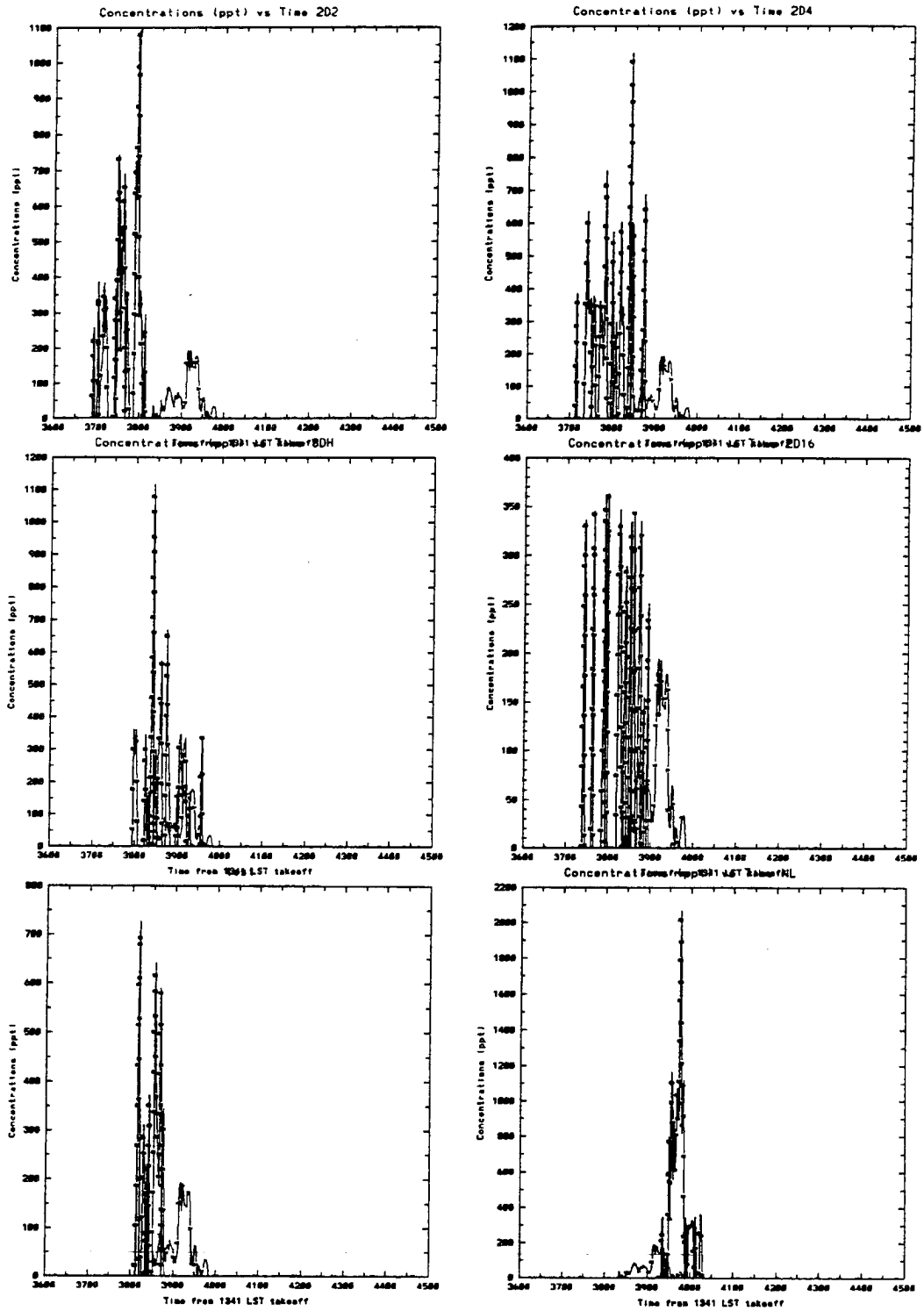

Figure 4.11: Concentration vs. time: A – observations; B – LPDM.

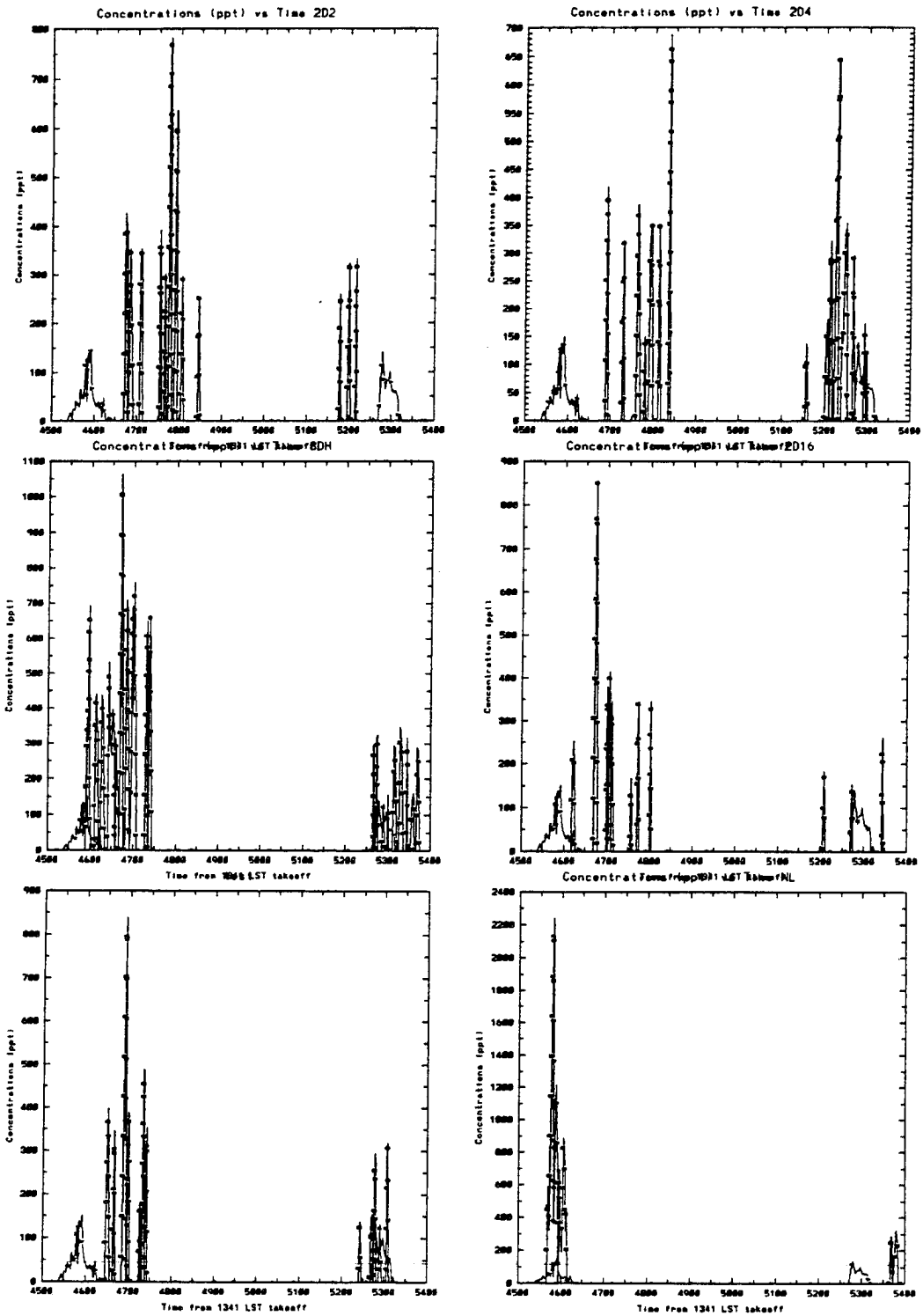

Figure 4.12: Concentration vs. time: A – observations; B – LPDM.

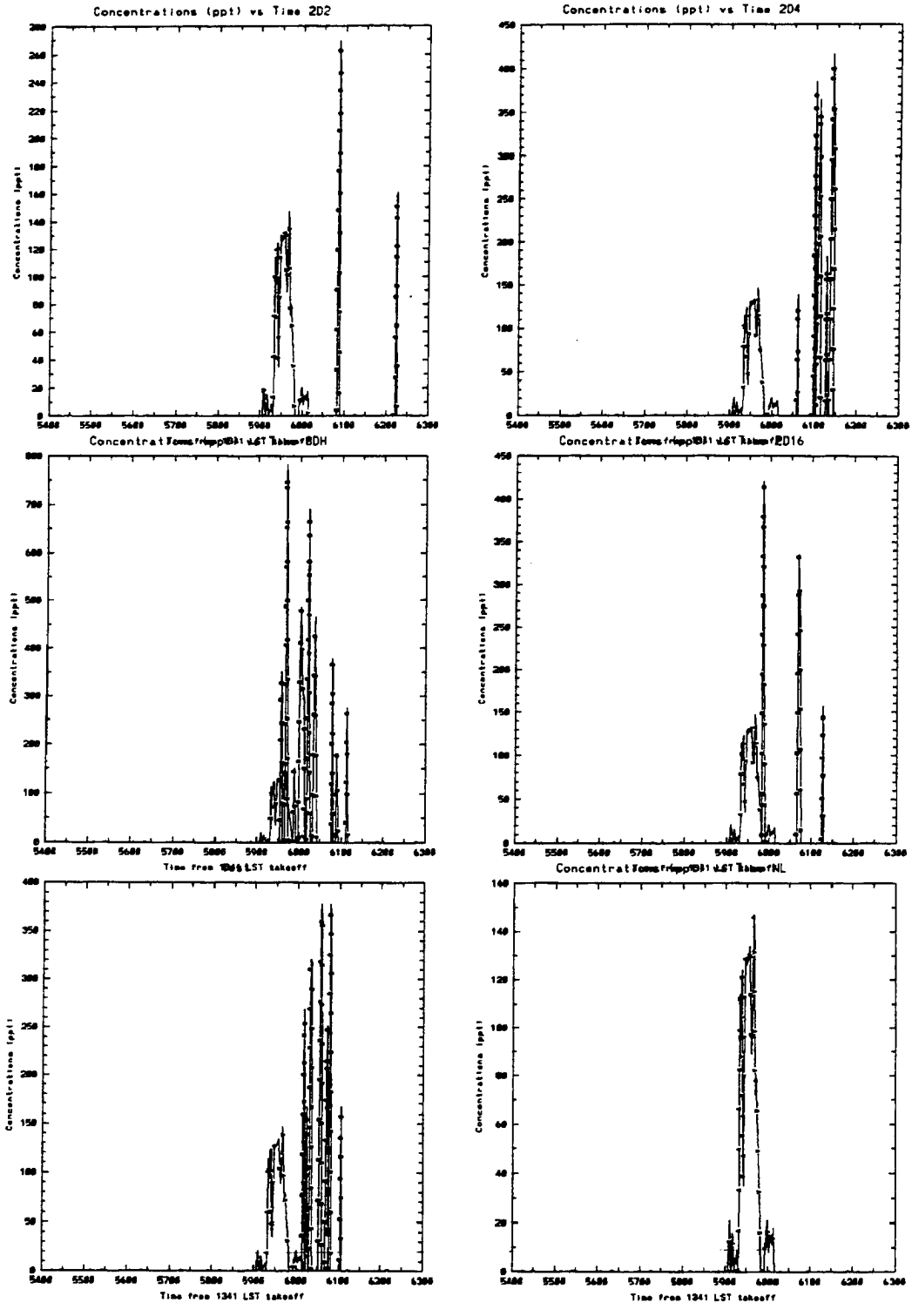

Figure 4.13: Concentration vs. time: A – observations; B – LPDM.

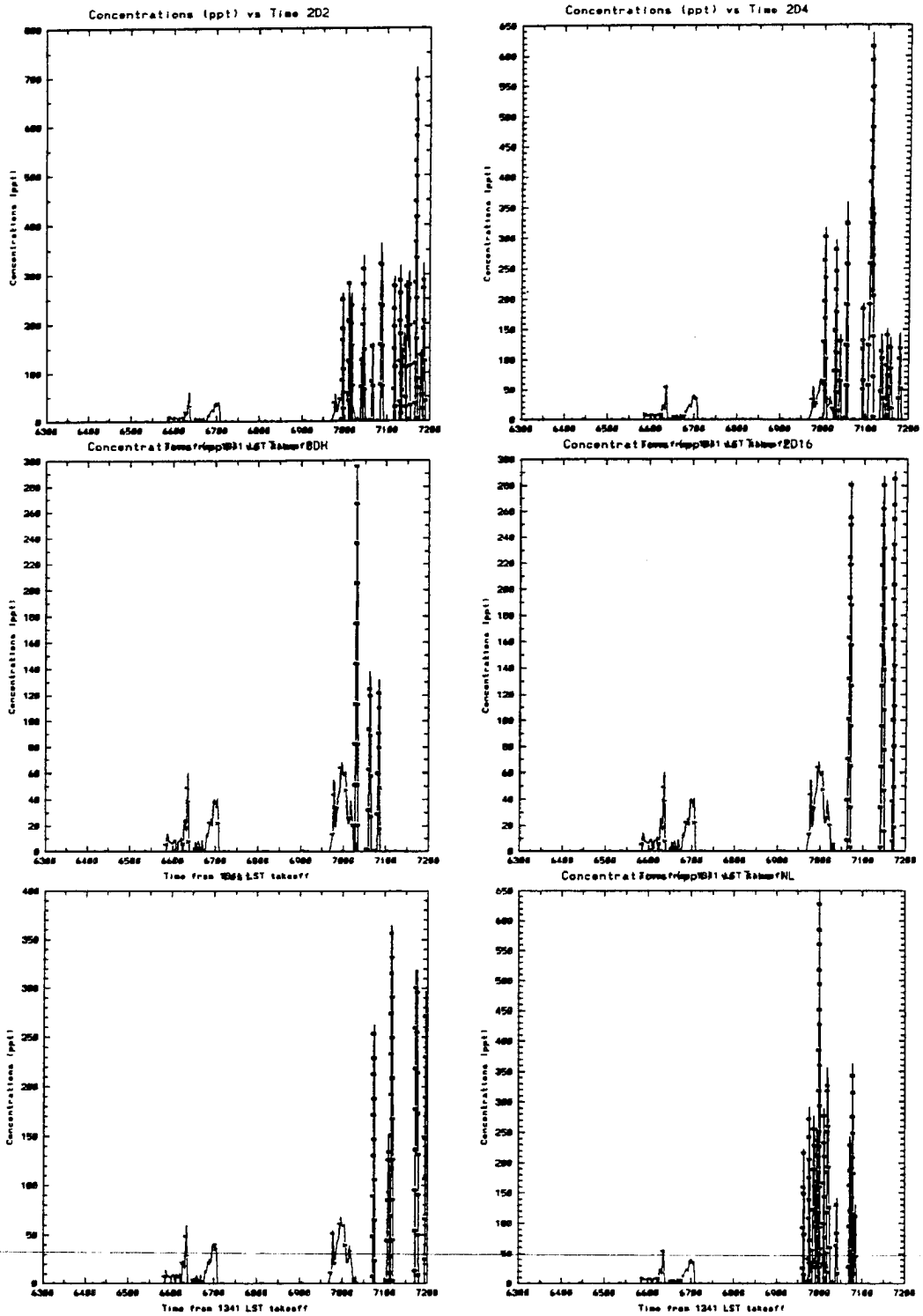

Figure 4.14: Concentration vs. time: A – observations; B – LPDM.

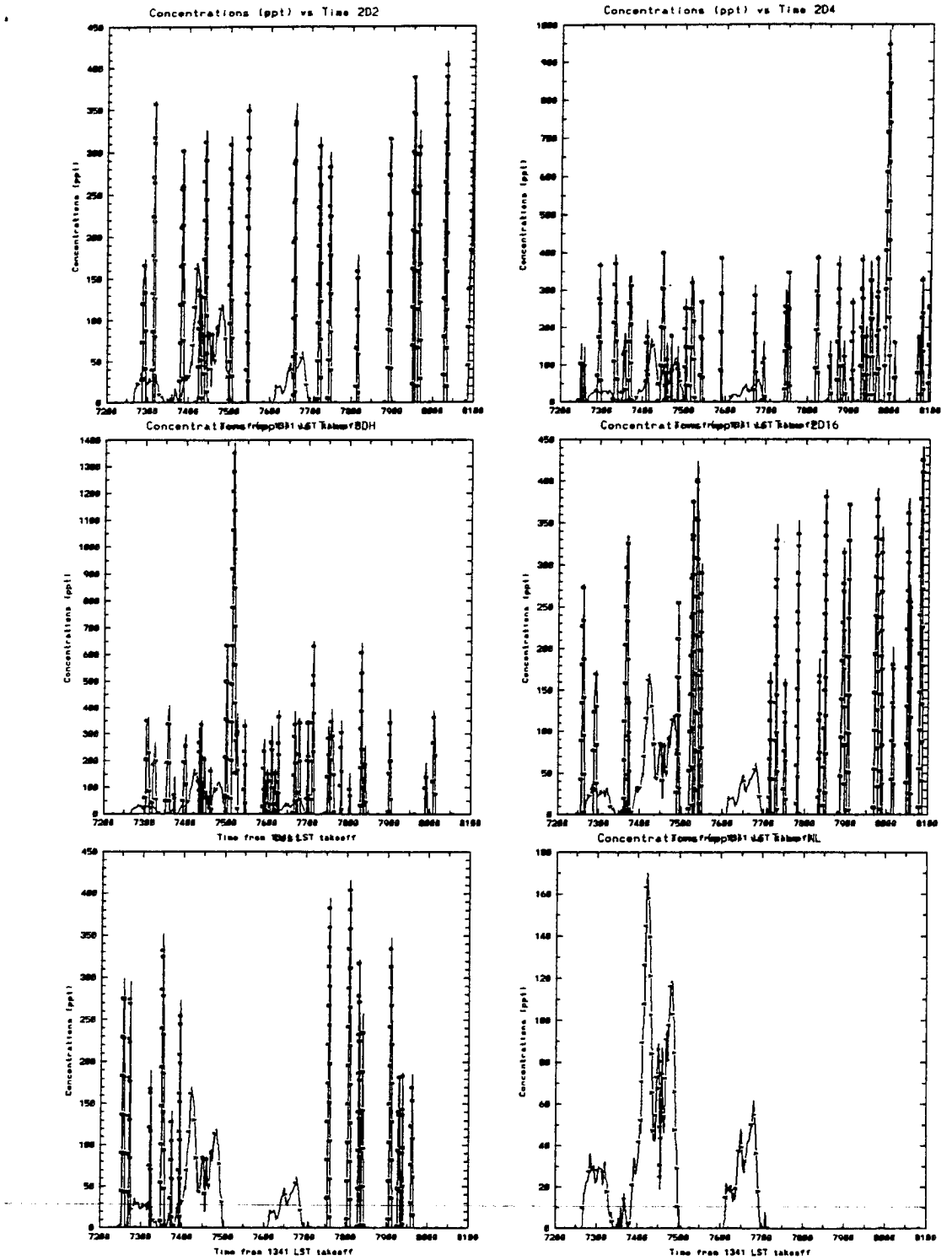

Figure 4.15: Concentration vs. time: A – observations; B – LPDM.

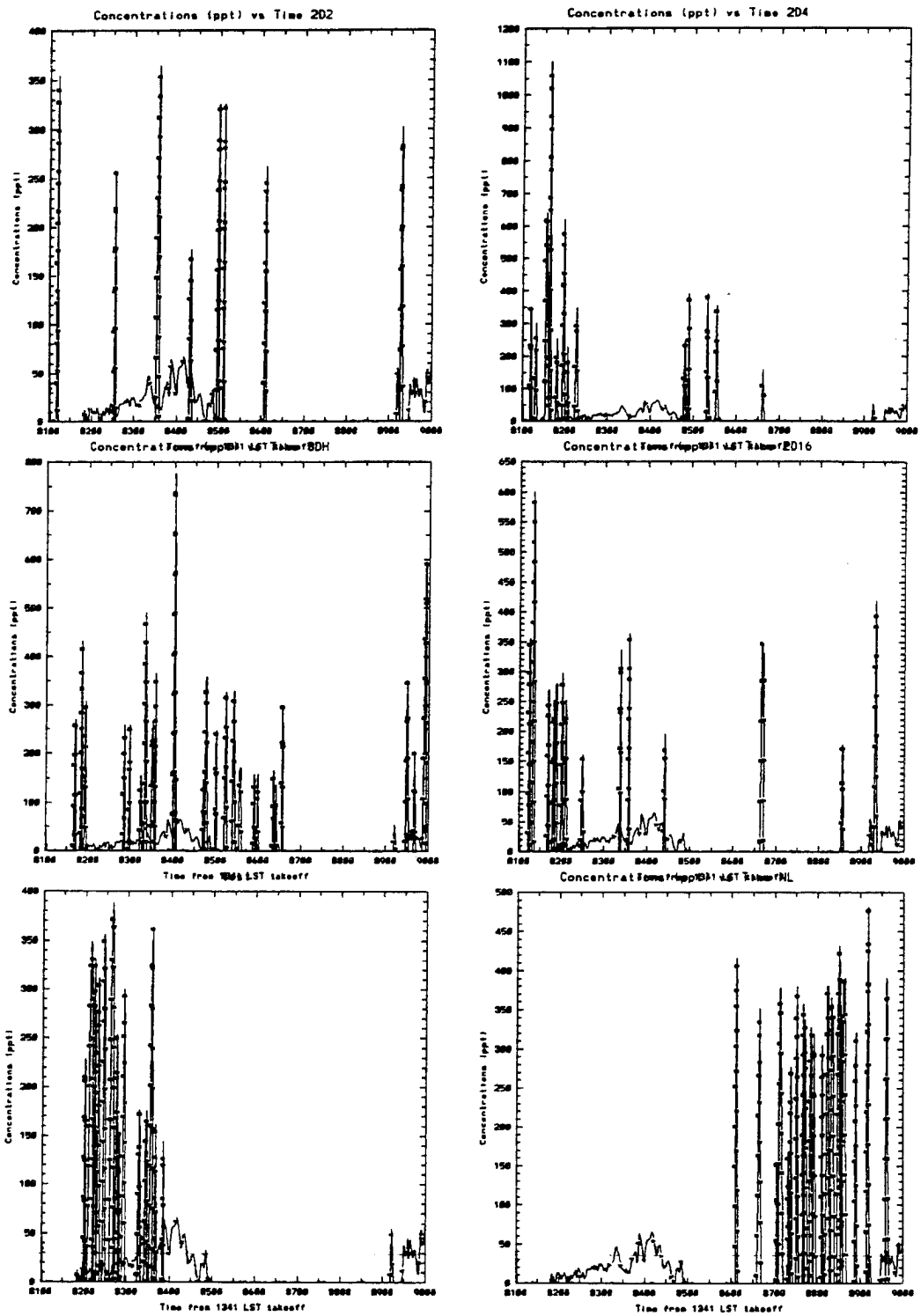

Figure 4.16: Concentration vs. time: A – observations; B – LPDM.

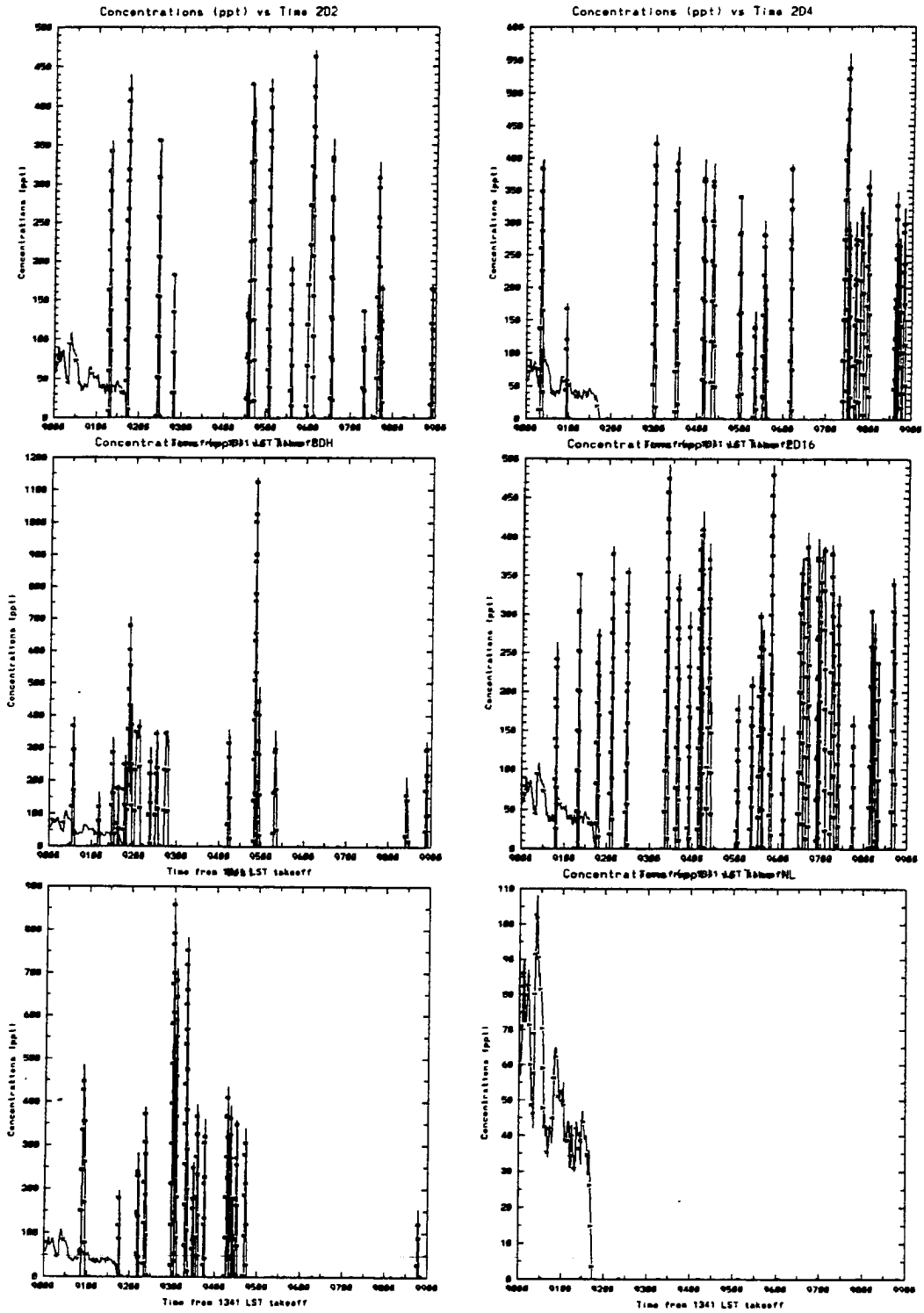

Figure 4.17: Concentration vs. time: A – observations; B – LPDM.

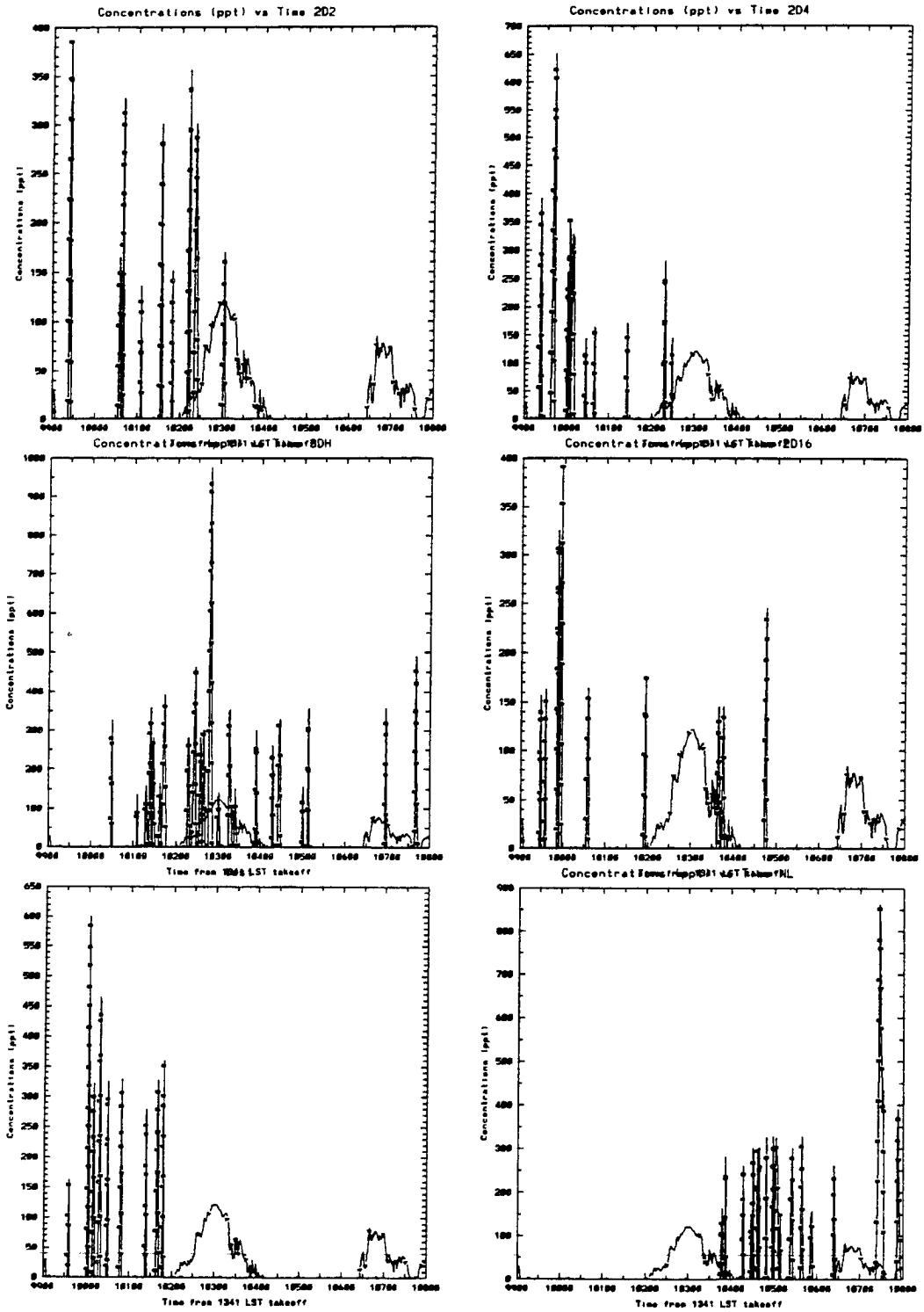

Figure 4.18: Concentration vs. time: A – observations; B – LPDM.

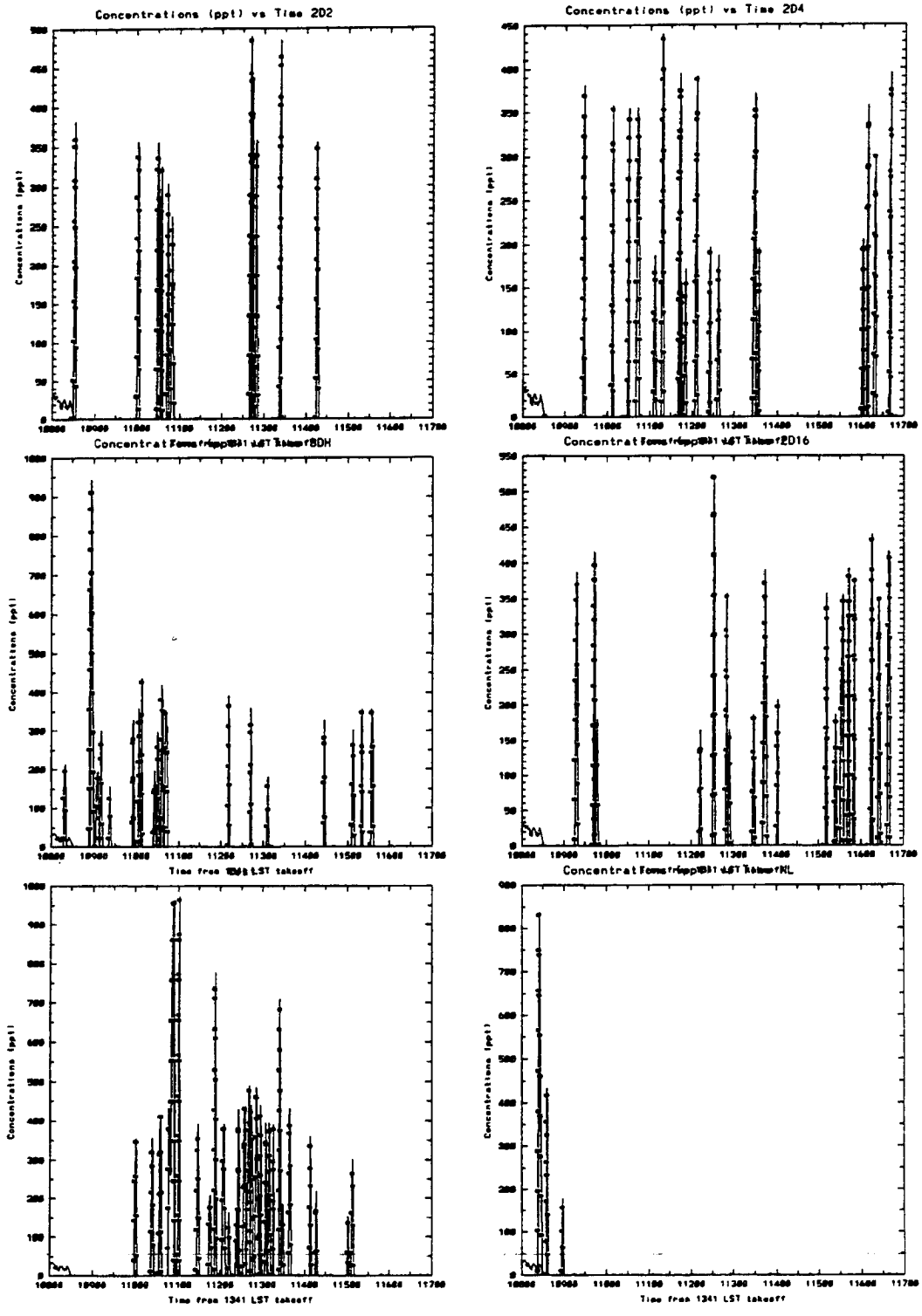

Figure 4.19: Concentration vs. time: A – observations; B – LPDM.

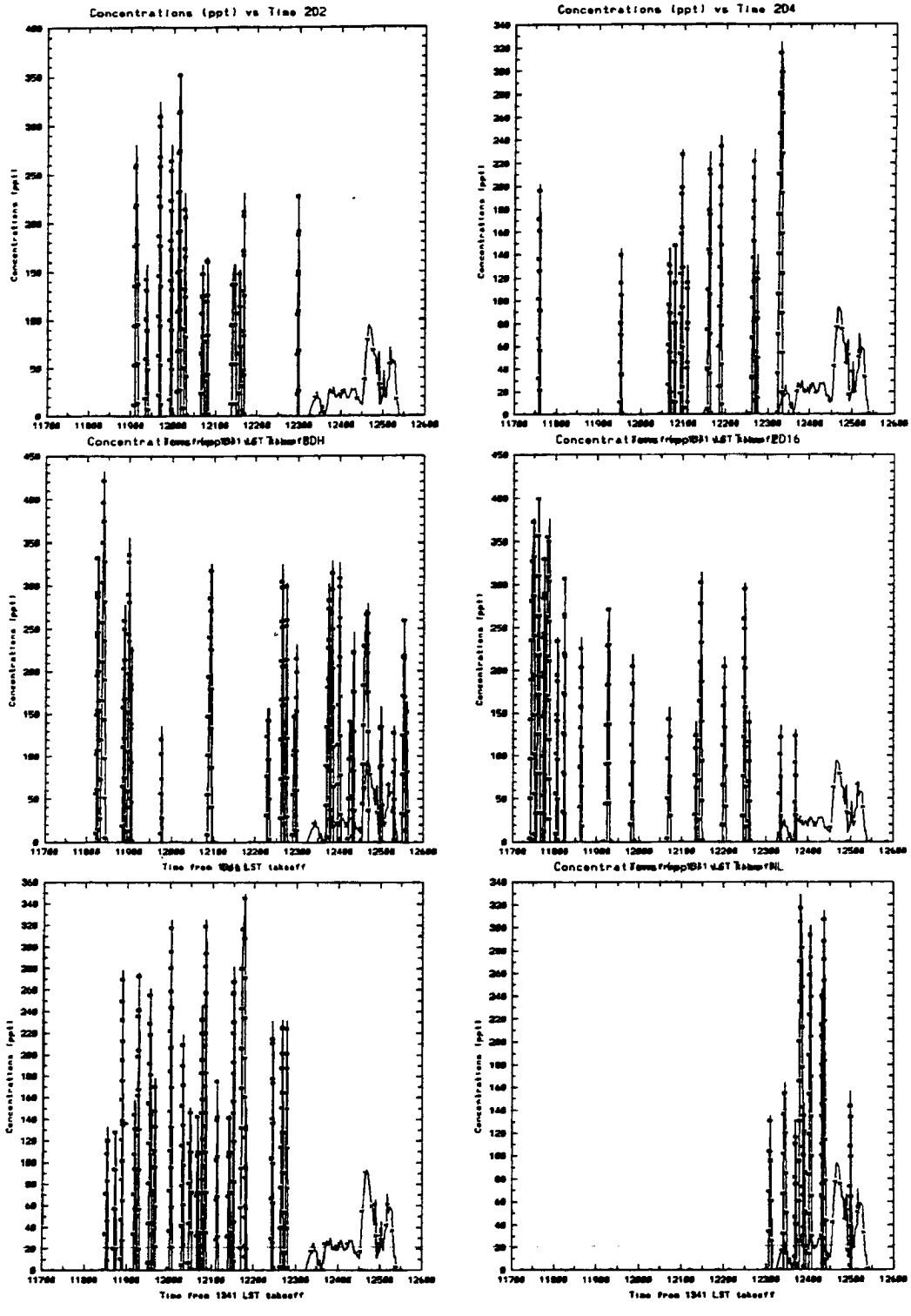

Figure 4.20: Concentration vs. time: A – observations; B – LPDM.

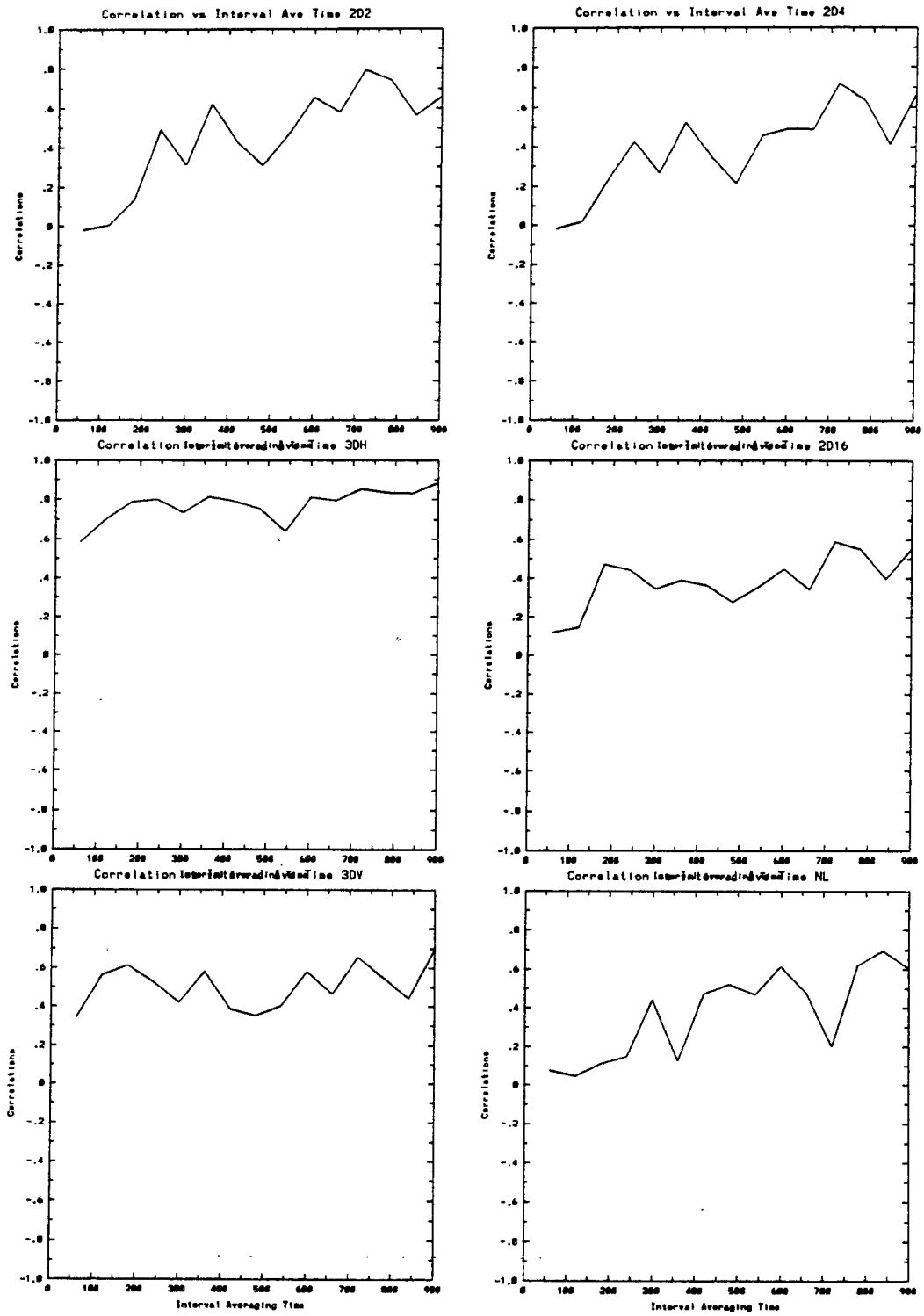

Figure 4.21: Correlation vs. interval averaging time.

times, ranging from 60 to 900 seconds. The results are displayed in Figure 4.21. It is clear that the 3DH shows remarkable correlations. The values range from .6 at 60 seconds to roughly .9 at 900 seconds. Notice that the 3DH line does not have the same amount of variability as the other plots. The 3DV results have the next best correlations, followed by 2D2 and 2D4. The similarity of 2D2 and 2D4 curves further supports the assertion that a 4km mesh is suitable for the 3D grids, and a 2 km mesh is not necessary. The NL and 2D16 show the least amount of correlation to the data, as expected. The order of agreement was quantified by integrating the area under the curves.

To give the reader a visual picture of the technique used is displayed in Figures 4.22 through 4.27. The software used to display the data is called $savi3D^{TM}$ and created by Supercomputer Systems Engineering and Services Company (SSESCO) of Minneapolis. The software allows the user to animate observational and model data, both LPDM and RAMS, at the same time. Figure 4.22 is an XY cross section taken 3 hours into the 3DH LPDM run. The flight path up to this time is shown as the solid yellow line. The blue segments within this line represent positions where the aircraft detected SF_6, and the orange segments are where both the LPDM and the plane detected SF_6. The red and white dots are the particle positions at this time. When the particles are released they are initially red. They turn white after undergoing one or more recirculations. It is apparent that the particles advect about 7 km, intercept the frontal boundary, and are advected aloft, at which time they can either undergo recirculation or proceed towards the other shoreline in the return flow aloft. The XZ cross section shown in Figure 4.23 is taken at the same time. Notice the complicated vertical structure. The effects of the return flow aloft is apparent, as particles located at this level have advected considerable distances.

The plume position 5 hours after release can be seen in Figure 4.24. There are nearly 80 percent recirculated particles, as shown by the large number of white dots. The lake breeze is beginning to collapse at this time, as evidenced by the solid white strip of particles about 5km inland. The vertical structure of the plume at 1741 LST is shown in Figure 4.25. Notice the general tilt downward over the lake of the area of highest particle density. A perspective view, taken from southwest of Zion, is shown in Figure

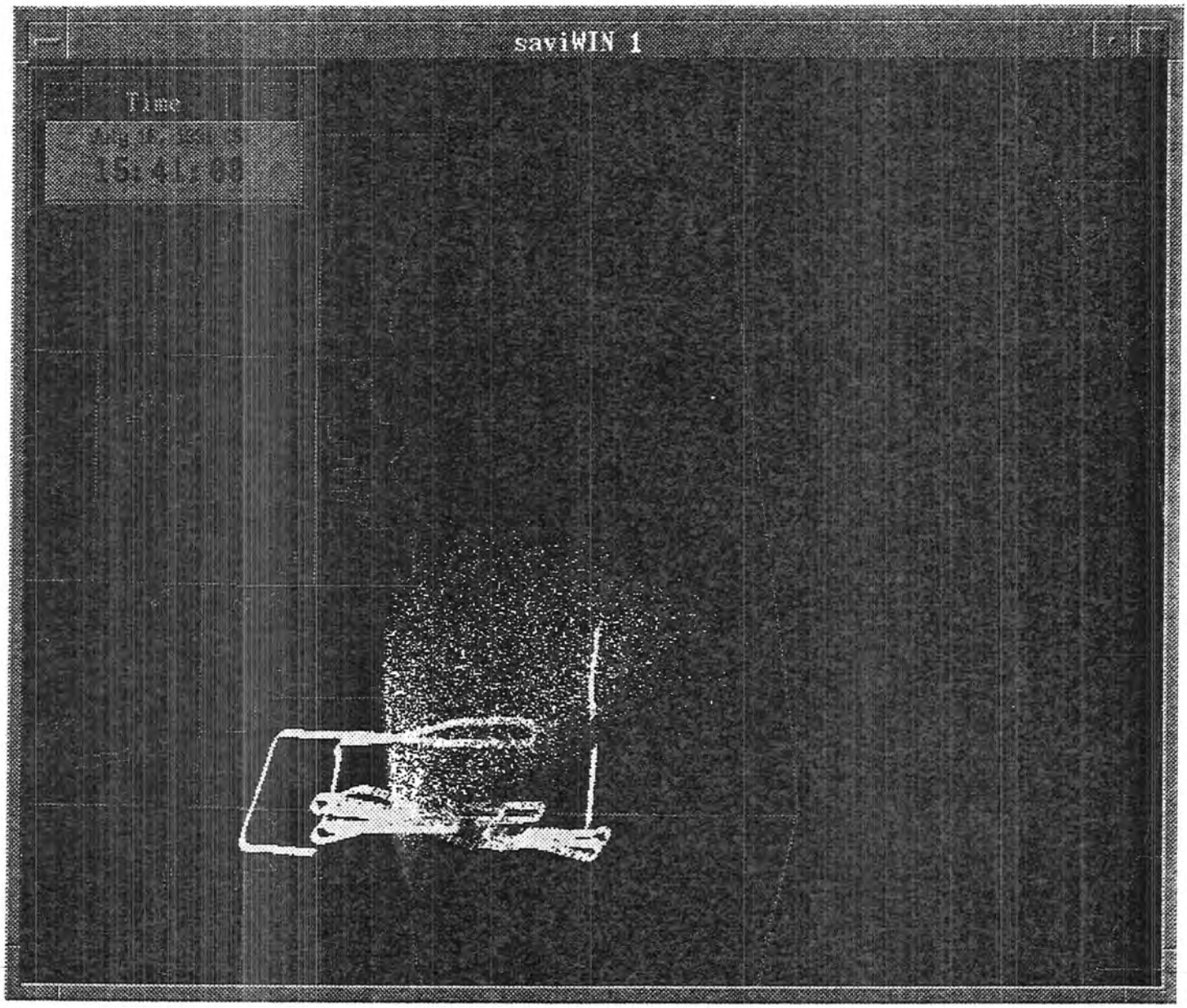

Figure 4.22: An XY cross section of the plume and flight path. Particles are emitted as red. White particles represent those that have undergone recirculation. The flight path is indicated by the yellow, orange, and blue line. The yellow indicates a null observation, orange a positive observation and LPDM value, and blue a positive observation and no LPDM value. Time is 1541 LST.

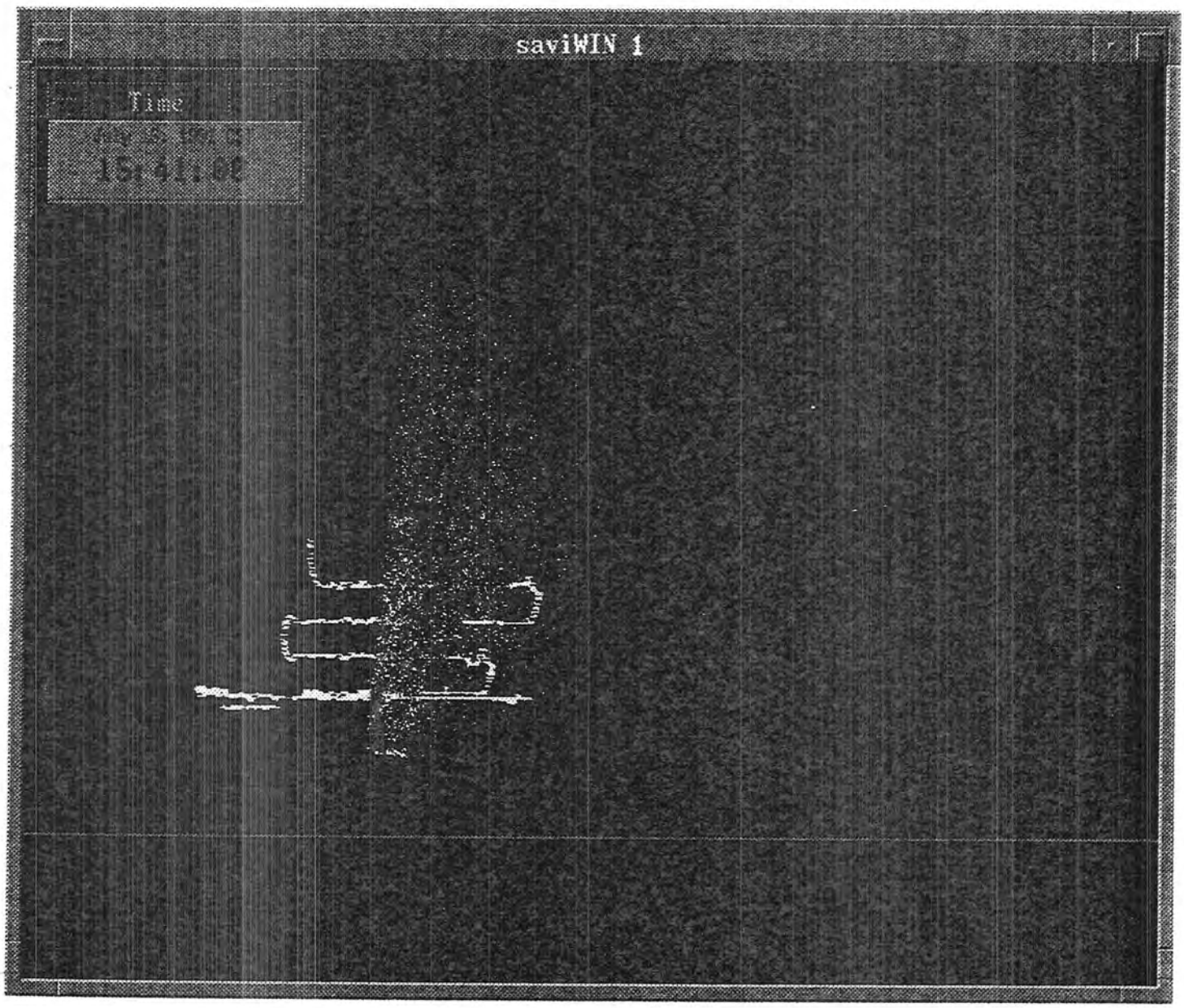

Figure 4.23: An XZ cross section of the plume and flight path. Particles are emitted as red. White particles represent those that have undergone recirculation. The flight path is indicated by the yellow, orange, and blue line. The yellow indicates a null observation, orange a positive observation and LPDM value, and blue a positive observation and no LPDM value. Time is 1541 LST.

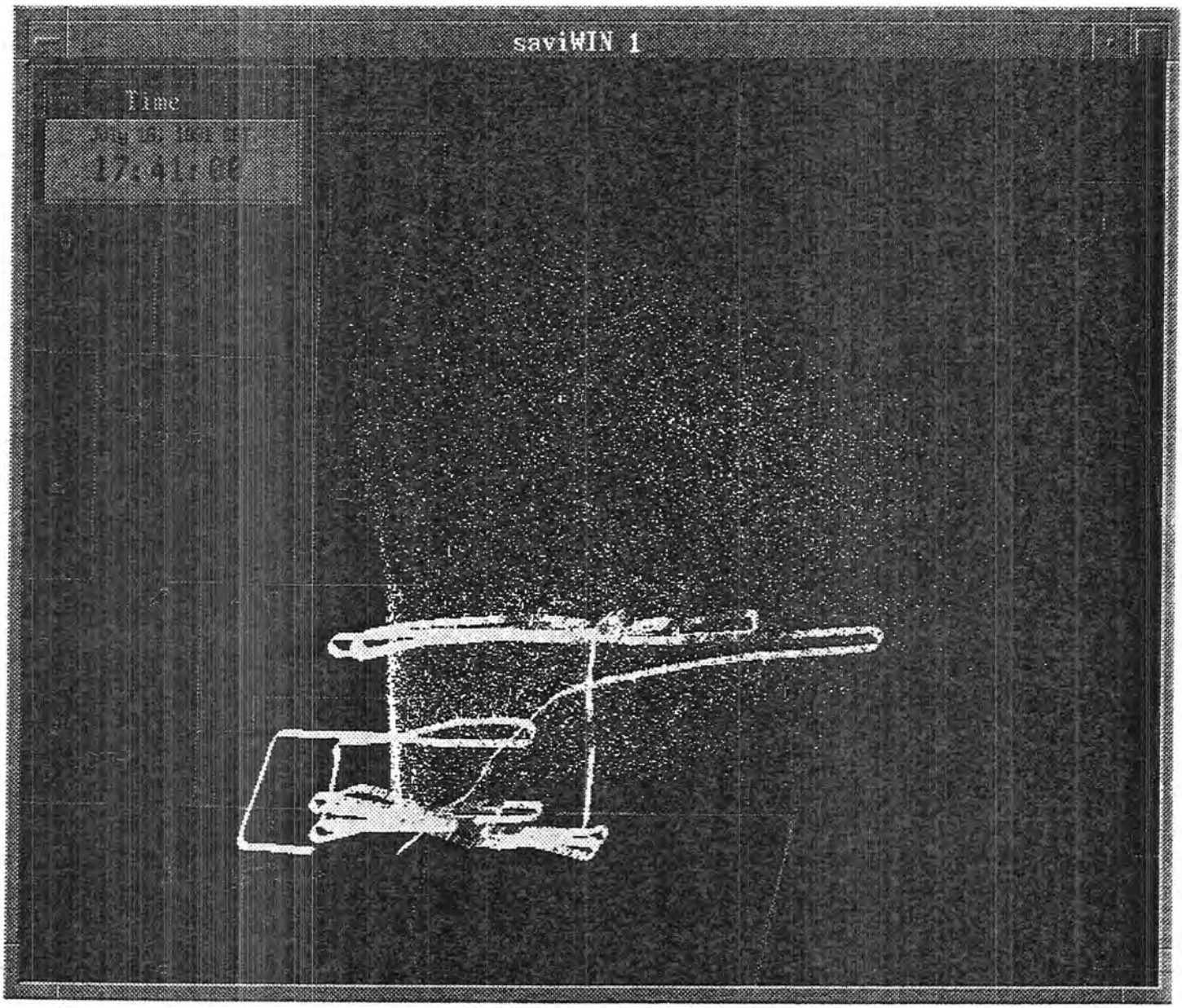

Figure 4.24: An XY cross section of the plume and flight path. Particles are emitted as red. White particles represent those that have undergone recirculation. The flight path is indicated by the yellow, orange, and blue line. The yellow indicates a null observation, orange a positive observation and LPDM value, and blue a positive observation and no LPDM value. Time is 1741 LST.

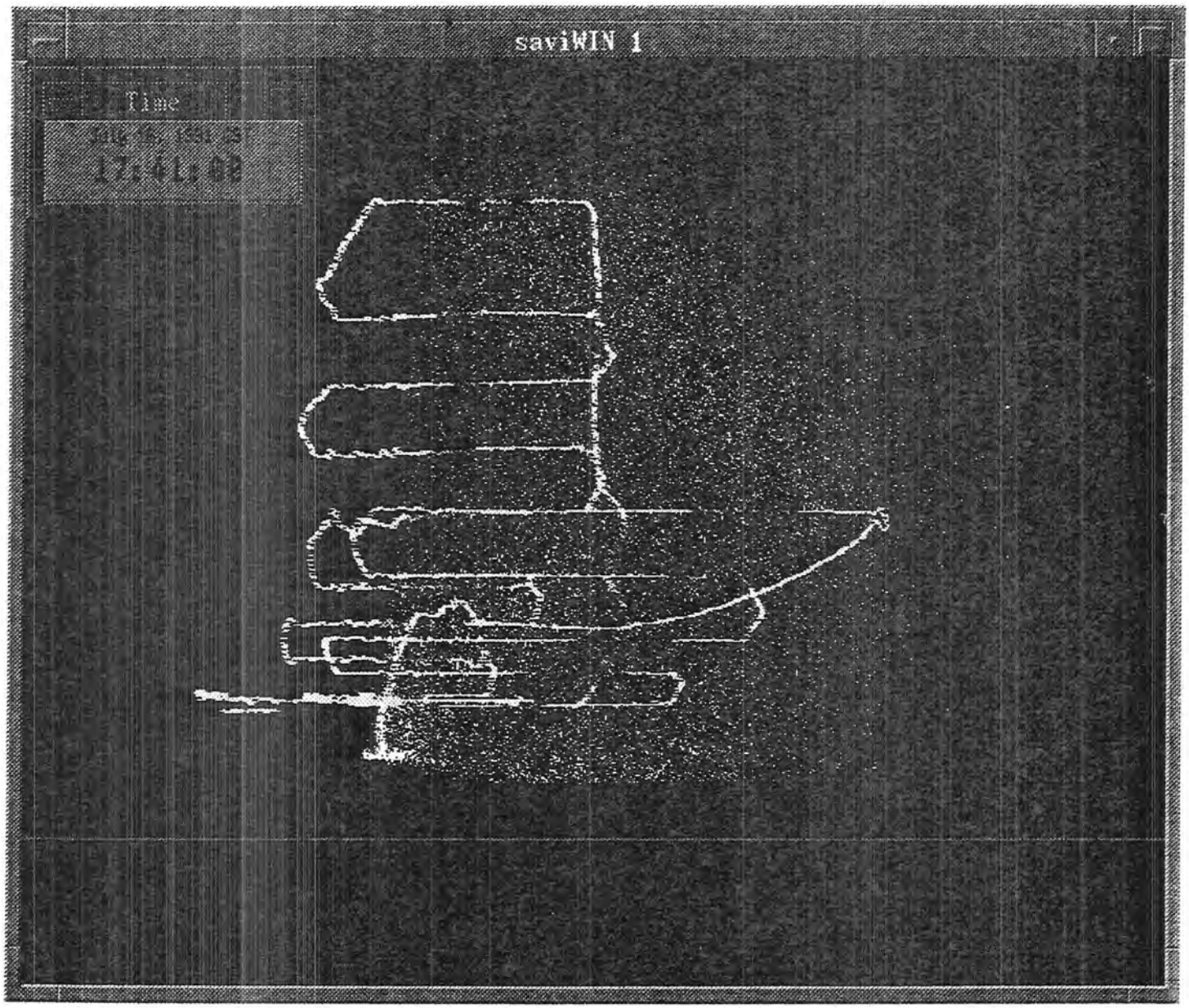

Figure 4.25: An XZ cross section of the plume and flight path. Particles are emitted as red. White particles represent those that have undergone recirculation. The flight path is indicated by the yellow, orange, and blue line. The yellow indicates a null observation, orange a positive observation and LPDM value, and blue a positive observation and no LPDM value. Time is 1741 LST.

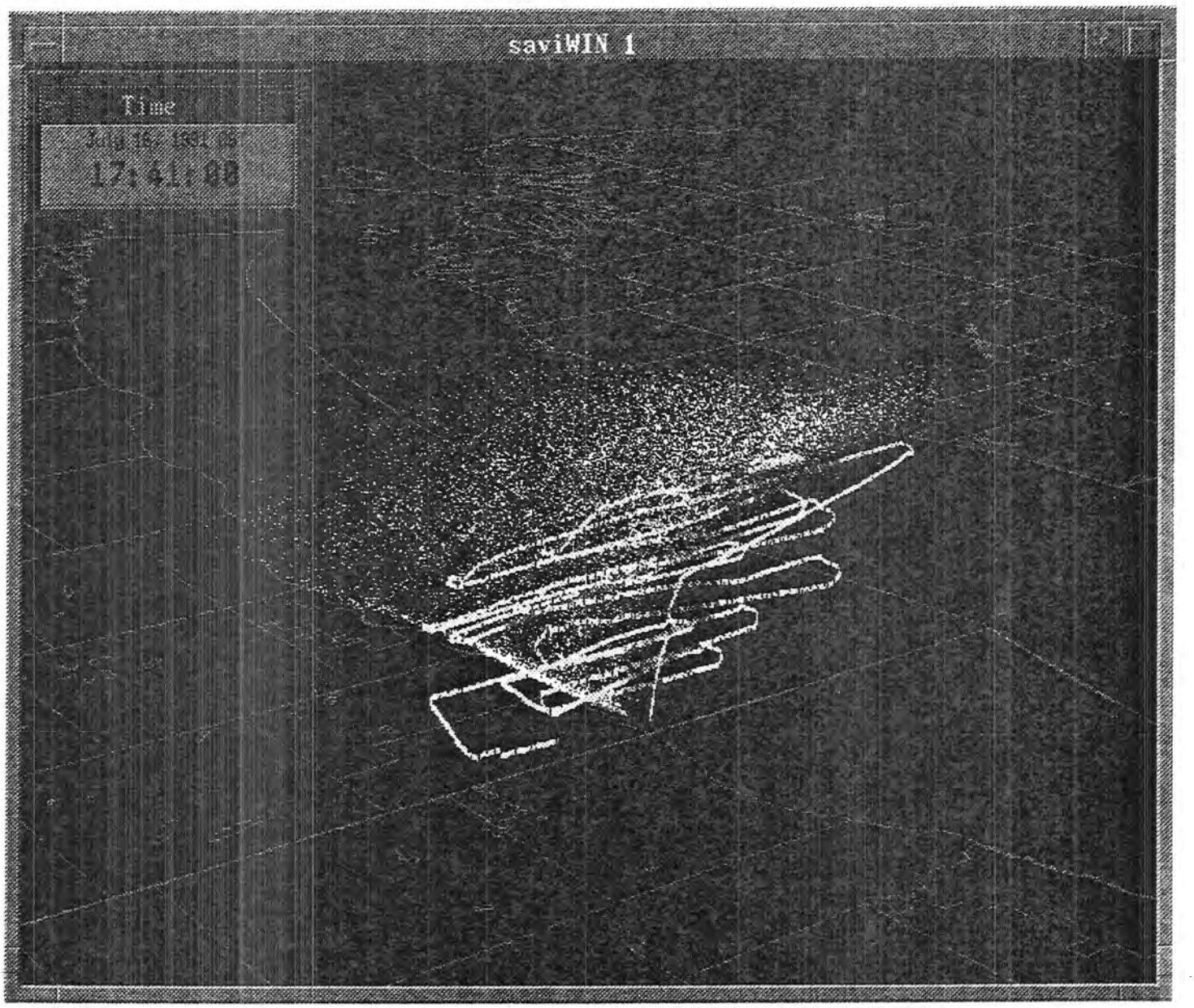

Figure 4.26: A perspective view of the plume and flight path from the southwest. Particles are emitted as red. White particles represent those that have undergone recirculation. The flight path is indicated by the yellow, orange, and blue line. The yellow indicates a null observation, orange a positive observation and LPDM value, and blue a positive observation and no LPDM value. Time is 1741 LST.

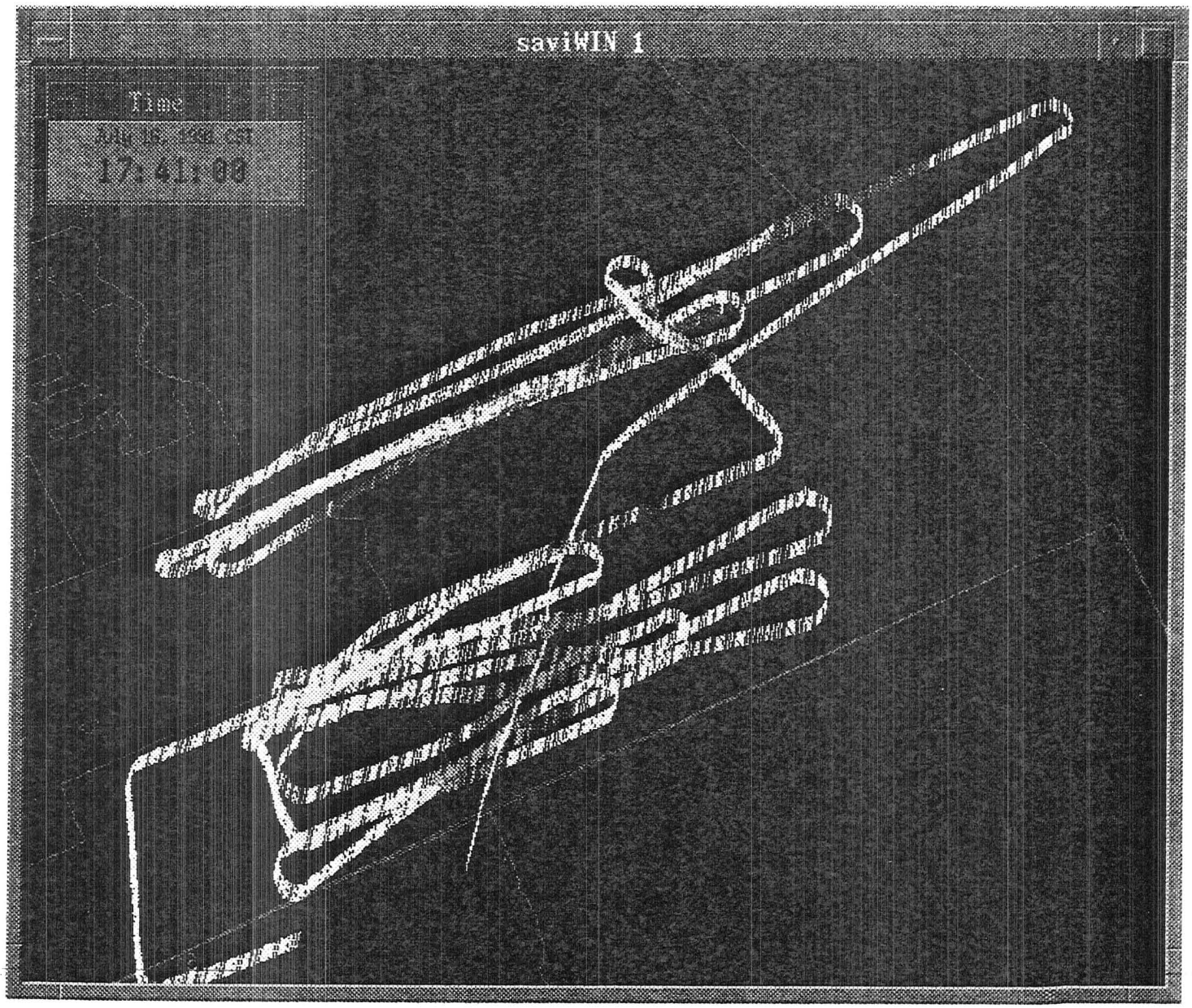

Figure 4.27: A perspective view, nearly overhead, of the flight path from the southwest. The flight path is indicated by the yellow, orange, and blue line. The yellow indicates a null observation, orange a positive observation and LPDM value, and blue a positive observation and no LPDM value. Time is 1741 LST.

4.26. Extracted at 1741 LST, this plot indicates a large amount of vertical transport as well as a perspective on the extent of the plume in the northern direction. Figure 4.27 is again taken from southwest perspective, at the same time, and represents the final flight path and shows the degree of agreement between the LPDM and the observations. Notice that nearly every segment of the flight path that is colored blue is interspersed with an orange segment, giving credence to the ability of the LPDM to represent the dispersion pattern of the tracer.

4.4 A Comparison of the ISCST and LPDM Models

One of the purposes of this study was to compare a Gaussian plume model to the LPDM. For this comparison the ISCST was run in an enhanced mode, where the meteorology from the 3DV run was used to drive the ISCST model. The 3DV results were used because the surface values were in excellent agreement with the observations. Normally the ISCST uses meteorological towers to supplement the nearest sounding. The information from the sounding is used to diagnose a probable PBL height. In this ISCST run the PBL height was supplied by the model, which varied from 1200 m at the time of the release to 1550 m by mid-afternoon. As mentioned in Chapter 1 there are some inherent weaknesses of Gaussian based models. As stated in Section 2, they are:

- Over-simplification of fundamental conservation relationships
- Inability to represent recirculation, i.e., wind profiles are unidirectional in the vertical
- The use of a constant stability class, although the terrain may be heterogeneous

Reviewing Table 4.1, it is apparent that the second difficulty listed above should be clearly visible in any comparison. Armed with the knowledge that the 3DH LPDM simulation is in agreement with the observations, at least 70 percent of the material should recirculate. In addition, a probable transport pattern scenario would be that the material is first advected to the frontal boundary, then it is carried aloft by the frontal updraft at which point it may either recirculate in proximity to the frontal zone, or be injected

into the return flow aloft. Since the wind aloft is southwesterly, and the surface winds are southeasterly, the ISCST will not predict either one of these situations correctly.

As seen in the meteorological plots from Section 3 of this study, near the shoreline the stability goes from a class A (unstable) Pasquill-Gifford class inland of the front to a class F (stable) front. This raises the probability that the third difficulty listed will be of concern.

Figures 4.28 through 4.35 show surface isopleths for an ISCST run in the left hand column, and surface isopleths for the 3DH LPDM simulation. The isopleths are produced using a logarithmic scale, with the contours in terms of the log of the concentration in *ppt*. The panels are in 15 minute increments, with each figure showing 30 minutes of data. The domain size in each panel is 37.5 km $\times$ 37.5 km. Figure 4.28 shows the solutions for 1245 LST in the top two panels, and those for 1300 LST in the bottom panel. The differences between the ISCST and LPDM are striking. As expected difficulty arises for the ISCST when the particles reach the frontal boundary and are transported aloft. Clearly the ISCST can not handle this situation. In addition, the use of the wrong stability class further complicates the situation. Notice how quickly the ISCST plume widens, this is not what was observed. The trend continues over the next 4 hours (see Figures 4.29 - 4.35). It is apparent that the ISCST model also has a tendency to overpredict the concentration values. Many of the isopleths were on the order of 100000 ppt while at the same time the LPDM predictions were on the order of 1000 ppt near the source and dropped off to roughly 100 ppts away from the source. The problems encountered by the ISCST were entirely predictable, and verified by the results. Clearly this model should not be applied to areas that mesoscale circulations can dominate.

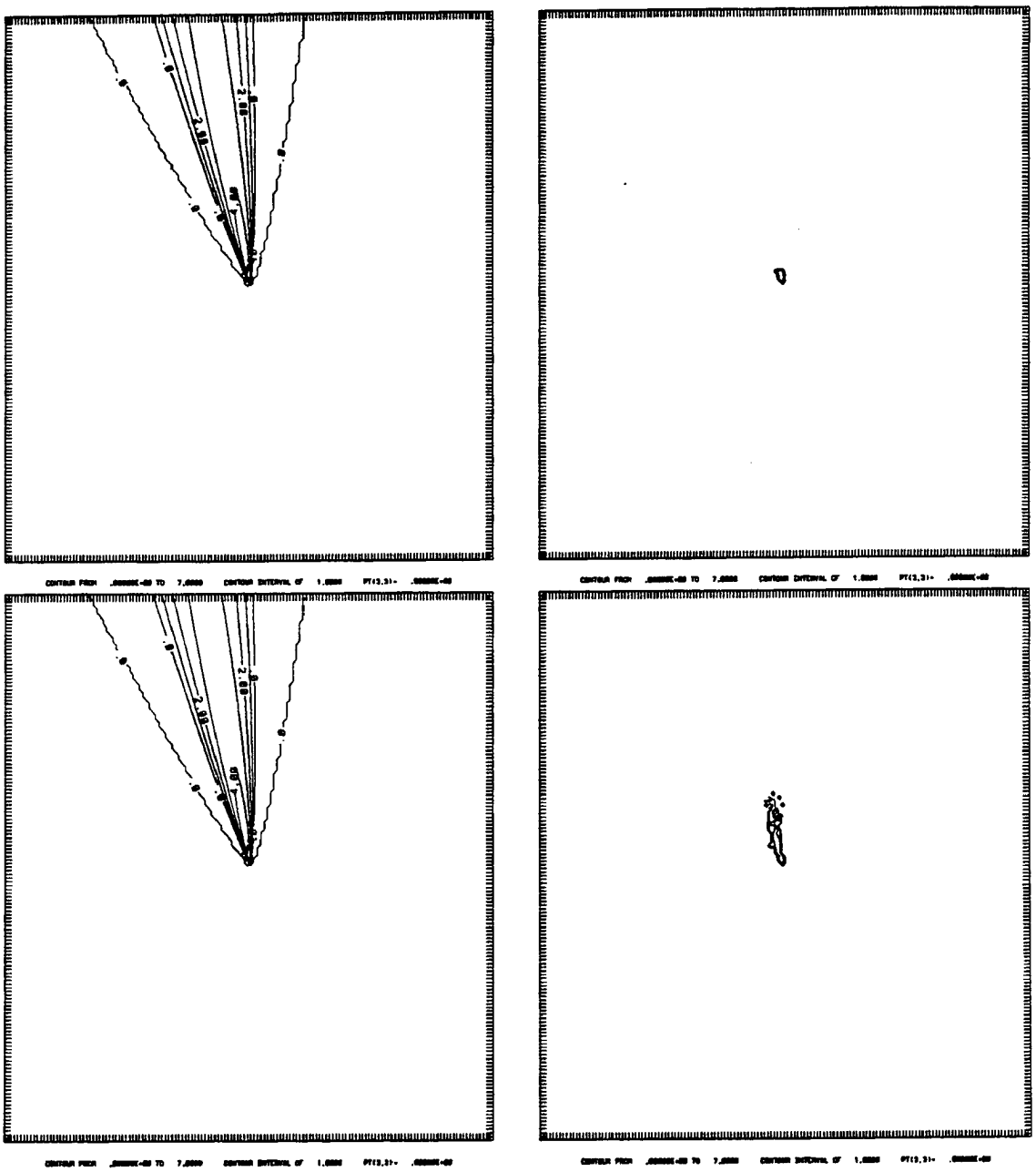

Figure 4.28: Surface isopleths in LOG (ppt). Left – ISCST; Right – LPDM.

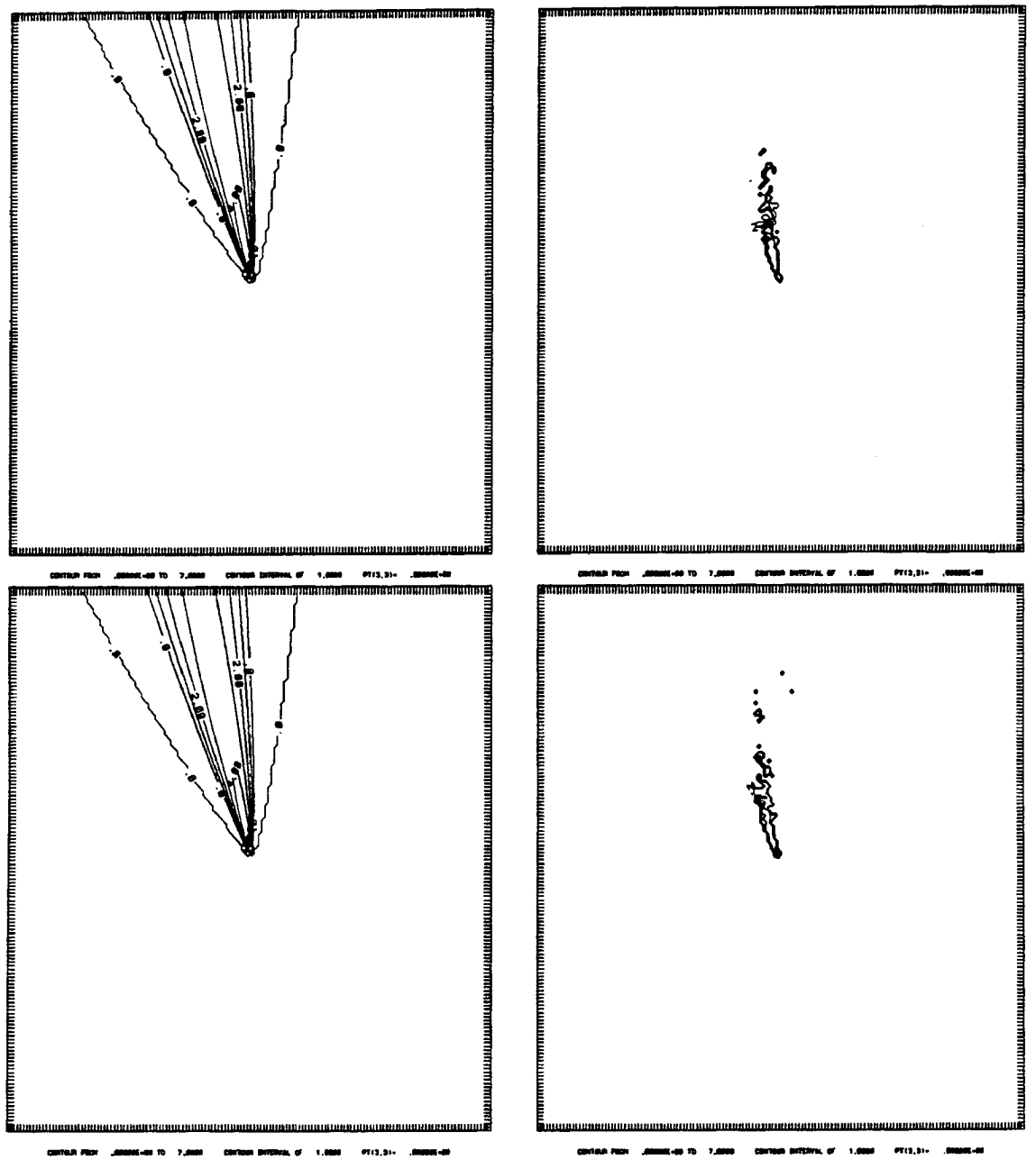

Figure 4.29: Surface isopleths in LOG (ppt). Left – ISCST; Right – LPDM.

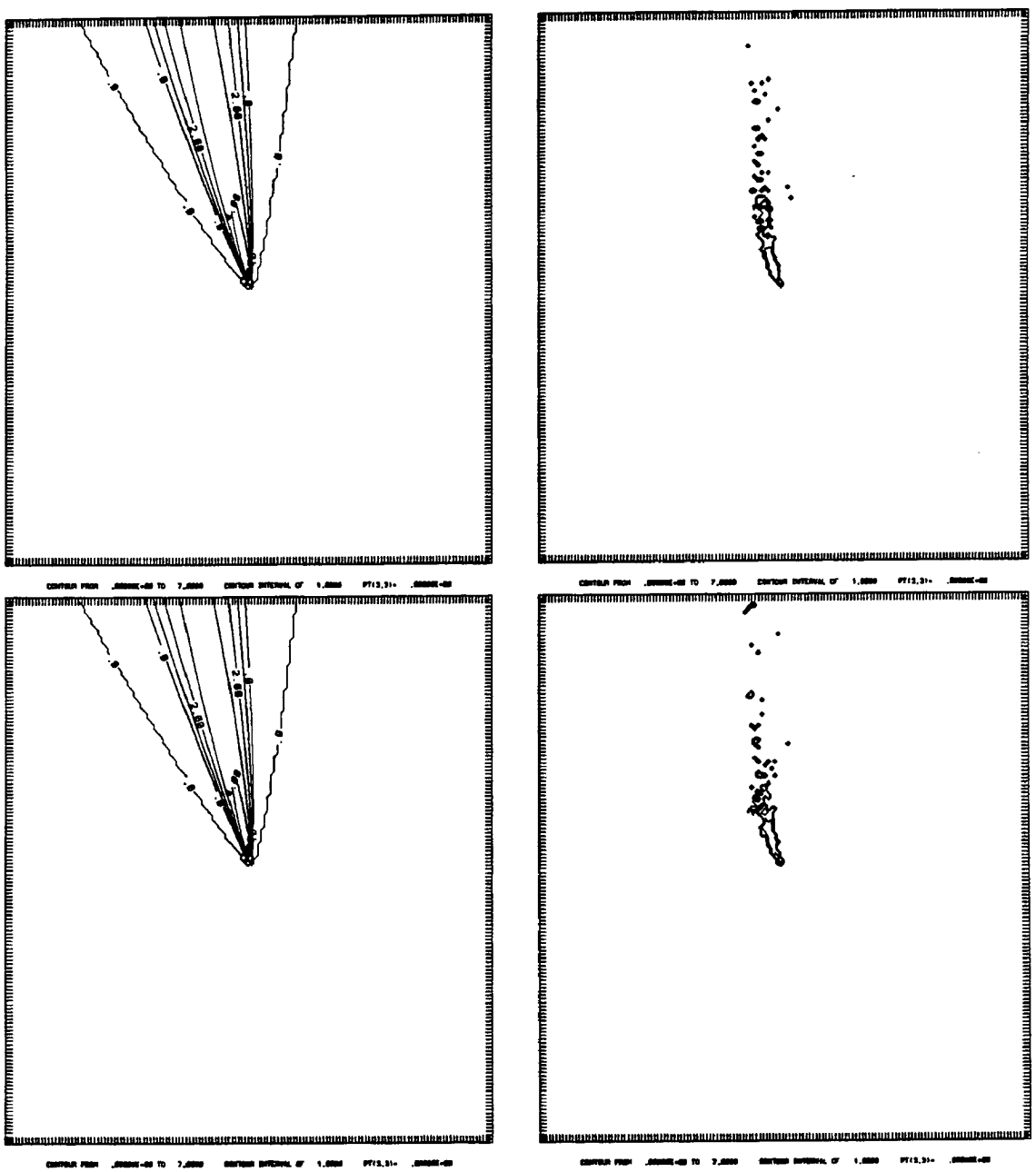

Figure 4.30: Surface isopleths in LOG (ppt). Left – ISCST; Right – LPDM.

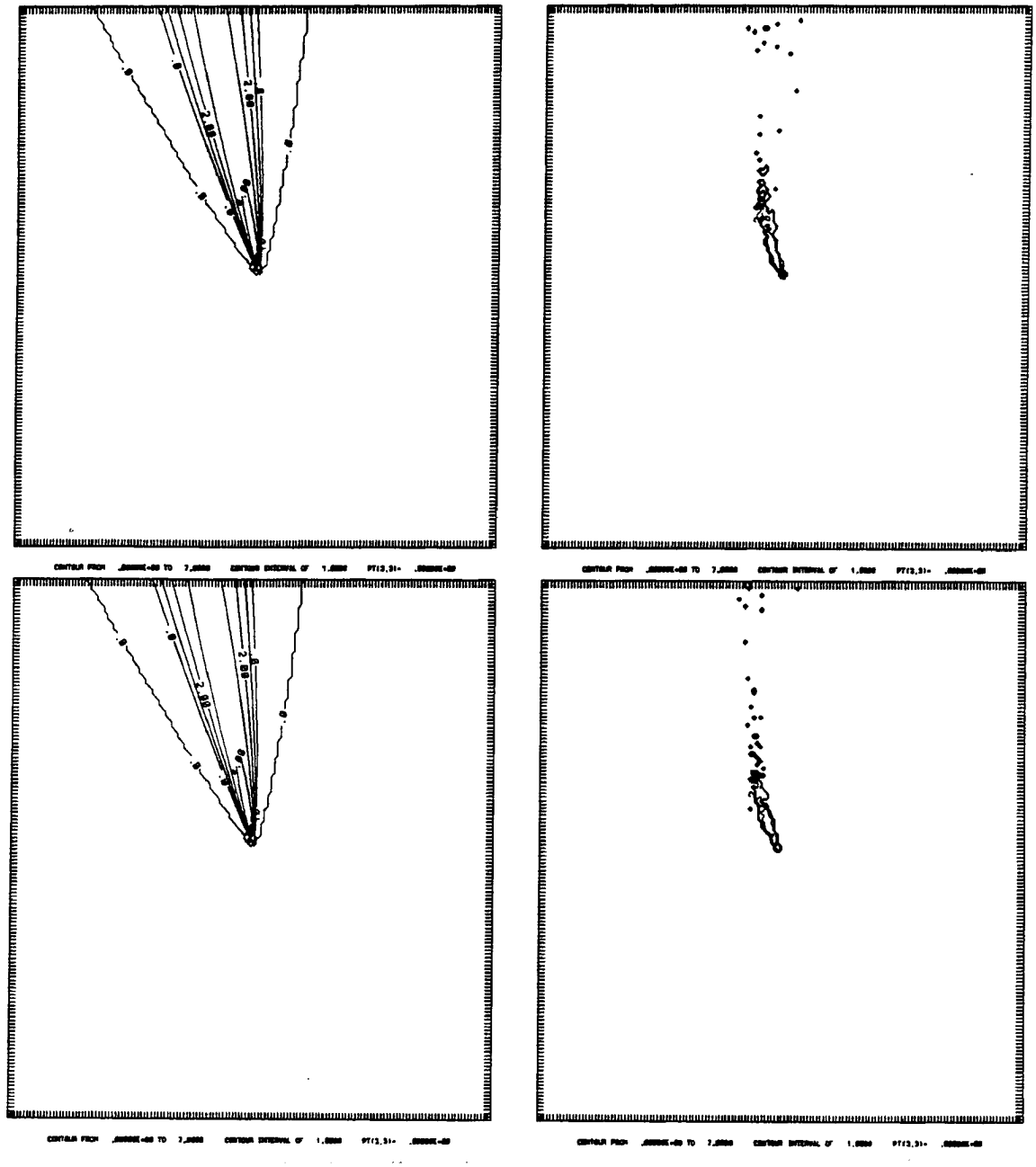

Figure 4.31: Surface isopleths in LOG (ppt). Left – ISCST; Right – LPDM.

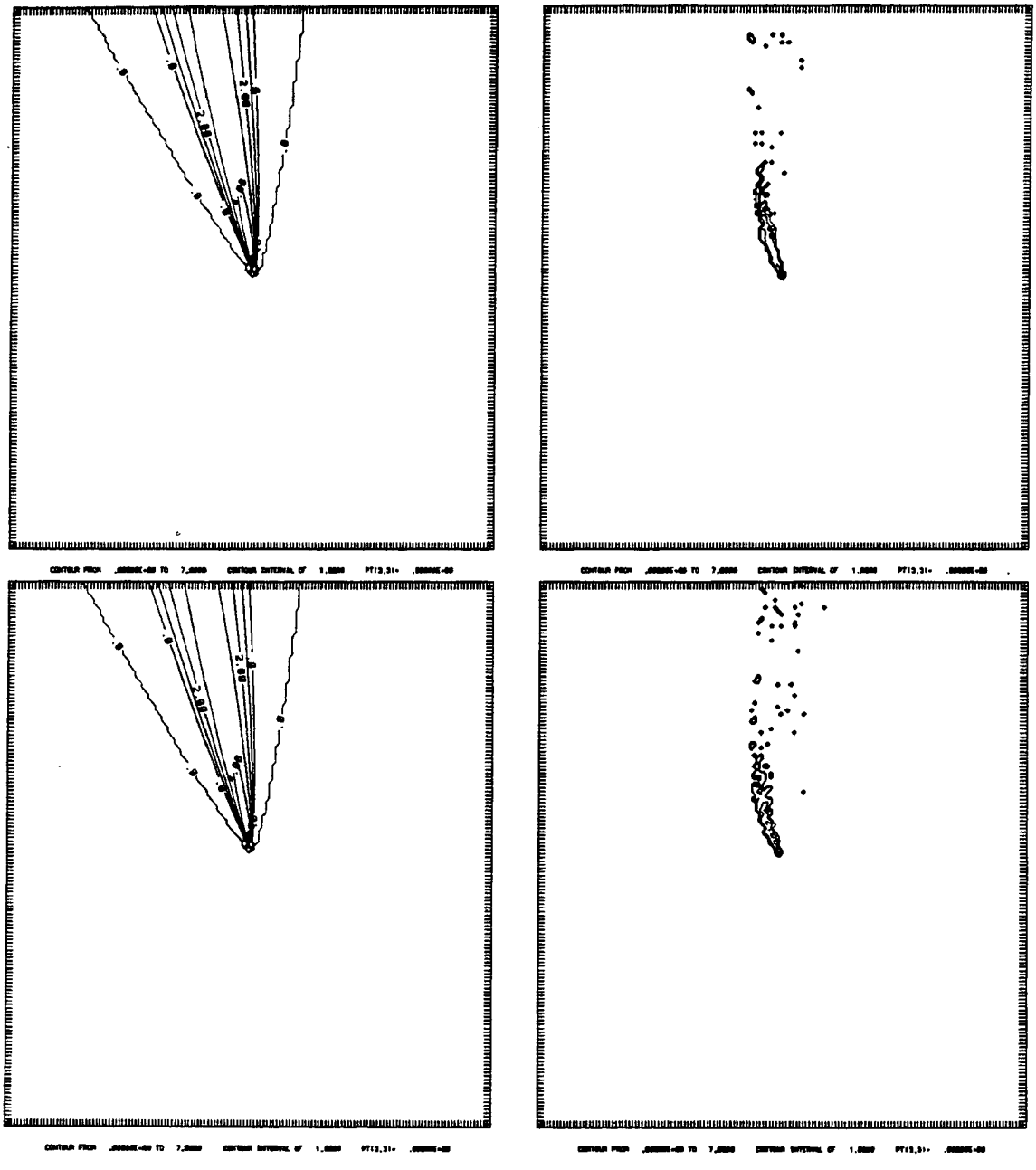

Figure 4.32: Surface isopleths in LOG (ppt). Left – ISCST; Right – LPDM.

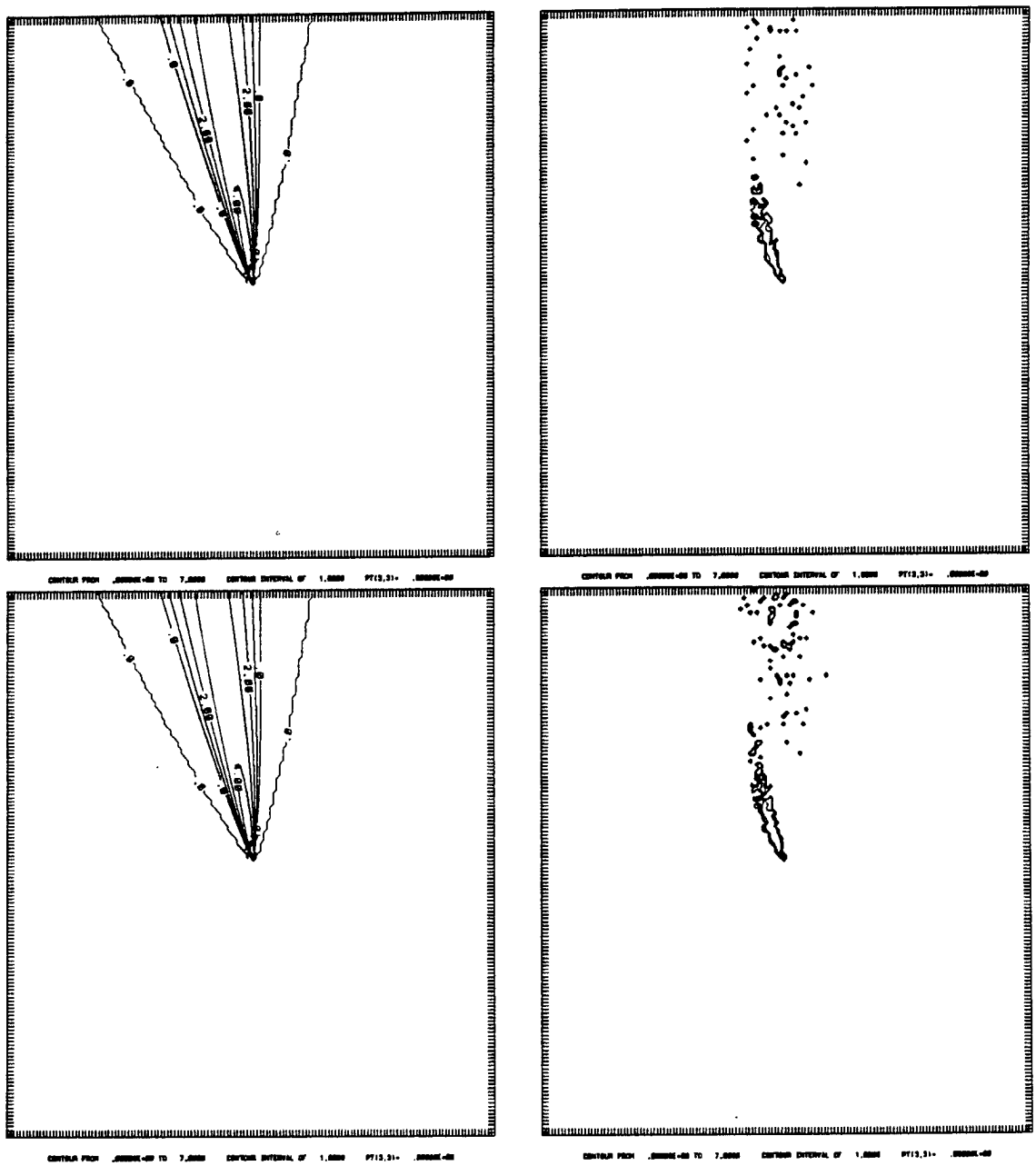

Figure 4.33: Surface isopleths in LOG (ppt). Left – ISCST; Right – LPDM.

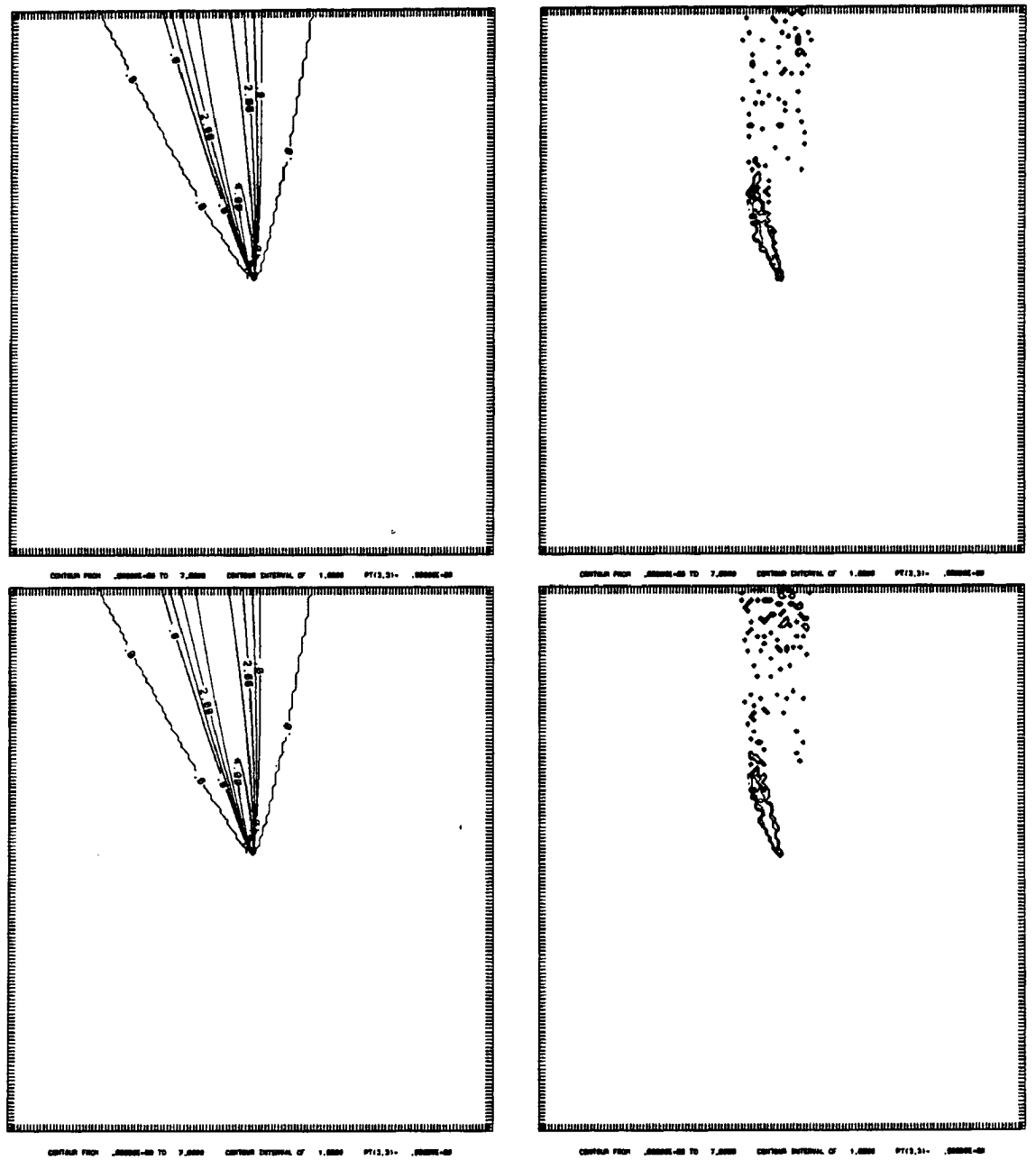

Figure 4.34: Surface isopleths in LOG (ppt). Left – ISCST; Right – LPDM.

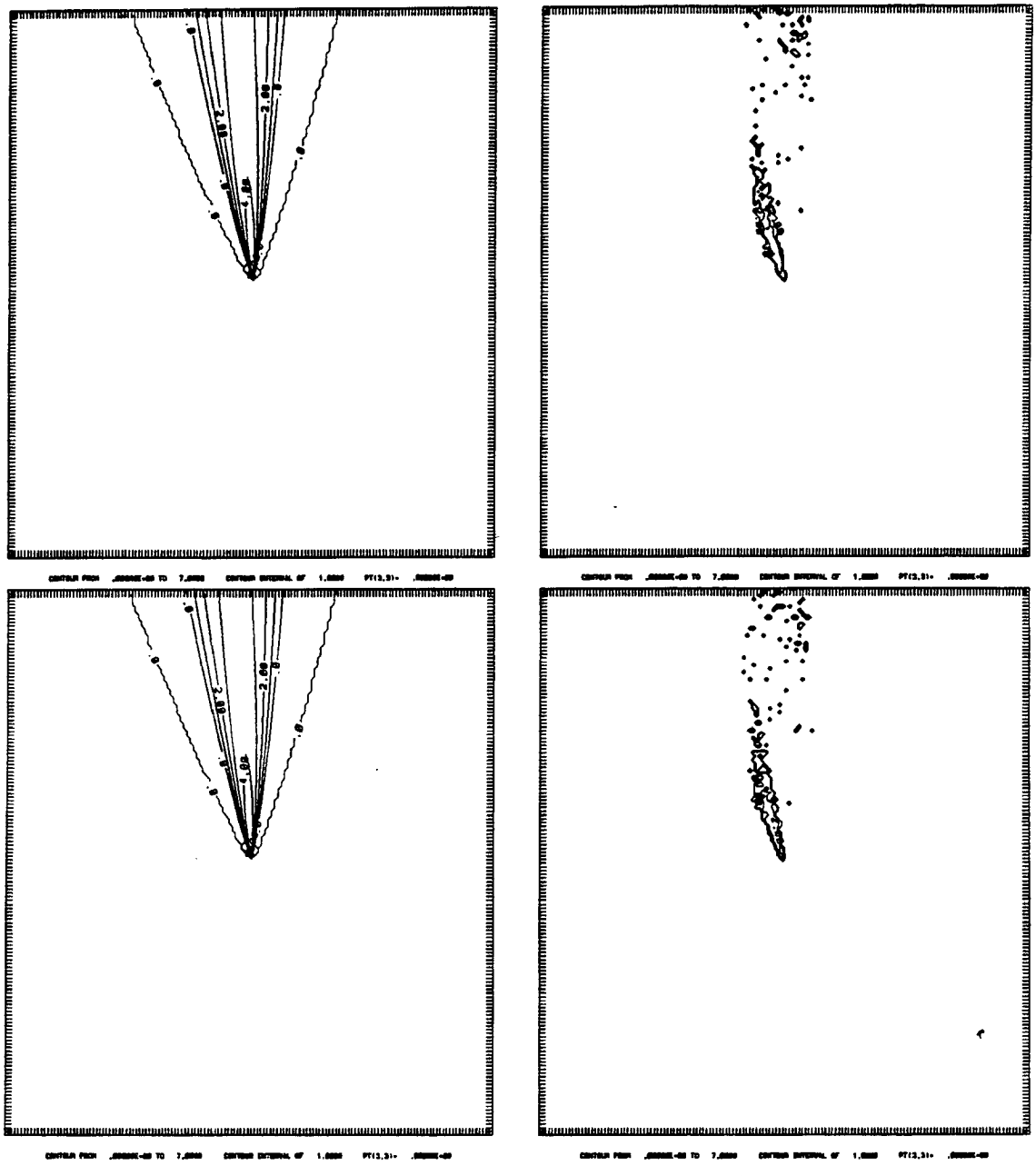

Figure 4.35: Surface isopleths in LOG (ppt). Left – ISCST; Right – LPDM.

Chapter 5

SUMMARY AND CONCLUSIONS

5.1 Summary

The introduction discusses some of the general air quality trends in the Lake Michigan basin, where a high number of days exceeded the federal ozone standards. The complex circulations and photochemistry associated with land lake interactions, and the urban buildup along the coastline are felt to be important causes of the large number of exceedances. A field program (LMOS) was developed to understand the source-receptor relationships in this region.

Chapter 2 provided the background information on the previous mesoscale dispersion studies. Of the 25 studies shown in Table 2.1 none attempt to provide a vertical distribution of the tracer at the resolution obtained from the LMOS aircraft data. The vertical distribution is particularly important for verifying numerical vertical transport in the land lake regime. In addition, a brief overview of the scope of the LMOS project was provided.

In the first section of Chapter 3 a discussion of the observations from July 16, 1991 were presented. They showed the presence of an anticyclone over the eastern U.S., typical of summertime eastern U.S. climatology, and generally conducive to formation of a lake breeze on the western shore of Lake Michigan. Geostrophic winds were strong preventing deep inland penetration, also contributing to the formation of a shallow, weak lake breeze.

The meteorological simulations were discussed in the next section. It was found that simulations with 4 km or less grid spacing simulated the event realistically. The NL and 2D16 simulations were not representative of the lake breeze of July 16, 1991. The 2D2 and 2D4 simulations showed a stronger convergence and inland penetration, while the 3D runs exhibited a realistic penetration, according to observations. A set of statistics

were run to verify the model results. Wind speed, direction, temperature, and dewpoint measured at the meteorological towers positioned around the Zion Nuclear Power Plant were correlated to meteorological towers extracted from the RAMS data set for the entire suite of simulations. The highest correlation was calculated using the 3DV data set, with the rest of the simulations showing similar results.

In Chapter 4 the meteorological data was used by the LPDM to mimic the SF_6 release of July 16, 1991. The release, from Waukegan Harbor, Illinois, was 4 hours in duration. The results from the LPDM demonstrated a remarkable impact of the lake breeze circulation on dispersion. It was found that upwards of 65 percent of the particles released by the LPDM underwent at least one re-circulation.

A simulated aircraft was flown through the resultant plume and a variety of correlations were computed with he actual aircraft data. This was found to be necessary because of the fine temporal and spatial resolution of the aircraft data versus the fixed temporal resolution of the LPDM derived fields. The LPDM results were somewhat different in terms of model accuracy as found from the results of the meteorological simulations. It was expected that the most highly correlated meteorological simulations would produce the best dispersion results. Contrary to this assumption, which will be discussed further later in this Chapter, the 3DH correlations were, on average the highest, followed by 3DV, 2D2, 2D4, 2D16, and finally NL. Overall, the LPDM showed excellent skill in predicting the spatial and temporal distribution of the concentration fields. This allowed a degree of certainty to be assured when comparing the best LPDM results to other models.

Near the end of Chapter 4, a brief comparison of the ISCST model and the LPDM was performed. A side by side comparison of the surface concentrations derived from the 2 models showed remarkable differences in structure and magnitude. The ISCST not only overpredicted the magnitudes, it also produced the typical Gaussian shape, with concentrations predicted to reach far inland. The LPDM concentrations were confined to be significant only in close proximity to the release.

5.2 Conclusions and Recommendations

There are several major and minor conclusions that can be drawn from the results of the study.

- The RAMS model showed remarkable skill simulating the lake breeze of July 16, 1991.

  As previously mentioned, it was believed that the most highly correlated meteorology would translate into the best dispersion results. However, the correlations of the meteorological observations and the simulations were surface based. All tower observations used were taken at 10 m or less. The winds that effect the plume the longest are those aloft, above the depth of the inflow, which was roughly 200 m in depth. The surface information was used because of the temporal and spatial sparseness of the upper air data.

- The RAMS/LPDM coupled model system results demonstrate skill in predicting the observed tracer concentration fields.

  The 3DH LPDM simulation results were highly correlated to those observed by the simulated aircraft. The fact that it had a higher correlation than the 3DV simulation is not surprising, since, as mentioned in the preceding paragraph, the meteorological validation was biased to near surface observations. The LPDM results point to a possible weakness in the system using nudging and data assimilation. The spatial sparseness of the upper air data and the NMC analysis could actually be the cause of this weakness. The NMC analysis is performed on a $2.5° \times 2.5°$ grid, which represents roughly 300×300 km. The rawinsonde stations are generally further apart than this. Thus any information used in nudging is obtained by interpolating between data points separated by distances much larger than the mesh size. If there is a strong localized ageostrophic component to the flow the solutions obtained by nudging will tend to diverge from the proper solution, since the information aloft has some basis on $2.5° \times 2.5°$ analysis.

- The lake plays a profound role in altering the wind patterns associated with the Lake Michigan basin.

  The results presented in Chapter 3 demonstrate this rather dramatically. Ageostrophic wind components developed throughout the periphery of the entire lake. On both shores, the lake breeze developed with a complex variety of magnitudes depending on the highly irregular shape of the coastline. In addition, a mesohigh developed over the southeastern portion of the lake. This in turn lead to a convergence zone southeast of the lake. Inspection of the surface winds leads to the conclusion that parcel trajectories originating from the mesohigh area could cover a full 360° of motion.

  The particle modeling results were equally dramatic. Table 4.1 displays the lake influence with clarity. With no lake present there were no particle recirculations, while the rest of the simulations showed that particle recirculations were undertaken by more than 65 percent of the particles. The no lake simulation showed a plume advecting to the northeast, while the other simulations indicate particles dispersing in directions ranging from the west to the east-northeast.

- The ISCST model does not produce realistic tracer concentration fields for this coastal regime.

  This was expected based on the weaknesses outlined in Chapters 2 and 4. It would be surprising if a Gaussian plume model would be more successful than the RAMS/LPDM couplet anywhere where surface heterogeneities, wind shear, or any other mechanisms that lead to vertical transport or heterogeneous stability class are present. It is inherent in the derivation of the Gaussian plume model equations that these situations are not represented realistically.

- The 3D RAMS/LPDM system demonstrated more skill in predicting the evolution of the tracer field than the 2D RAMS/LPDM system, despite one of the 2D simulations employing a ΔX one half the size of the finest ΔX used by the 3D simulations.

This was a result of the strong convergence and inland penetration predicted by the 2D system. Considering that the plane is sampling the plume at roughly 1 second intervals, it would be expected that the precise prediction of the location of the lake breeze front is crucial to the predictions produced by the LPDM simulations. As noted in Chapter 3 the 2D simulations reached the 8 km tower location, and, thus went past this location to some degree, while the 3D simulations did not penetrate past this point. Assume, for instance, that the 2D frontal position prediction was 1 km too far inland (actually it was more than this). With respect to the motion of the plane, which was travelling at roughly 70 m s^{-1}, this is over 14 sampling periods. Clearly, this will decrease the magnitude of any correlation calculated.

- A grid spacing around 4 km in the horizontal direction is necessary to correctly model the lake breeze of July 16, 1991.

  This conclusion, of course, is more general than an application to this particular day. This comes from experience in modeling land/lake breezes, and a suite of sensitivity studies used to decide on the configuration of the various meteorological simulations performed in this study. The suggestion that at least $4\Delta X$ is needed to resolve a feature (Pielke, 1984), implies that the characteristic length of the lake breeze for this day was 16 km during the earlier hours of its development. During the first two hours of lake breeze onset the horizontal size of the inflow is roughly 16 km in magnitude. The horizontal extent of the feature does increase in magnitude as the simulation time approaches mid-afternoon, as indicated by the late onshore arrival of the 2D16 lake breeze front.

5.2.1 Recommendations for Further Research

There are several ideas for future work that will hopefully be pursued.

- A similar set of simulations should be performed for June 26, 1991. This day was another day with a tracer release and was characterized by a stronger lake breeze.
- Examine how the lake impacts the photochemistry of the region. Some of this work has begun using the Urban Airshed Model (Morris et al., 1992)

- One should use NAPAP gridded emissions data to ascertain the impact of the lake upon emissions from the entire region. Even a simple volume release from Chicago would provide information about the dispersion of Chicago's pollutants. This should be contingent on the incorporation of realistic urban land use data into RAMS.
- A series of comparisons with other EPA approved models, such as the Offshore Coastal Dispersion model (OCD) (Hanna et al., 1985). This model is a Gaussian model, but has corrections for internal boundary layers and dispersion over water.
- Find the cause for the superadiabatic layer present in the homogeneous simulations.
- Pray that there is not a nuclear accident at the Zion Nuclear Power Plant. They use a Gaussian based model with more simplifications than ISCST.
- Experiment with effects of nudging on operational use.

REFERENCES

Bowne, N., M. Koerber, D. Lawler, 1991: Lake Michigan ozone study 1991 field program. *84th Annual Meeting & Exhibition*, Vancouver, BC, Air and Waste Management Association, Paper 91-69.5.

Chen, C. and W.R. Cotton, 1983: A one-dimensional simulation of the stratocumulus-capped mixed layer. *Bound.-Layer Meteor.*, **25**, 289-321.

Chen, C. and W.R. Cotton, 1987: The physics of the marine stratocumulus-capped mixed layer. *J. Atmos. Sci.*, **44**, 2951-2977.

Gerritson, S.L., 1992: Multi-state ozone control strategy development in the Lake Michigan region. *Proc. 85th Annual Air & Waste Management Association*, June 21-26, Kansas City.

Haney, J.L., S.G. Douglas, L.R. Chinkin, D.R. Souten and C.S. Burton, 1989: Ozone air quality scoping study for the lower Lake Michigan air quality region. Final Report, Systems Application Inc., SAISAPP-89/101, 197 pp.

Hanna, S.R., L.L. Schulman, R.J. Paine, J.E. Pleim, and M. Baer, 1985: Development and evaluation of the offshore and coastal dispersion model. *J. Air Poll. Control Assoc.*, **35**, 1039-1047.

Klemp, J.B. and R.B. Wilhelmson, 1978a: The simulation of three-dimensional convective storm dynamics. *J. Atmos. Sci.*, **35**, 1070-1096.

Klemp, J.B. and R.B. Wilhelmson, 1978b: Simulations of right- and left-moving storms produced through storm splitting. *J. Atmos. Sci.*, **35**, 1097-1110.

Lee, T.J., 1992, Ph.D. Dissertation: The impact of vegetation on the atmospheric boundary layer and convective storms. Department of Atmospheric Science, Colorado State University, 137 pp.

Louis, J.F., 1979: A parametric model of vertical eddy fluxes in the atmosphere. *Bound.-Layer Meteor.*, **17**, 187-202.

Lyons, W.A., 1970: Numerical simulation of Great Lakes summertime conduction inversions. *Proc. 13th Conference on Great Lakes Research*, International Association for Great Lakes Research, 369-387.

Lyons, W.A., 1975: Satellite detection of air pollutants. In: *Remote Sensing Energy-Related Studies*, T.N. Vaziroglu, Ed., John Wiley, New York, 263-290.

Lyons, W.A., and H.S. Cole, 1976: Photochemical oxidant transport: Mesoscale lake breeze and synoptic aspects. *J. Appl. Meteor.*, **15**, 733-743.

Lyons, W.A. and L.E. Olsson, 1973: Detailed meso-meteorological studies of air pollution dispersion in the Chicago lake breeze. *Mon. Wea. Rev.*, **101**, 387.

Lyons, W.A. and S.R. Pease, 1973: Detection of particulate air pollution plumes from major point sources using ERTS-1 imagery. *Bull. Amer. Meteor. Soc.*, **54**, 1163-1170.

Lyons, W.A. and H.S. Cole, 1974: The use of monitoring network and ERTS-1 data to study inter-regional pollution transport of ozone in the Gary-Chicago-Milwaukee Corridor. 67th Annual Meeting of the Air Pollution Control Association, Paper #74-241, Denver, Colorado.

Lyons, W.A., J.L.Eastman, R.A. Pielke, C.J. Tremback, G.W. Wilkerson, 1992: The use of a mesoscale prognostic model to design a field tracer experiment for the Lake Michigan ozone study. *Proc. 85th Annual Air & Waste Management Association*, June 21-26, Kansas City.

McNider, R.T., M.D. Moran, and R.A. Pielke, 1988: Influence of diurnal and inertial boundary layer oscillations on long-range dispersion. *Atmos. Environ.*, **22**, 2445-2462.

Melli, P. and P. Zannetti, 1992: Environmental Modeling. Computational Mechanics Publications, Southampton, Boston, MA, 379 pp.

Moran, M.D., 1992, Ph.D. Dissertation: Numerical modelling of mesoscale atmospheric dispersion. Department of Atmospheric Science, Colorado State University, 758 pp.

Morris, R.E., M.A. Yocke, T.C Myers, V. Mirabella, 1992: Overview of the Variable-Grid Urban Airshed Model (UAM-V). *Proc. 85th Annual Air & Waste Management Association*, June 21-26, Kansas City.

Pielke, R.A., 1981: An overview of our current understanding of the physical interactions between the sea- and land-breeze and the coastal waters. *Ocean Mgt.*, **6**, 87-100.

Pielke, R.A., 1984: *Mesoscale meteorological modeling.* Academic Press, New York, N.Y., 612 pp. (Translated into Chinese with corrections by the Chinese Meteorological Press, 1990.)

Pielke, R.A., G. Dalu, M.D. Moran, M. Uliasz, T.J. Lee, and R.A. Stocker, 1991: Impacts of land surface characteristics on atmospheric dispersion. *Preprints, Seventh Joint Conference on Applications of Air Pollution Meteorology with AWMA*, New Orleans, Louisiana, AMS, January 14-18, 1991, 302-307.

Pielke, R.A., W.R. Cotton, R.L. Walko, C.J. Tremback, M.E. Nicholls, M.D. Moran, D.A. Wesley, T.J. Lee, and J.H. Copeland, 1992: A comprehensive meteorological modeling system – RAMS. *Meteor. Atmos. Phys.*, **49**, 69-91.

Smith, F.B., 1968: Conditioned particle motion in a homogeneous turbulent field. *Atmos. Environ.*, **2**, 491-508.

Tremback, C.J. and R. Kessler, 1985: A surface temperature and moisture parameterization for use in mesoscale numerical models. *Preprints, 7th AMS Conference on Numerical Weather Prediction*, June 17-20, Montreal, Quebec, Canada, American Meteorological Society, Boston, 355-358.

Tremback, C.J., J. Powell, W.R. Cotton, and R.A. Pielke, 1987: The forward-in-time upstream advection scheme: Extension to higher orders. *Mon. Wea. Rev.*, **115**, 540-555.

Tripoli, G.J. and W.R. Cotton, 1982: The Colorado State University three-dimensional cloud/mesoscale model – 1982. Part I: General theoretical framework and sensitivity experiments. *J. de Rech. Atmos.*, **16**, 185-220.

Uliasz, M. and R.A. Pielke, 1991: Lagrangian-Eulerian dispersion modeling system for real-time mesoscale applications. *Proc. Third Topical Meeting on Emergency Response and Preparedness*, Chicago, Illinois, April 16-19, 1991.

Wang, W. and T.T. Warner, 1988: Use of four-dimensional data assimilation by Newtonian relaxation and latent-heat forcing to improve a mesoscale-model precipitation forecast: A case study. *Mon. Wea. Rev.*, **116**, 2593-2613.

Xian, Zejin, 1991, M.S. Thesis: A 2-D model study of the influence of the surface on mesoscale convection during the Indian monsoon. Department of Atmospheric Science, Colorado State University, 110 pp + appendix.